



**NTNU – Trondheim**  
Norwegian University of  
Science and Technology

# Dehydrogenation of propane by carbon supported metal catalysts

**Eirik Østbye Pedersen**

Chemical Engineering and Biotechnology

Submission date: June 2013

Supervisor: Edd Anders Blekkan, IKP

Co-supervisor: Andrey S. Volynkin, IKP

Norwegian University of Science and Technology  
Department of Chemical Engineering



# Declaration of Authorship

I declare that this is an independent work according to the exam regulations of the Norwegian University of Science and Technology (NTNU).

Trondheim, June 7, 2013

---

Eirik Østbye Pedersen





# Preface

This master's thesis was written on behalf of the Department of Chemical Engineering at the Norwegian University of Science and Technology during the time period of January - June 2013. The work presented in this thesis is a continuation of a specialization project work performed during the fall semester of 2012. This project culminated in a report, and parts of this thesis, including some results, have been gathered from said report.

The thesis has been written under the supervision of Professor Edd Anders Blekkan who is first and foremost given thanks for his invaluable academic guidance. Additional thanks is given to co-supervisor Ph.D candidate Andrey S. Volynkin for his guidance regarding both the practical experimental work and theoretical issues. Engineer Karin Wiggen Dragsten is also thanked for her training with various instruments and her helpfulness with various technical issues. Post.doc fellow Navaneethan Muthuswamy and Ph.D candidate Ida Hjorth are also given a special thanks for their help with the voltammetric setup. Regina M. Barr of Altamira Instruments is thanked for providing training with the pulse chemisorption instrument. Lastly, fellow student Eirik Djuve is thanked for his cooperation with the aforementioned specialization project, helping to lay the groundwork for the work presented in this thesis.

The main purpose of this project was to prepare, characterize and test various carbon supported platinum catalysts for the dehydrogenation of propane. The characterization methods applied included thermogravimetric analysis, hydrogen chemisorption: volumetric and pulse method, BET surface area measurements and CO stripping voltammetry. The original plan was to compare the carbon supported catalysts to a hydrotalcite supported catalyst, but due to time limitations, no hydrotalcite supported catalyst was prepared. Four different carbon supported catalysts supported on three different carbon allotropes were prepared, characterized and tested. Four additional catalysts supported on carbon black, were also prepared and tested, but not characterized.

# Abstract

In this thesis, the catalytic properties of carbon supported Pt catalysts were investigated for the dehydrogenation of propane.

Using a polyol process, Pt/Carbon catalysts active for propane dehydrogenation were successfully prepared using carbon black, graphite and a conical platelet CNF as supports.

The catalysts were characterized using BET surface area measurements, TGA, volumetric and pulse hydrogen chemisorption and CO stripping voltammetry. The BET measurements found surface areas in the order carbon black > CNF > graphite with good measurement accuracy. The three subsequent methods were found impractical for the catalysts investigated due to poor measurement accuracy for the TGA compared to the size of the target value. The volumetric chemisorption was found unable to produce linear isotherms, likely caused by hydrogen-carbon interactions and the pulse experiment failed to find an optimal adsorption temperature that combined a manageable rate of desorption with a high rate of adsorption. The CO stripping voltammetric experiment was found able to determine the dispersion of the carbon black and graphite supported catalysts and found the dispersion of Pt/Carbon black > graphite, with some uncertainty associated with the results.

Experimental work was put into optimizing the catalyst activity measurement conditions and achieve an acceptable trade-off between pressure drop, deactivation rate and conversion levels. This was found at 500 °C, 50 mL/min feed flow rate, 50 mg sample mass diluted with inerts and 0.5 %wt. Pt content in the catalysts.

A kinetic study was performed and on a Pt/Carbon black catalyst, the propane dehydrogenation reaction was found to follow power law kinetics with a propane order of 0.9 and hydrogen order of  $-1.1$ . The accuracy of the measurements were better for the propane order than for hydrogen.

The three different supports were compared for catalytic activity and it was found that the activity of Pt/Carbon black > graphite > CNF. The likely cause was the lower dispersion of the graphite supported catalyst compared to that of the carbon black supported catalyst. As the CNF supported catalyst was found less active than the graphite supported catalyst, it is likely that the CNF supported catalyst also had a low dispersion. The low dispersions is most likely caused by a combination of the low surface areas and the surface chemistries of the CNF and graphite supports.

# Sammendrag

I dette arbeidet ble de katalytiske egenskapene til Pt katalysatorer på karbonbærere undersøkt for dehydrogenering av propan.

Ved bruk av en polyol prosess ble Pt/Karbon katalysatorer, som ble funnet aktive for propan dehydrogenering, syntetisert. Bærermaterialene som ble brukt var carbon black, grafitt og et konisk platelet karbonnanofiber (CNF) pulver.

Katalysatorene ble karakterisert ved hjelp av BET overflatemålinger, TGA, hydrogenkjemisorpsjon med volumetrisk og pulsmetode og CO stripping voltammetri. BET målingene fant at overflatearealet til carbon black > CNF > grafitt med god målenøyaktighet. De tre neste metodene ble vist å være upraktiske for katalysatorene som ble undersøkt. TGA viste for lav målenøyaktighet i forhold til måltallets størrelse. Volumetrisk kjemisorpsjon ble funnet til ikke å kunne produsere lineære isotermer, antakelig grunnet hydrogen-karbon interaksjoner. For pulskjemisorpsjonen ble det ikke funnet en optimal adsorpsjonstemperatur som kombinerte en håndterbar lav desorpsjonsrate med en tilstrekkelig høy adsorpsjonsrate. CO stripping voltammetrieksperimentet ble brukt til å påvise dispersjonen til katalysatorene på carbon black of grafitt bærer og det ble funnet at dispersjonen til Pt/Carbon black > grafitt, med noe måleusikkerhet knyttet til eksperimentet.

Eksperimentelt arbeid ble lagt ned i å optimalisere driftsbetingelsene for målingene av katalytisk aktivitet med mål om å finne et akseptabelt kompromiss mellom trykkfall, deaktivierungsrate og omsetningsnivåer. Dette ble funnet ved 500 °C, 50 mL/min gassfoderate, 50 mg prøvemasse fortynnet med inerter og 0.5 vekt% Pt innhold i katalysatorene.

Et kinetikkeksperiment ble utført og på Pt/Carbon black katalysatoren ble det funnet at propan dehydrogeneringsreaksjonen følger power law kinetikk med propanorden på 0.9 og hydrogenorden på -1.1. Nøyaktigheten til disse bestemmelsene var bedre for propanordenen enn for hydrogen.

De tre forskjellige bærermaterialene ble sammenliknet for katalytisk aktivitet og det ble funnet at aktiviteteten til Pt/Carbon black > grafitt > CNF. Den mest sannsynlige årsaken var den lavere dispersjonen påvist på katalysatoren på grafittbærer i forhold til på carbon black. Siden katalysatoren på CNFbærer ble funnet å være mindre aktiv enn katalysatoren på grafittbærer, er det sannsynlig at katalysatoren på CNFbærer også har lav dispersjon. De lave dispersjonene er mest sannsynlig forårsaket av en kombinasjon av de lave overflatearealene og overflatekjemien til CNF og grafittbæerne.

# Table of Contents

<b>Declaration of Authorship</b>	<b>i</b>
<b>Preface</b>	<b>iii</b>
<b>Abstract</b>	<b>iv</b>
<b>Sammendrag</b>	<b>v</b>
<b>Table of Contents</b>	<b>vi</b>
<b>Symbols and Abbreviations</b>	<b>viii</b>
<b>1 Introduction</b>	<b>1</b>
<b>2 Theory</b>	<b>2</b>
2.1 Propane Dehydrogenation . . . . .	2
2.2 Carbon in Catalysis . . . . .	4
2.3 Catalyst Synthesis . . . . .	7
2.4 Catalyst Characterization . . . . .	7
2.5 Catalyst Testing . . . . .	12
2.6 Gas Chromatography . . . . .	14
<b>3 Experimental</b>	<b>16</b>
3.1 Catalyst Synthesis . . . . .	16
3.2 Catalyst Characterization . . . . .	16
3.3 Catalyst Activity Measurements . . . . .	19
<b>4 Results</b>	<b>23</b>
4.1 Catalyst Synthesis . . . . .	23
4.2 Catalyst Characterization . . . . .	23
4.3 Catalyst Activity Measurements . . . . .	29
<b>5 Discussion</b>	<b>36</b>
5.1 Catalyst Synthesis Results . . . . .	36
5.2 Catalyst Characterization Results . . . . .	36
5.3 Catalyst Activity Results . . . . .	40
<b>6 Future Work</b>	<b>48</b>
<b>7 Conclusion</b>	<b>50</b>

<b>Bibliography</b>	<b>51</b>
<b>Appendix A Chemicals</b>	<b>I</b>
<b>Appendix B Catalyst Synthesis Details</b>	<b>II</b>
<b>Appendix C BET Measurements</b>	<b>VI</b>
<b>Appendix D TGA Measurements</b>	<b>VIII</b>
<b>Appendix E Hydrogen Chemisorption Measurements</b>	<b>XII</b>
E.1 Volumetric Method . . . . .	XII
E.2 Pulse Method . . . . .	XIV
<b>Appendix F CO Stripping Voltammetry Measurements</b>	<b>XVI</b>
<b>Appendix G Activity Measurements</b>	<b>XVIII</b>
G.1 Experimental Raw Data . . . . .	XVIII
G.2 Deactivation Model . . . . .	XXVII
G.3 Kinetic Study . . . . .	XXVIII
G.4 Selected Chromatograms . . . . .	XXX
<b>Appendix H Micro GC Calibration Data</b>	<b>XXXII</b>
<b>Appendix I Simulation Data</b>	<b>XXXIV</b>
<b>Appendix J Risk Assessment</b>	<b>XXXVI</b>

# Symbols and Abbreviations

Symbol	Unit	Description
$a$		Power law order of propane
$A_0$	$\text{nm}^2$	Surface area of one adsorbate molecule in BET measurements
$A_i$	$\mu\text{Vs}$	Response of component $i$ in GC measurements
$A_{IS}$	$\mu\text{Vs}$	Response of the internal standard in GC measurements
$A$	$\text{nm}^2$	Total surface area in BET measurements
ASTM		American Society for Testing and Materials
$b$		Power law order of hydrogen
BET		Brunauer Emmett and Teller
$C_{K^*}$	$\text{g}^{-1}$	Concentration of sites deactivated by coking
$C_t$	$\text{g}^{-1}$	Total concentration of active sites
CNF		Carbon nanofiber
CNT		Carbon nanotube
$D$	%	Dispersion
DSC		Differential Scanning Calorimetry
$E$	V	Electrode potential
$E_t^a$	V	Anodic turn-round potential
$E_t^c$	V	Cathodic turn-round potential
EG		Ethylene glycol
$F_{A,0}$	mol/s, mL STP/min	Inlet molar flow of component A
$F_A$	mol/s, mL STP/min	Outlet molar flow of component A
$F_i$	mol/s, mL STP/min	Molar flow of component $i$
$F_B$	mol/s, mL STP/min	Outlet molar flow of component B
$F_T$	mol/s, mL STP/min	Total molar flow
FBD		Fluidized bed dehydrogenation
GC		Gas chromatography
GFCB		Gas Flow Controller Box
$I$	$\text{mA}/\text{cm}^2$ , $\text{A}/\text{mmol}$	Current density
IR		Infrared (spectroscopy)
$k$	$\text{mol}/\text{g cat s}$	Reaction rate constant
$k_B$	J/K	Boltzmann constant
$m$	g, mg	Mass, weight
$M_m$	g/mol	Molar mass of metal
MFC		Mass Flow Controller
MS		Mass Spectroscopy

$n_s$	mol	Number of surface metal moles
$N_0$		Number of molecules in a BET monolayer
$N_A$	$\text{mol}^{-1}$	Avogadro's number
OV-1		Capillary GC column with methyl polysiloxane as the stationary phase.
$p$	bar	Partial pressure
$p_{Ref}$	bar	Reference partial pressure
$P$	mmHg	Adsorption pressure
$P_0$	mmHg	Equilibrium, /saturation pressure
PC		Pressure Controller
PLOT U		Porous Layer Open Tubular GC column type U
PLS		Pulse loop size
PM		Pressure Meter
$Q_{CO}$	$\mu\text{C}$	Desorption charge of a CO monolayer
$R$	$\text{mol/g cat s}$	Reaction rate
$R_A$	$\text{mol/g cat s}$	Rate of consumption of component $A$
$R_A^0$	$\text{mol/g cat s}$	Initial rate of consumption of component $A$
$R_B$	$\text{mol/g cat s}$	Rate of production of component $B$
$R_{Ref}$	$\text{mol/g cat s}$	Reference reaction rate
$RF_i$	$\mu\text{V s}$	Response Factor of component $i$ in GC measurements
$RF_{IS}$	$\mu\text{V s}$	Response Factor of the internal standard in GC measurements
$RRF_i$		Relative response factor of component $i$
RHE		Reversible hydrogen electrode
$S_B$	%	Selectivity of component B
$S_{CO}$	$\text{cm}^2$	Surface area of CO monolayer
$S_{BET}$	$\text{m}^2/\text{g}$	BET specific surface area
STAR		Steam Active Reforming
STP		Standard temperature and pressure
SV		Safety Valve
$t$	min, h	Time
$t_0$	min, h	Reference time
$T$	K, °C	Temperature
TC		Thermocouple
TCB		Temperature Controller Box
TCD		Thermal conductivity detection/detector
TGA		Thermogravimetric analysis
$TOF_A$	$\text{s}^{-1}$	Turnover frequency for consumption of component $A$
$TOF_B$	$\text{s}^{-1}$	Turnover frequency for production of component $B$
$v$	$\text{mV/s}$	Voltammetric scan rate
$V$	mL	Volume
$V_a$	$\text{mL STP/g cat}$	Volume of adsorbed gas
$V_0$	$\text{mL STP/g cat}$	Volume of adsorbed gas in a monolayer
$V_m$	$\text{mL/mol}$	Molar volume of an ideal gas

Vulcan		A carbon black brand name
$W$	g	Catalyst weight
$x_m$	%	Weight fraction of metal in a catalyst
$X_A$	%	Conversion of component A
$X_{eq}$	%	Equilibrium conversion
$Y_i$		Gas phase mole fraction of component $i$ .
$Y_{IS}$		Gas phase mole fraction of the internal standard.
$\alpha$	$\text{mL}^{-1}$	Slope value in the BET equation
$\Delta H_{298K}^0$	$\text{kJ/mol}$	Standard heat of reaction at 1 bar and 298 K.
$\Delta t$	s	Time between pulses
$\eta$	$\text{mL}^{-1}$	Intercept value in the BET equation
$\varphi_A$		Deactivation function
$\chi$		Ratio of desorption rate constants for the $2^{nd}$ and $1^{st}$ adsorption layer
3vw		Three-way-valve
*		Free active site
$H^*$		Adsorbed hydrogen



# 1. Introduction

Propylene, or propene, is one of the major industrial chemical intermediates that serves as one of the main building blocks of the petrochemical industry. It is used as a feedstock for a variety of petrochemical products including polypropylene, propylene oxide, cumene and acrylonitrile. The main routes of producing propylene are steam cracking of light alkanes and fluid catalytic cracking of gas oil in refineries with steam cracking providing for 68 % of propylene production as of 2002[1].

Due to ethylene being the key building block of the petrochemical industry, steam cracking technology have always been designed to maximize ethylene yield, with propylene and other light olefins only being produced as by-products. Consequently, as the demand of key propylene derivatives, most notably polypropylene, have increased rapidly in later years, steam crackers have struggled to meet the growing demand of propylene[2].

An inherent weakness of the steam cracking process is its relatively low selectivity towards its desired product, which is ethylene[3]. The flexibility in the process to change its desired product to propylene is also very limited[2]. Adding that the building of steam cracking plants is highly capital cost intensive, more and more attention has been spent on the alternate production paths to light olefins[3].

Among several alternative paths to light olefins including methanol to olefins, Fischer-Tropsch synthesis[3] and olefin metathesis[1], the selective dehydrogenation of propane is already commercialized and is therefore of particular interest. This process has also in more recent years recieved heightened attention due to a radical decrease of the propane price following the recent developments in shale gas production in North America[4].

At the high reaction temperatures required for propane dehydrogenation, secondary reactions such as cracking and coke formation are expected to occur. Catalyst deactivation by coking is rapid and the process requires continous catalyst regeneration causing high operation costs[3]. Consequently, substantial research efforts are dedicated to the development of better catalysts with focus on catalyst lifetime, activity, selectivity and regenerative properties.

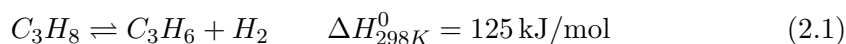
In this project, the catalytic properties of carbon supported Pt catalysts will be investigated. As carbon supported catalysts are not regenerable by traditional means, they are not commercially interesting as propane dehydrogenation catalysts. However, their catalytic properties are interesting as carbon supported catalysts previously have been reported as having superior properties in comparison to earlier type catalysts with respect to both activity and selectivity[5, 6]. The catalysts will be prepared, characterized and tested. The characterization techniques that are to be employed are: thermogravimetric analysis, BET surface area measurements, volumetric hydrogen chemisorption, hydrogen pulse chemisorption and CO stripping voltammetry.

# 2. Theory

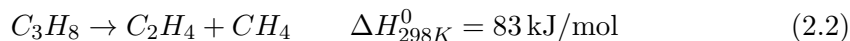
## 2.1 Propane Dehydrogenation

### 2.1.1 Chemistry

The propane dehydrogenation reaction equation is presented in equation (2.1).



Reaction (2.1) is highly endothermic and results in an increase in mole number. Propane dehydrogenation is therefore thermodynamically favoured by high temperatures and low pressures. To reach acceptable conversion levels, the feed gas is diluted with inerts and heated[1]. Depending on the process configuration, reactor temperature is kept between 750 and 920 K[3]. At these high reaction temperatures, secondary reactions such as cracking (2.2) and hydrogenolysis (2.3) of propane[7] in addition to coking are expected to occur[3, 7].



Cracking can occur both catalytically or thermally, but thermal cracking is usually not important below 650 - 700 °C. Hydrogenolysis is a catalytic reaction, taking place at Pt-sites. It is, in contrast to dehydrogenation of propane, a structure sensitive reaction, favouring steps and kinks on the Pt surface[8]. The reaction enthalpies shown are calculated using values from Aylward & Findlay[9].

### 2.1.2 Kinetics

The reaction mechanism of reaction (2.1) is not known in detail, but several suggested mechanisms exist[8]. Kinetic studies have however shown good fits with Langmuir-Hinshelwood kinetic models[10, 11] and power law models[12]. A power law kinetic expression of reaction (2.1) is shown in equation (2.4)[13].

$$R = k p_{C_3H_8}^a p_{H_2}^b \quad (2.4)$$

Here,  $R$  is the rate of reaction,  $k$  is the temperature dependent reaction constant,  $p$  is component partial pressure and  $a$  and  $b$  are the reaction orders with respect to  $C_3H_8$  and  $H_2$  respectively. The reaction orders can be determined by measuring the

reaction rate while varying the partial pressure of the monitored reactant and keeping partial pressure of the other reactant constant. A log-log plot of  $R$  versus the partial pressure of the monitored reactant should yield a linear plot with a slope equal to the reaction order of the monitored reactant.

### 2.1.3 Catalysis

Several catalyst systems including Pt,  $\text{Cr}_2\text{O}_3$  and Pt-Sn on  $\gamma\text{-Al}_2\text{O}_3$  or  $\text{Zn}/\gamma\text{-Al}_2\text{O}_3$  are employed commercially[1, 3]. Pt is considered highly active for propane dehydrogenation. To achieve high Pt dispersions, a high surface area support like  $\gamma\text{-Al}_2\text{O}_3$  is used. This support contains acid sites which are believed to promote the cracking reaction (2.2) as well as coking[7, 14]. The acid sites of  $\gamma\text{-Al}_2\text{O}_3$  are neutralized by application of alkaline promoters like potassium[7]. The addition of Sn is known to improve both activity, selectivity and deactivation resistance of Pt/ $\gamma\text{-Al}_2\text{O}_3$  by interaction with the support and increasing Pt dispersion[15]. The addition of Sn in particular inhibits reaction (2.3)[7].

The dominant deactivation mechanism in propane dehydrogenation catalysts is coking[3]. Coke formed during dehydrogenation of propane is believed to primarily deposit on the acid sites of the support but it is known to also deposit on the active metal by a different mechanism than for acid site coking[16]. The coke on the metal is believed to be formed via a complex mechanism starting with di- or oligomerization of adsorbed propylene to either hexene or an aromatic compound serving as a coke precursor. The addition of hydrogen to the feed gas is known to suppress coke formation and increase deactivation resistance as it is believed to adsorb competitively with propylene on the same surface sites[14].

### 2.1.4 Industrial Production

Several process configurations exist for the dehydrogenation of propane. All have installed a system for catalyst regeneration and heat supply but differ in the way this is performed and in reactor design[3]. A simplified flow sheet of the propane dehydrogenation general process is shown in Fig. 2.1.

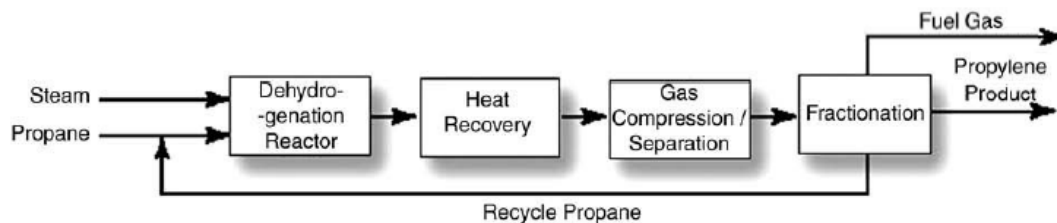


Figure 2.1: Simplified flow sheet of a general propane dehydrogenation process. Source: Aitani[1].

In Fig. 2.1 propane is fed to the reactor along with a diluent, most commonly steam. As the cracking (2.2) and coking products are the thermodynamically stable products at the high reaction temperatures, the reactor effluent needs to be quenched by heat recovery to stop further reaction. Due to the inherent difficulty associated with

the separation of propylene from propane, the separation units required are quite complex. The conversion per pass is limited by thermodynamics, so a large recycle stream is required. The result of these two properties is that the compression and separation units in a dehydrogenation plant account for nearly 85% of total capital costs[3].

The Oleflex process uses radial flow adiabatic moving bed reactors in series with interstage fired heaters. Catalyst regeneration is provided by burning in air in a separate regenerator. The Catofin process uses between 3 and 8 adiabatic fixed bed reactors in parallel. The reactors are taken off stream one at the time to be regenerated by burning in air. The reaction heat is provided by the heat produced by regeneration, stored in the catalyst bed, as well as preheating the feed in a fired heater. The Steam Active Reforming (STAR) process uses multiple parallel fixed bed reactors contained in a furnace similar to a steam reformer furnace. It is regenerated in a similar way to the Catofin process. The FBD-4 or Snamprogetti process uses a fluidized bed reactor with continuous circulation of catalyst between the reactor and a regenerator, similar to an older fluid catalytic cracking reactor[3].

## **2.2 Carbon in Catalysis**

### **2.2.1 General**

Carbon can be used both as a catalyst in its own right, and as a catalyst support. Carbon is an interesting catalyst support material due to several properties. It is known to be resistant to acidic and basic media, it can be shaped into different forms, its surface properties can be modified to different degrees of hydrophilicity, and recovery of the active metal is made easy by burning off the carbon. Carbon's electronic properties make it particularly suitable as a fuel cell catalyst support[17]. Carbon has several allotropes that has been used as catalyst supports including graphite, carbon black, activated carbon, carbon nanotubes and nanofibers.

### **2.2.2 Carbon Black**

Carbon black is elemental carbon of high purity produced by incomplete combustion or thermal decomposition of liquid or gaseous hydrocarbons under controlled conditions. It is an amorphous carbon allotrope with a high surface-to-volume ratio [18]. The high surface area makes it suitable as a catalyst support for noble metals as high metal dispersions are achievable at high metal loads. Commercially available carbon blacks are for this reason widely employed as fuel cell catalyst supports[19].

### 2.2.3 Graphite

Graphite is a crystalline carbon allotrope with a structure as shown in Fig. 2.2. It consists of planar graphene sheets in layers held together by weak intermolecular forces. It has a variety of uses and is used in catalysis for its thermal and chemical stability[20] and can also be used to form intercalated compounds where the active metal is deposited between the graphene sheets[21].

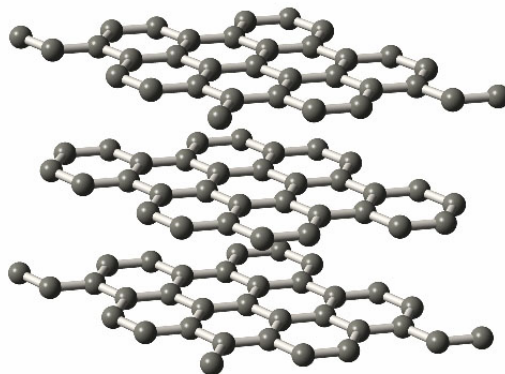


*Figure 2.2: Graphite's planar, layered structure. Source: MBI Institut[22].*

### 2.2.4 Carbon Nanotubes and Nanofibers

Carbon nanotubes (CNTs) and carbon nanofibers (CNFs) come in a variety of forms as shown in Fig. 2.3. The structures are built up of graphene sheets and differ in the way these sheets are aligned in relation to each other. The different structures are known to have different properties as the varying graphene edge densities provide for different electronic properties between the structures[17]. These unique electronic properties give rise to interesting catalytic properties and CNF supported catalysts have previously been reported to have superior properties to other catalysts with respect to both activity and selectivity[5, 6].

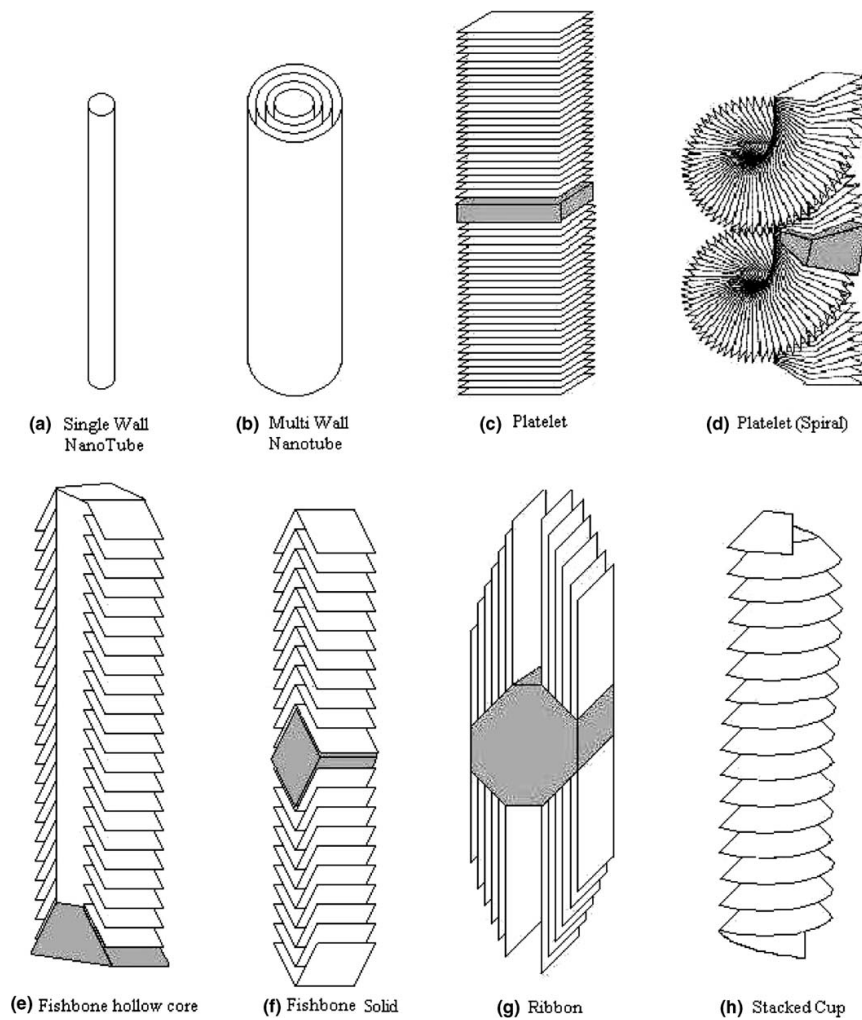


Figure 2.3: Diagram of the accepted carbon nanotube and nanofiber structures. Source: Martin-Gullon et al.[23].

Scanning electron microscopy images of the CNF type used later in this thesis are shown in Fig. 2.4.

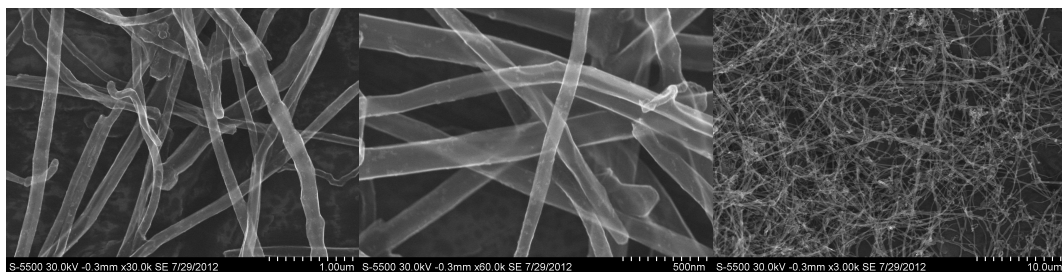


Figure 2.4: Scanning electron micrographs of carbon nanofibers. Source: Volynkin[24].

## 2.3 Catalyst Synthesis

The polyol process is a catalyst preparation method that has been proven able to produce highly dispersed Pt/Carbon catalysts with small and narrowly distributed particle sizes. The process can produce catalysts with Pt content over 50 %wt., making it a suitable method for producing fuel cell catalysts[17, 25]. It is based on the conventional polyol process first reported by Fievet et al.[26].

In the polyol process, a metal salt is dissolved in a liquid polyol where the metal ions will be reduced under heating to form a metal colloid suspension. The polyol acts as both solvent and reducing agent. For Pt/Carbon catalyst synthesis, ethylene glycol is commonly applied. Ethylene glycol will oxidize to form glycolic acid, which exists in its deprotonated glycolate form in alkaline solution. The glycolate anions will adsorb on the Pt colloid surface and act as a stabilizing agent for the colloid suspension by providing an electrostatic repulsive force between the metal particles. Consequently, there exists a strong relationship between the metal particle size and the concentration of glycolate anions. It is therefore favourable to perform the polyol process in an alkaline solution to decrease particle size and achieve a high dispersion[25].

For Pt/Carbon catalysts produced with the polyol process, it has been shown that the Pt content on carbon supports, significantly decreases with increasing pH. The undeposited Pt remains in the suspension and is lost. The modification to the polyol process suggested by Oh et al.[25] therefore consists of adding a pH adjustment step to the process in order to increase the Pt content on the carbon support without significantly increasing particle size. Increasing the pH increases the electrostatic attractive forces between Pt colloids and carbon support and maintains the repulsive forces between Pt particles[25].

A weakness of this method is that not all Pt will deposit on the support, but remain in the suspension. The catalysts prepared with this method will therefore need to be characterized for Pt content.

## 2.4 Catalyst Characterization

### 2.4.1 The Brunauer-Emmett-Teller Method

The information presented under this section is gathered from Chorkendorff & Niemantsverdriet[27]. The Brunauer-Emmett-Teller(BET) method is a commonly applied technique used to determine the specific surface area of a catalyst. The method uses adsorption of an inert gas, typically N<sub>2</sub>, to determine surface area by measuring the adsorption - desorption isotherm. The principle underlying the method is that the total surface area can be found by determining the monolayer coverage of the adsorbate molecule and multiplying with the area covered by one adsorbed molecule. The assumptions that govern the BET theory are:

1. Dynamic equilibrium between adsorbate and adsorbent, i.e. the rate of adsorption is equal to the rate of desorption in any layer.
2. In the first layer, molecules adsorb on equivalent adsorption sites.

3. The molecules in any layer make up the adsorption sites for the molecules in the subsequent layer.
4. Adsorbate-adsorbate interaction are negligible.
5. The adsorption-desorption conditions are equal for all layers above the first.
6. The adsorption energy for the 2<sup>nd</sup> and higher layers is equal to the condensation energy.
7. The multilayer grows to infinite thickness as the adsorption pressure approaches the saturation pressure.

By applying these assumptions, equation (2.5) can be derived.

$$\frac{P}{V_a(P_0 - P)} = \frac{1}{\chi V_0} + \frac{(\chi - 1)}{\chi V_0} \frac{P}{P_0} \quad (2.5)$$

Equation (2.5) is commonly known as the BET equation. Here  $P$  is the adsorption pressure,  $P_0$  is the equilibrium pressure of the condensed gas, or saturation pressure,  $V_a$  is the volume of adsorbed gas,  $\chi$  is the ratio of desorption rate constants for the second and the first layer and  $V_0$  is the volume of the gas adsorbed in the first monolayer. Plotting the left hand side of equation (2.5) versus  $P/P_0$ , yields a linear curve with a slope equal to  $(\chi - 1)/\chi V_0$  and an intercept at  $1/\chi V_0$ . By setting the slope value as  $\alpha$  and the intercept as  $\eta$ , rearranging gives the monolayer volume by equation (2.6).

$$V_0 = \frac{1}{\alpha + \eta} \quad (2.6)$$

Using ideal gas law (2.7), this can be converted to the number of molecules adsorbed in a monolayer.

$$N_0 = \frac{PV_0}{k_B T} \quad (2.7)$$

Here  $k_B$  is the Boltzmann constant, and  $T$  is temperature. Knowing the surface area covered by a single adsorbate molecule  $A_0$ , e.g. 0.162 nm<sup>2</sup> for N<sub>2</sub> at 77 K, the total area  $A = N_0 A_0$  is found. Accordingly, the specific surface area,  $S_{BET}$ , is found by dividing  $A$  with the catalyst sample mass.

### 2.4.2 Thermogravimetric Analysis

Thermogravimetric analysis (TGA) is a characterization technique in which the mass of a sample is monitored over a range of temperatures and time in a temperature controlled environment with a controlled atmosphere. The technique is usually performed in conjunction with differential scanning calorimetry (TGA-DSC) in order to monitor the heat development in the sample. The method can be used to determine the thermal stability of the sample material, and when performed in an oxidative atmosphere, used to determine the weight fraction of the non-combustible components of a sample material, e.g. the Pt content in a Pt/Carbon catalyst. In order to analyse the off-gases produced during temperature programmed treatment,



TGA is often performed in conjunction with mass spectroscopy (TGA-MS), infrared spectroscopy (TGA-IR) and/or gas chromatography (TGA-GC)[28].

### 2.4.3 Hydrogen Chemisorption

Chemisorption is a characterization technique applied to determine the dispersion of a catalyst. The method uses a chemisorbing gas, commonly hydrogen or CO to determine the number of surface metal atoms present in the catalyst by estimating the monolayer coverage of a chemisorbing species. Several chemisorption techniques are employed in order to estimate the monolayer coverage including volumetric chemisorption and pulse chemisorption.

The volumetric chemisorption method that is used to determine the dispersion is governed by ASTM International (American Society for Testing and Materials) in order to produce comparable results. The method assumes that the adsorbate gas chemisorps selectively on the surface atoms and is in dynamic equilibrium with the gas phase. Data is collected by gradually increasing the partial pressure of the adsorbate gas and measuring the adsorption volume at constant temperature producing an adsorption isotherm, called the 1<sup>st</sup> isotherm. The ASTM method then evacuates the sample chamber and repeats the pressure increase producing the 2<sup>nd</sup> isotherm assumed to represent the weakly adsorbed species. The difference between the 1<sup>st</sup> and 2<sup>nd</sup> isotherm is then assumed to be the chemisorbed species. The isotherm produced is then extrapolated to determine the monolayer coverage.

Pulse techniques are generally considered less accurate than volumetric methods, but offer practical advantages under experimental conditions. Pulse experiments are performed by continually flowing an inert gas over a catalyst bed and introducing a small, known amount of adsorbing gas to the system in successive pulses. The adsorption volume is determined by measuring the gas slipping through the catalyst bed. The gas slip will increase with successive pulses and eventually stabilize. It is then assumed that monolayer coverage has been reached and it is determined by adding the adsorption volume of the preceding pulses. Two conditions are necessary for ensuring the reliability of this method[29]:

1. A fast rate of gas adsorption
2. A negligible slow rate of gas desorption

Hydrogen is a commonly used adsorbate which is known to chemisorb dissociatively, as by reaction (2.8)[27].



Here, \* is a free active site and  $H*$  is adsorbed hydrogen. This gives an adsorption stoichiometry of 2. Having determined the monolayer coverage, the total number of active sites is then found by equation (2.9) assuming ideal gas.

$$n_s = \frac{2V_0}{V_m} \quad (2.9)$$

Here  $n_s$  is the total molar number of active sites, or surface metals atoms,  $V_0$  is the adsorbed volume of hydrogen at monolayer coverage and  $V_m$  is the molar volume equal to 22414 mL/mol derived by the ideal gas law. The definition of catalyst dispersion is the fraction of metal atoms exposed to the surface[13]. It is consequently found by equation (2.10).

$$D = \frac{n_s M_m}{x_m W} \quad (2.10)$$

Here  $M_m$  is the molar mass of the metal,  $x_m$  is the metal weight fraction in the catalyst and  $W$  is the catalyst sample mass.

#### 2.4.4 Cyclic Voltammetry

Cyclic voltammetry is a type of potentiodynamic electrochemical measurement. It is performed in a 3-electrode system consisting of a working electrode, a reference electrode and a counter electrode. The working electrode will contain the analyte. The reference electrode acts as a half cell with a known reduction potential, and the counter electrode's role is to supply the electrons needed for the electrode reactions at the working electrode [30, 31].

A potential is imposed on the working electrode through a potentiostat and ramped linearly over time. When it reaches a set potential, the ramp rate is inverted and the potential is lowered back to the initial potential. This is performed while simultaneously measuring the current at the counter electrode. The inversion can be repeated many times during the experiment, creating a triangular potential waveform as shown in Fig. 2.5a. Following some cycles, the system will respond in a quasi-stationary manner described by a cyclic voltammogram, exemplified by Fig. 2.5b[31].

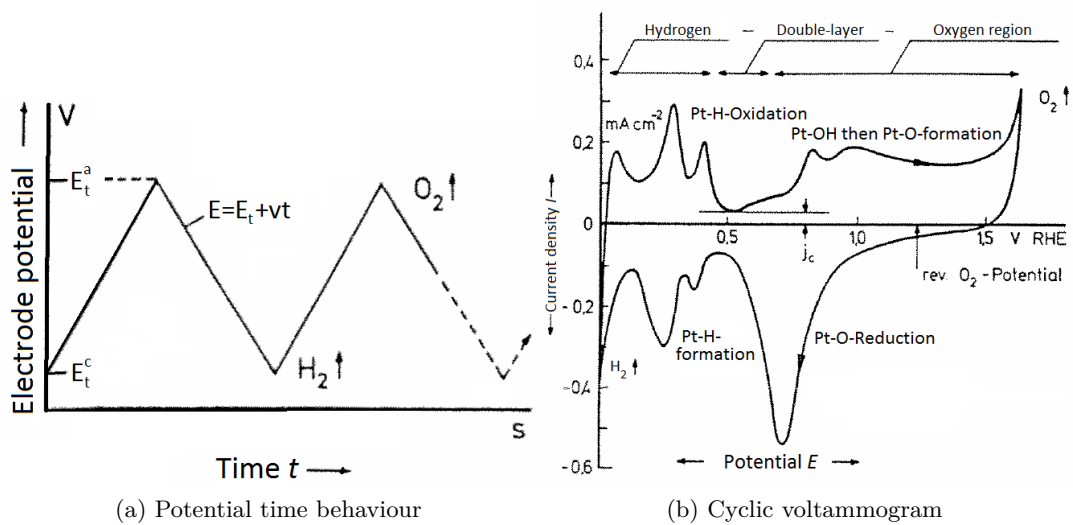


Figure 2.5: Potential-time behaviour at the working electrode (a) and cyclic voltammogram of Pt in 1M KOH at 20°C and  $v = 100$  mV/s (b).

Source: Hamann et al.[31].

Here,  $E$  is electrode potential,  $E_t^c$  and  $E_t^a$  are the cathodic and anodic turn-round potentials and  $v$  is the potential ramp rate. As shown in Fig. 2.5b, different electrode reactions occur at different potentials, and the shape, and scale of the voltammogram can be used to determine several electrochemical properties[31].

CO stripping voltammetry is a type of cyclic voltammetric experiment in which the working electrode is first saturated with CO before the CO is stripped from the surface at increasing potential[32]. The resulting voltammogram will resemble Fig. 2.6.

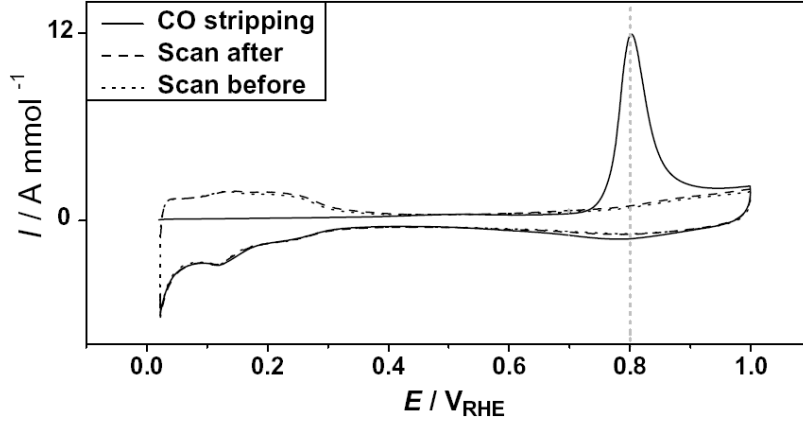


Figure 2.6: Cyclic voltammogram for CO stripping of a Pt/Vulcan sample, produced at 10 mV/s in 0.5M HClO<sub>4</sub>. Adapted from Ochal et al.[33].

Here, the peak at approximately 0.8 V represents the CO desorption and is believed to correspond to a monolayer of CO[32]. The desorption charge,  $Q_{CO}$  is found by integrating the peak area and dividing by the potential ramp rate,  $v$ . By using equation (2.11)[34], the CO surface area,  $S_{CO}$ , can be found.

$$S_{CO} = Q_{CO}/0.420 \text{ mC/cm}^2 \quad (2.11)$$

The constant in equation (2.11) corresponds to a monolayer of adsorbed CO assuming linear bonding between CO and adsorbent[32], i.e. 1:1 adsorption stoichiometry. By assuming a specific Pt surface area of  $8^{-16} \text{ cm}^2/\text{atom}$  (average of the (111), (110) and (100) crystal planes[35]), the molar number of surface Pt atoms,  $n_s$ , can be determined by dividing  $S_{CO}$  with  $8^{-16} \text{ cm}^2$  and dividing by Avogadro's number,  $N_A$ , equal to  $6.022 \cdot 10^{23} \text{ mol}^{-1}$ . Knowing  $n_s$ , the dispersion can be determined as described earlier by equation (2.10).

## 2.5 Catalyst Testing

### 2.5.1 The Differential Reactor

The testing of catalysts is an important step towards determining a catalyst's suitability for performing a chemical reaction. There are several methods of investigating a catalyst's activity but a common method is to use the fixed bed differential reactor[27]. The differential reactor is easy to use, easy to construct, has low construction costs and can be adapted to provide near ideal conditions regarding gas-catalyst contact and minimization of concentration and temperature gradients[36]. This makes it a suitable reactor setup for determining a catalyst's kinetic properties and deactivation properties with comparable results. A differential fixed bed reactor is made by using a small amount of catalyst, and/or diluting the catalyst bed with inerts, as shown in Fig. 2.7.

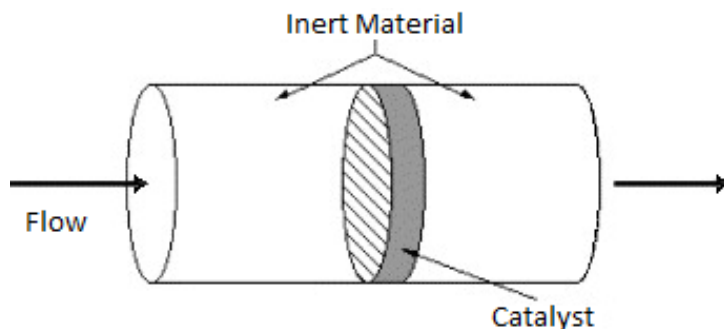


Figure 2.7: Differential fixed bed reactor schematic. Source: Richardson et al.[37].

### 2.5.2 Catalyst Activity

A catalyst's initial activity can be described by the conversion it yields at specific operation conditions. The conversion of a species  $A$  is defined as moles of  $A$  reacted, divided by moles of  $A$  fed as shown in equation (2.12).

$$X_A = \frac{F_{A,0} - F_A}{F_{A,0}} \quad (2.12)$$

Here,  $F$  is molar flow at the reactor outlet,  $F_0$  molar flow at the reactor inlet and subscript  $A$  denotes the monitored reactant, which in systems with more than one reactant species should be the limiting reactant[13]. Conversion can be used for rapid screening of catalysts in comparison of their initial activities, but does not provide enough information to determine the suitability of a catalyst. Another important quality of a catalyst is its selectivity, which is defined as the fraction of converted  $A$  which has been converted to the desired product  $B$ . Comparison of the selectivities of catalysts should be done at the same conversion level. For an  $A \rightarrow B$  reaction

system with possible side reactions, the selectivity of  $B$  is defined by equation(2.13).

$$S_B = \frac{F_B}{F_{A,0}X_A} \quad (2.13)$$

The reaction rate per unit mass of a catalyst, which provides more information on a catalysts properties than the conversion is in a fixed bed reactor related to the conversion by reaction (2.14)[13].

$$F_{A,0}X_A = \int_0^W R_A dW \quad (2.14)$$

Here,  $R_A$  is the rate of consumption of component  $A$  per unit mass of catalyst and  $W$  is the mass of catalyst in the reactor. When testing under differential reactor conditions, with the conversion levels significantly lower than the equilibrium conversion, the rate can be assumed constant throughout the catalyst bed, and equation (2.14) is reduced and rearranged to equation (2.15)[13].

$$R_A = \frac{F_{A,0}X_A}{W} \quad (2.15)$$

Consequently, the rate of production of component  $B$ ,  $R_B$ , is found by  $S_B R_A$ . Another commonly reported catalyst activity measurement is the specific activity, or turnover frequency. Turnover frequency is defined as the number of moles converted per number of moles of active sites, or surface metal atoms, in the catalyst per unit time[13]. Turnover frequency provides comparable information on the activity of the catalysts active sites, but requires a measurement of the catalyst's dispersion. The turnover frequency of a catalyst can be determined by reaction (2.16).

$$TOF_A = \frac{R_A M_m}{x_m D} \quad (2.16)$$

Here,  $M_m$  is the molar mass of the catalyst metal,  $x_m$  is the metal mass fraction in the catalyst and  $D$  is the metal dispersion. Turnover frequency for production of  $B$ ,  $TOF_B$ , is then found by  $S_B TOF_A$ .

### 2.5.3 Catalyst Deactivation

A catalyst's activity is not constant, but will decline with use and the catalyst in a reactor will eventually have to be regenerated or replaced. A catalyst's lifetime may be on the timescale of years in the case of the Fe based ammonia synthesis catalyst, or seconds in the case of the catalytic cracking catalyst[38].

Deactivation may be caused by several means including mechanical failure, fouling, volatilization, phase changes, compound formation, sintering, poisoning and coking of which the three latter are the most important. The causes often appear alongside one another and are often difficult to diagnose[39].

When testing a catalyst's properties under changing conditions, it is important to have a catalyst that deactivates at a negligible slow rate relative to the time scale of the experiment. If this is not achievable, a mathematical model predicting the activity loss over time may be used to correct for deactivation and minimize the information loss. Several such models have been used to predict catalyst deactivation[39]. From Holmen[38], deactivation by coking is modeled using the deactivation function,  $\varphi_A$ , defined as the fraction of active sites that are still active, as shown in equation (2.17).

$$\varphi_A = \frac{C_t - C_{K^*}}{C_t} \quad (2.17)$$

Here  $C_t$  is the total concentration of active sites, while  $C_{K^*}$  is the concentration of sites deactivated by coking. Catalyst activity is connected to the deactivation function by the relation shown in equation (2.18).

$$\frac{R_A}{R_A^0} = \varphi_A(t) \quad (2.18)$$

Here,  $R_A$  is reaction rate as defined by equation (2.15) and  $R_A^0$  is reaction rate at  $t = 0$ . By fitting experimental deactivation data from a differential reactor, an expression for  $\varphi_A(t)$  can be found and data corrected for activity loss may be determined by extrapolation[38].

## 2.6 Gas Chromatography

Gas chromatography (GC) is a separation technique used to quantitatively and qualitatively determine the compositions of gas mixtures. It separates components by partitioning between two phases. The mobile phase consists of the injected gas sample and an inert carrier gas, and the stationary phase is a solid or a liquid with high surface area packed in, or coated on the wall of a GC column. The different sample components equilibrate into the stationary phase by adsorption or absorption and separate based on their different affinities for the stationary bed. The components are consequently eluted from the column at different times, called elution times, and can be quantitatively measured by a concentration measurement method, commonly thermal conductivity detection (TCD)[40].

Micro GC is a high speed chromatography method designed for rapid analysis of gas mixtures. It commonly employs long capillary wall coated columns with high carrier gas flows to achieve fast and efficient separation[41].

A GC apparatus needs to be calibrated with relevant gases in order to function as a qualitative and quantitative analysis tool. This is done by analysing gas mixtures with known compositions and identifying component elution times and response factors for the concentration detection apparatus. One calibration method is the internal standard method described by Grob et al.[41]. In the internal standard method an inert gas, which needs to be present at all measurements in known amounts, serves as the internal standard. All other components are quantitatively determined relative

to the amount of the internal standard. When calibrating, each component is given a response factor as defined by equation (2.19).

$$RF_i = \frac{A_i}{Y_i} \quad (2.19)$$

Here  $A_i$  is the response, or integrated peak area of the elution peak identified to belong to component  $i$  and  $Y_i$  is the mole fraction of component  $i$ . A response factor is also produced for the internal standard ( $RF_{IS}$ ), and the relative response factor is defined by equation (2.20).

$$RRF_i = \frac{RF_i}{RF_{IS}} \quad (2.20)$$

When performing quantitative analysis, the mole fraction of component  $i$  is found by equation (2.21).

$$Y_i = \frac{A_i}{A_{IS}} \frac{Y_{IS}}{RRF_i} \quad (2.21)$$

Here  $Y_{IS}$  is the molar fraction of the internal standard determined using  $A_{IS}$  and  $RF_{IS}$ . Consequently, the total molar flow  $F_T$  of the system is found dividing  $F_{IS}$ , which is known, by  $Y_{IS}$  and the molar flow of component  $i$ ,  $F_i$ , by  $Y_i F_T$ .

# 3. Experimental

## 3.1 Catalyst Synthesis

To synthesize Pt/Carbon catalysts, a polyol process similar to the method described by Muthuswamy[34] was used.

First, a Pt colloid stock suspension was prepared by dissolving  $\text{H}_2\text{PtCl}_6 \cdot 6\text{H}_2\text{O}$  in ethylene glycol (EG). The solution was then added 1M NaOH in EG before being heated to 145 °C for 3 h under stirring and bubbling of Ar before cooling overnight.

The stock suspension was sonicated in an ultrasound bath for 5 min before having an amount adjusted to the target Pt-load extracted for catalyst synthesis. The extracted suspension was heated to 170 °C under stirring and bubbling of Ar, and cooled to room temperature. The carbon support material was weighed in and added to 96 %vol. ethanol and sonicated for 5 min before being mixed with the Pt suspension. The resulting mixture was sonicated for 5 min before being added 0.54M HCl and additional 96 %vol. ethanol. The final mixture was sonicated for 5 min before heated to 55 °C for 18 h under stirring and bubbling of Ar.

The resulting catalyst was separated from the solution by centrifugation and thoroughly washed with water (deionized) and acetone before being dried at 70 °C overnight.

Two different stock suspensions were prepared and used. Three different commercial carbons were used as supports: Carbon black (Vulcan XC-72R, hereafter referred to as Vulcan), CNF (Conical platelets, Sigma-Aldrich) and Graphite (Sigma-Aldrich). The target metal loads for the produced catalysts were 2 %wt. and 0.5 %wt.

To investigate the stock suspension's stability over time, another 0.5% Pt/Vulcan catalyst, hereafter referred to as the 0.5% Pt/VulcanB catalyst, was prepared two months after the first, using an identical synthesis procedure.

To investigate the acid concentration's effect in the synthesis procedure. Three more vulcan supported catalysts, hereafter referred to as the 0.5% Pt/VulcanC, D and E respectively, were prepared with 1 day apart. The first used an identical synthesis procedure as the first 0.5% Pt/Vulcan catalyst. The second increased the HCl addition by a factor of 1.5, and the third by a factor of 2.

## 3.2 Catalyst Characterization

### 3.2.1 The Brunauer-Emmett-Teller Method

The BET method with nitrogen adsorption was performed using a Micromeritics Tristar II instrument with the purpose of determining the specific surface areas.



The samples were weighed in a quartz sample tube and installed in a degassing apparatus. There the sample tubes were evacuated under heating to 200 °C over night. The sample tubes were then cooled to room temperature and transferred to the BET instrument. Pretreatment consisted of evacuation at room temperature and leak tests. The analysis was performed with the sample tubes submerged in liquid nitrogen at  $-195.85$  °C.

Analysis was performed on the 2% Pt/Vulcan, 0.5% Pt/Vulcan, 0.5% Pt/CNF and 0.5% Pt/Graphite catalysts as well as the untreated vulcan, CNF and graphite supports. Two parallel analyses were performed for each sample.

### 3.2.2 Thermogravimetric Analysis

Thermogravimetric analysis (TGA) was performed using a Netzsch STA 449 C instrument with the purpose of determining the catalysts' Pt content.

The sample was weighed in a crucible and installed in the instrument. The temperature program was defined as follows: Temperature increase from room temperature to 900 °C at a ramp rate of 10 °C/min. Steady temperature at 900 °C for 1 h. Measurement stop and cooling back to room temperature. The atmosphere chosen was air (20/80 v/v O<sub>2</sub>/N<sub>2</sub>, 20 mL/min) and Ar (10 mL/min) as a protective gas throughout the analysis.

Analysis was performed on the 2% Pt/Vulcan and the 0.5% Pt/Vulcan catalysts as well as the untreated vulcan support to serve as correction. Multiple parallel analyses were performed.

### 3.2.3 Hydrogen Chemisorption - Volumetric Method

Volumetric hydrogen chemisorption measurements were performed using a Micromeritics ASAP 2020 instrument with the purpose of determining the catalysts' dispersion.

The catalyst sample was weighed and placed in a 9 mm inner diameter fixed bed u-tube quartz reactor together with quartz wool. Pretreatment consisted of flushing the system reactor in He flow followed by evacuation for 2 h at room temperature, repeating the procedure at 120 °C for 30 min, heating to 500 °C under hydrogen flow for reduction and repeat flushing and evacuation at 120 °C for another 30 min with intermittent leak testing of the apparatus.

The analysis was performed at 35 °C with an equilibration interval of 20 s to produce the first isotherm. The reactor was subsequently evacuated and the chemisorption analysis was repeated to produce the second isotherm.

Analysis was performed on the 2% Pt/Vulcan, 0.5% Pt/Vulcan and 0.5% Pt/CNF catalysts. Multiple parallel analyses were performed.

### 3.2.4 Hydrogen Chemisorption - Pulse Method

Hydrogen pulse chemisorption was performed on the 0.5% Pt/Vulcan catalyst using an Altamira Instruments BenchCAT 1000 HP Hybrid apparatus with the purpose of determining the catalyst's dispersion.

The catalyst sample was weighed and placed in a 4 mm inner diameter fixed-bed u-tube quartz reactor together with quartz wool. Pretreatment consisted of flushing the system in Ar flow at 175 °C for 1 h, reduction in 10/90 v/v H<sub>2</sub>/Ar flow at 450 °C for 2 h and cooling in Ar flow to the analysis temperature.

Analyses were conducted using two different pulse loops at 500 and 50  $\mu$ L. The pulse interval was varied between 80 and 200 s and the adsorption temperature was set at 35, 0, -72 and -46 °C. The three latter temperatures were achieved by keeping the reactor in an ice bath, a dry ice/ethanol bath and a dry ice in 30/70 v/v ethanol/ethylene glycol slurry bath respectively.

### 3.2.5 CO Stripping Voltammetry

CO stripping voltammetric measurements were performed using a Princeton Applied Research potentiostat, type Versastat MC. The electrochemical cell was a conventional three-electrode system with a reversible hydrogen electrode (RHE) as the reference electrode and a Pt wire as the counter electrode in 0.5M H<sub>2</sub>SO<sub>4</sub>(aq) electrolyte. The working electrode was prepared by depositing a catalyst ink on a disc type glassy carbon electrode, as described by Muthuswamy[34]. The electrode was then dried under N<sub>2</sub> flow. Then the deposition was repeated, dried again, then coated in a 0.05 %wt. Nafion in water solution before being dried a third time. The catalyst ink was prepared by dispersing the catalyst sample in deionized water and sonicating for 1 h. The RHE was prepared by first filling the electrode with electrolyte, then imposing a -3.5 V potential between the RHE and the Pt-wire for approximately 30 s, causing hydrogen evolution at the RHE, partially filling the electrode.

First, the electrolyte was purged under bubbling of N<sub>2</sub> for 30 min. Then, the working electrode was conditioned by cyclic voltammetry between 0.05 and 1.2 V, first at a potential ramp rate of 100 mV/s for 50 cycles, then at 10 mV/s for 10 cycles. Saturation of CO was performed by bubbling the electrolyte with CO for 2 min while keeping a potential of 50 mV on the working electrode. Excess CO was removed by purging the electrolyte under bubbling of N<sub>2</sub> for 30 min, maintaining the working electrode potential. Cyclic voltammetry was then performed between 0.05 and 1.2 V, at a potential ramp rate of 10 mV/s for 3 cycles to strip the adsorbed CO. All procedures were performed at room temperature.

Analyses were conducted on the 2% Pt/Vulcan, 0.5% Pt/Vulcan and 0.5% Pt/Graphite catalysts. Attempt was also made to analyze the 0.5% Pt/CNF catalyst.

## 3.3 Catalyst Activity Measurements

### 3.3.1 Experimental Setup

The catalyst activity measurements were performed using a testing apparatus with a flow chart as shown in Fig. 3.1 with a figure description provided below.

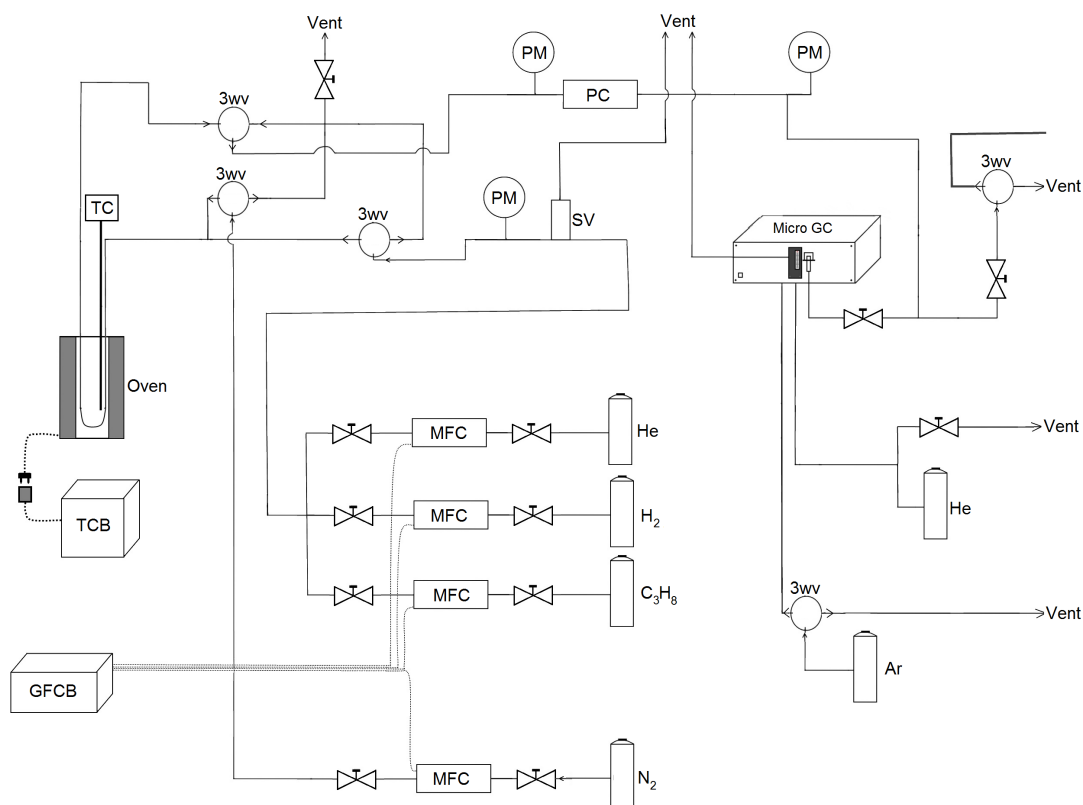


Figure 3.1: Flow Chart of the catalyst testing apparatus. GC: Gas chromatograph, GFCB: Gas flow controller box, MFC: Mass flow controller, TC : Thermocouple, TCB : Temperature controller box, PC: Pressure controller, PM: Pressure meter, SV: Safety valve, 3wv: Three way valve.

The feed gases are fed from bottles or from a central gas distribution system through mass flow controllers to maintain control of the feed gas composition. Three three-way-valves are in place to direct the feed gases to the reactor or to bypass it. The reactor is a 4 mm inner diameter fixed-bed u-tube quartz reactor seated in an oven and fitted with a thermocouple. The reactor temperature is controlled by the temperature controller connected to the thermocouple and the oven. A pressure controller connected to a safety valve is in place to vent the feed gas should the pressure exceed safety limits. The effluent gases are analyzed with micro gas chromatography using an Agilent 3000A Micro GC instrument fitted with four columns described in Table 3.1. The gas passing through the micro GC is subsequently vented.

Prior to experimental testing, the micro GC instrument was calibrated using the

internal standard method with nitrogen as the internal standard. For calibration results, see Appendix H.

*Table 3.1: Micro GC Apparatus Description*

Column	Column Type	Detector	Carrier Gas
A	Molecular Sieve	TCD	He
B	PLOT U	TCD	Ar
C	Alumina	TCD	Ar
D	OV-1	TCD	Ar

### 3.3.2 Optimization of Testing Parameters

Various test were conducted in order to optimize the testing parameters for the catalyst activity measurements. In order to obtain differential reactor conditions, a manageable pressure drop across the catalyst bed and reproducible results, tests were conducted at various temperatures, flow rates, catalyst Pt loads and with and without catalyst dilution. Testing was performed using the 2 % Pt/Vulcan as well as the 0.5 % Pt/Vulcan catalyst.

Approximately 50 mg of catalyst was loaded into the reactor together with the inert dilutant and quartz wool to keep the catalyst bed in place. The catalyst was pretreated in 50 mL/min 20/80 v/v H<sub>2</sub>/He flow under heating to 500 °C with a constant ramp rate of 10 °C/min. The pretreatment served as in situ reduction to negate any possible oxidation. The gas flow then was sent to bypass the reactor, changed to the flow conditions described in Table 3.2 and analyzed by micro GC. The feed gas was then sent back to the reactor and the effluent gas composition was analysed by micro GC at approximately 4 min intervals for 45 min, then following at approximately 19 min intervals. The catalyst activity was monitored for a total time on stream of approximately 4 to 20 h depending on the experiment's requirements.

*Table 3.2: Catalyst Testing Optimization Parameters*

Constant Parameters	
Composition	10/40/50 v/v/v H <sub>2</sub> /C <sub>3</sub> H <sub>8</sub> /N <sub>2</sub>
Outlet Pressure	1 bar
Varied Parameters	
Catalyst Dilution	0 and 20/80 w/w Cat/SiC
Temperature	475, 500, 525 °C
Catalyst metal load	2 and 0.5 %wt.
Flow Rate	50, 75, 100 mL/min

In order to determine if differential reactor conditions were achieved, the equilibrium conversion of reaction (2.1) was determined by simulation using UniSim Design. The equilibrium conversions shown in Appendix I served as comparison to the determined conversion levels.

The flow rate variation experiments were conducted by starting at a total flow rate of 50 mL/min and increasing at regular intervals before adjusting back to 50 mL/min. The transition was made using 2 methods. The first method directly adjusted the feed flow with the reactor on stream. The second method first flushed the reactor in 100 mL/min 35/65 v/v H<sub>2</sub>/N<sub>2</sub> flow for 1 h, then the reactor was taken off stream and the feed gas was adjusted and analyzed before the reactor was taken back on stream.

### 3.3.3 Kinetic Study

A kinetic study was conducted using the 0.5% Pt/Vulcan catalyst. The purpose was to determine the reaction orders  $a$  and  $b$  in the power law kinetic expression (2.4). The catalyst was diluted, loaded and pretreated as described earlier in chapter 3.3.2, and left on stream for 3 h in 50 mL/min 10/40/50 v/v/v H<sub>2</sub>/C<sub>3</sub>H<sub>8</sub>/N<sub>2</sub> flow at 500 °C to pass the initial period of rapid deactivation. Then, the feed composition was changed at 30-45 min intervals after stability was reached in accordance with Table 3.3. When investigating the propane order, the propane flow was varied under constant hydrogen flow while the nitrogen flow was adjusted to maintain a constant total flow of 50 mL/min. When investigating the hydrogen order, the hydrogen flow was varied. The transition between different feed gas compositions was handled using the same two methods performed when changing the flow rate described under chapter 3.3.2.

*Table 3.3: Kinetic Study Testing Conditions*

<b>Propane Order</b>	
H <sub>2</sub> Concentration	10 % vol
C <sub>3</sub> H <sub>8</sub> Concentrations	40, 30, 20, 50, 60 % vol
<b>Hydrogen Order</b>	
C <sub>3</sub> H <sub>8</sub> Concentration	40 % vol
H <sub>2</sub> Concentrations	10, 7, 14, 20 % vol

### 3.3.4 Blank Tests

Before comparing the various carbon supported catalysts, the untreated supports were tested to check for catalytic activity. This was performed by loading, diluting, and pretreating the supports in the same manner as described with the catalysts in chapter 3.3.2. The activity measurements conditions were chosen as described in Table 3.4, and the activity was monitored until no activity was detected. The tested supports were vulcan, CNF and graphite.

### 3.3.5 Catalyst Support Comparison

Activity measurements were performed on the catalysts prepared using different carbon supports. Based on the results from the optimization experiments, operation conditions were chosen as described by Table 3.4. Approximately 50 mg of catalyst was loaded into the reactor along with the inert dilutant and quartz wool. Using

different catalysts, pretreatment and activity measurements were performed as described in chapter 3.3.2. The catalysts' activities were monitored for a total of 6 h time on stream and two parallel tests were conducted for each catalyst.

*Table 3.4: Activity Measurement Operation Conditions*

<b>Catalyst Properties</b>	
Supports	Vulcan, CNF, Graphite
Metal load	0.5%wt.
<b>Operation Conditions</b>	
Bed dilution	20/80 w/w Cat/SiC
Temperature	500 °C
Gas flow	50 mL/min
Outlet pressure	1 bar
<b>Feed Gas Composition</b>	
H <sub>2</sub>	10 %vol
C <sub>3</sub> H <sub>8</sub>	40 %vol
N <sub>2</sub>	50 %vol

### 3.3.6 Vulcan Supported Catalysts Comparison

In order to investigate the stability over time for the Pt-colloid stock suspension, the activity of the 0.5% Pt/VulcanB catalyst was investigated and compared to that of the 0.5% Pt/Vulcan catalyst. The catalyst was loaded, diluted and pretreated as described in chapter 3.3.2. Operation conditions were chosen as described by Table 3.4. Total time on stream was 6 h, and 2 parallel tests were conducted.

In order to investigate the acid concentration's effect on the catalyst synthesis procedure, the activity of the 0.5% Pt/VulcanC, 0.5% Pt/VulcanD and 0.5% Pt/VulcanE catalysts were investigated and compared to each other. The catalysts were loaded, diluted and pretreated as described in chapter 3.3.2. Operation conditions were chosen as described by Table 3.4. Total time on stream was 6 h.

# 4. Results

## 4.1 Catalyst Synthesis

The catalyst synthesis procedure that was followed successfully produced Pt/Carbon catalysts that proved active for propane dehydrogenation. When varying the target metal load and the type of support, the procedure required slight altering. A total of 8 catalysts were successfully synthesized, as shown in Table 4.1. For details about the synthesis of the various catalysts, see Appendix B.

Table 4.1: Prepared Pt/Carbon catalysts

No.	Support	$x_m$ [%wt.]	Suspension	Notes on preparation
1	Vulcan	2	1	-
2	Vulcan	0.5	2	With dilution of stock suspension
3	Graphite	0.5	2	As no. 2
4	CNF	0.5	2	1.5xliquids, aged stock suspension
5	Vulcan	0.5	2	as no.2, aged stock suspension
6	Vulcan	0.5	2	as no.5
7	Vulcan	0.5	2	as no.6, with 1.5x HCl addition
8	Vulcan	0.5	2	as no.6, with 2x HCl addition

When going from 2 to 0.5 % load, the amount of stock suspension used was approximately quartered and had to be diluted in order to not dry out during the 170 °C heating period. Dilution was done with EG and 1M NaOH in EG at the same volume ratio as used when preparing the stock suspension.

To accommodate for the low density and consequently high volume of the CNFs used, the amount of liquids used had to be increased in order to ensure complete wetting of the solids for the entirety of the 18 h heating period. This was done by increasing the aforementioned dilution, as well as increasing the amount of ethanol and 0.54M HCl added.

## 4.2 Catalyst Characterization

### 4.2.1 BET Results

The BET experiments produced adsorption-desorption isotherms shown in Appendix C along with experimental details. Using adsorption values at  $P/P_0$  ratios between 0.05

and 0.35, BET isotherms were produced. The BET isotherms for the vulcan samples are shown in Fig. 4.1, the CNF samples are shown in Fig. 4.2, and the graphite samples are shown in Fig. 4.3.

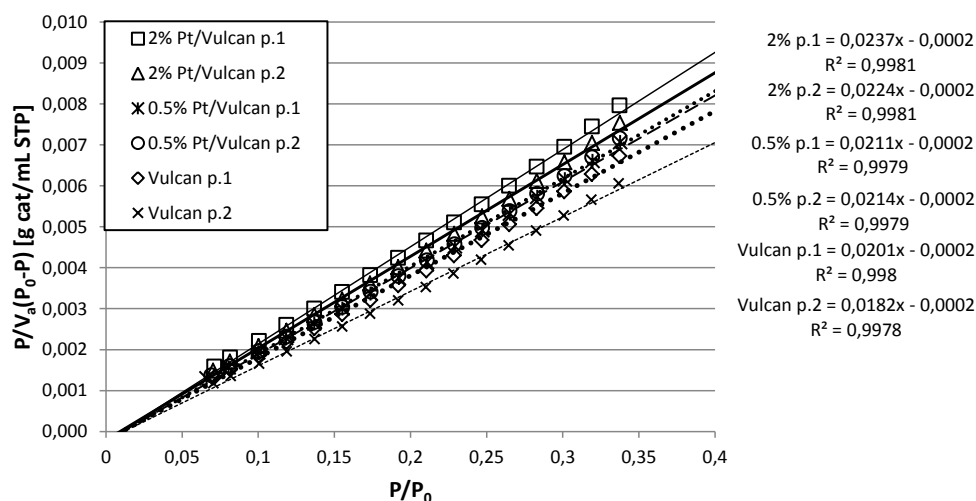


Figure 4.1: BET isotherms for the vulcan supported samples. Linear regression lines and formulas are added.

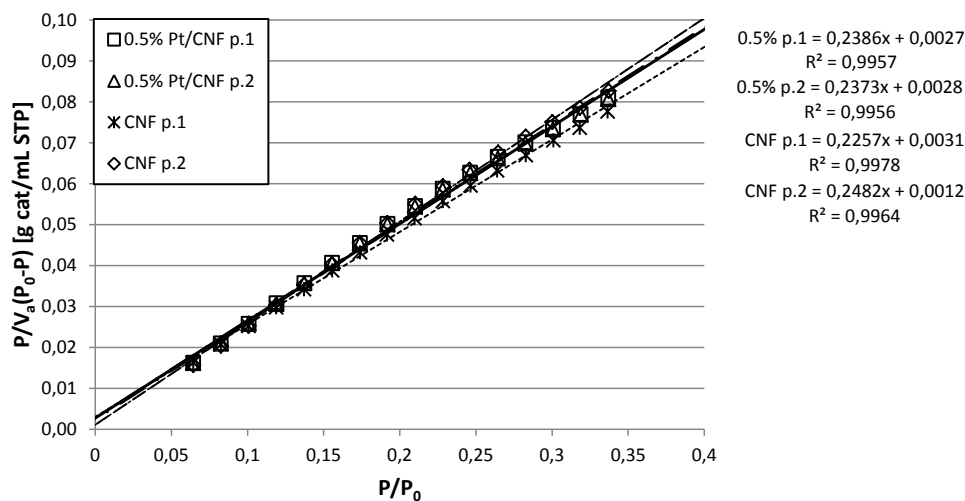


Figure 4.2: BET isotherms for the CNF supported samples. Linear regression lines and formulas are added.



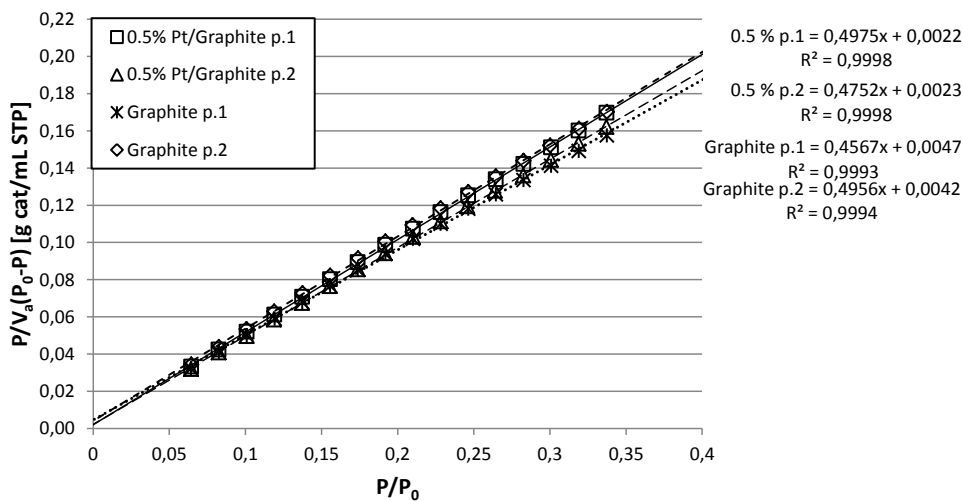


Figure 4.3: BET isotherms for the graphite supported samples. Linear regression lines and formulas are added.

From the regression formulas shown in Figs. 4.1 to 4.3, BET surface areas are calculated and shown in Table 4.2.

Table 4.2: BET Surface Area Measurement Results

Sample	$S_{BET}$ [m <sup>2</sup> /g]	
	Parallel 1	Parallel 2
2% Pt/Vulcan	185	196
0.5% Pt/Vulcan	209	206
Vulcan	219	242
0.5% Pt/CNF	18	18
CNF	19	22
0.5% Pt/Graphite	9	9
Graphite	9	9

#### 4.2.2 Thermogravimetric Analysis

Due to the lack of accuracy and poor reproducibility displayed by the TG analyses, it was chosen not to report the Pt content determined by TGA. Thermograms are shown in Appendix D. All dispersion determinations are made assuming a Pt content equal to its nominal value.

#### 4.2.3 Hydrogen Chemisorption - Volumetric Method

Due to the overall poor quality and poor reproducibility of the results gained with the volumetric chemisorption method, it was chosen not to report any dispersions determined using this method. Detailed results and adsorption isotherms are shown in Appendix E.1.

#### 4.2.4 Hydrogen Chemisorption - Pulse Method

Due to the failure to achieve optimal measurement conditions for the pulse chemisorption experiments, it was chosen not to report any dispersions determined using this method. Throughout most of the experiments, the desorption rate was found too high to produce viable results. At the  $-72^{\circ}\text{C}$  experiment, it was found that the adsorption rate was too low. Pulse data for the  $0$ ,  $-72$  and  $-46^{\circ}\text{C}$  experiments is shown in Figs. 4.4 to 4.6. Data for the rest of the experiments is shown in Appendix E.2.

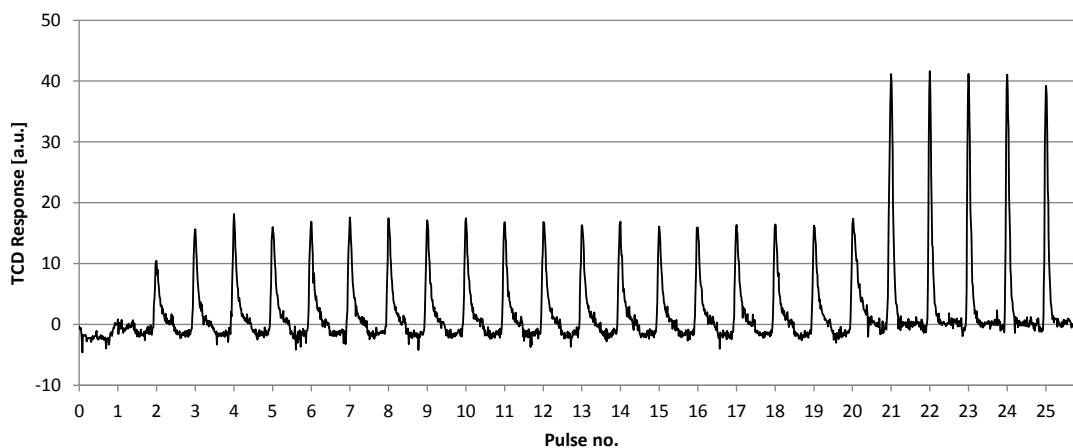


Figure 4.4: Pulse data showing TCD response versus pulse number for hydrogen chemisorption on the 0.5% Pt/Vulcan catalyst at  $0^{\circ}\text{C}$ . 20 adsorption pulses (left) and 5 calibration pulses (right) are shown. Pulse loop size =  $50\ \mu\text{L}$ , Time between pulses = 80 s.

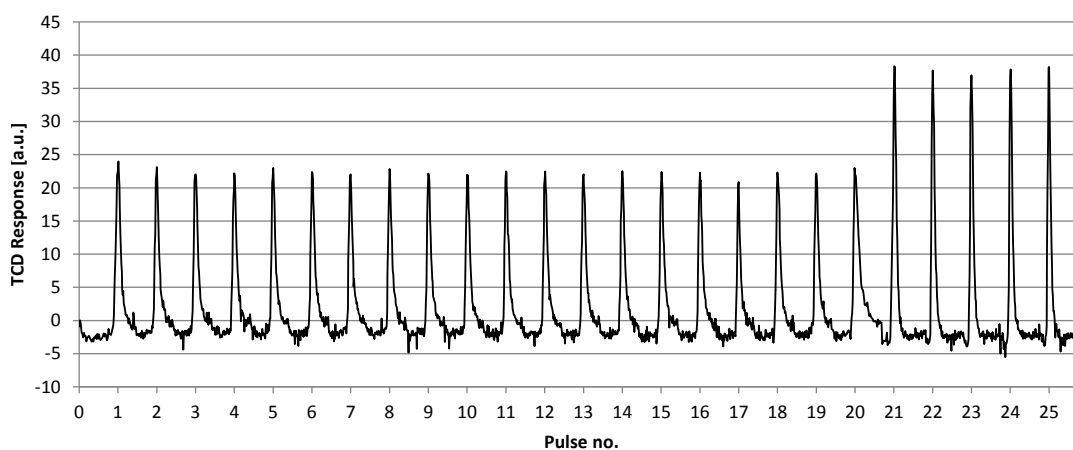


Figure 4.5: Pulse data showing TCD response versus pulse number for hydrogen chemisorption on the 0.5% Pt/Vulcan catalyst at  $-72^{\circ}\text{C}$ . 20 adsorption pulses (left) and 5 calibration pulses (right) are shown. Pulse loop size =  $50\ \mu\text{L}$ , Time between pulses = 80 s.

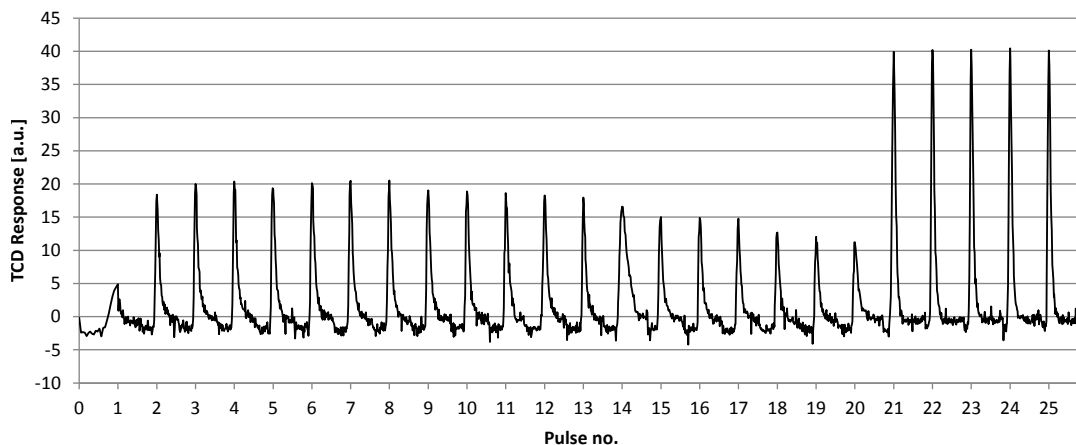


Figure 4.6: Pulse data showing TCD response versus pulse number for hydrogen chemisorption on the 0.5% Pt/Vulcan catalyst at  $-46$  to  $-41^{\circ}\text{C}$ . 20 adsorption pulses (left) and 5 calibration pulses (right) are shown. Pulse loop size =  $50\ \mu\text{L}$ , Time between pulses = 80 s.

#### 4.2.5 CO Stripping Voltammetry

CO stripping voltammograms are shown in Figs. 4.7 to 4.9. Two voltammetric cycles are shown, the first producing the stripping peak at approximately 800 mV, the second producing the baseline.

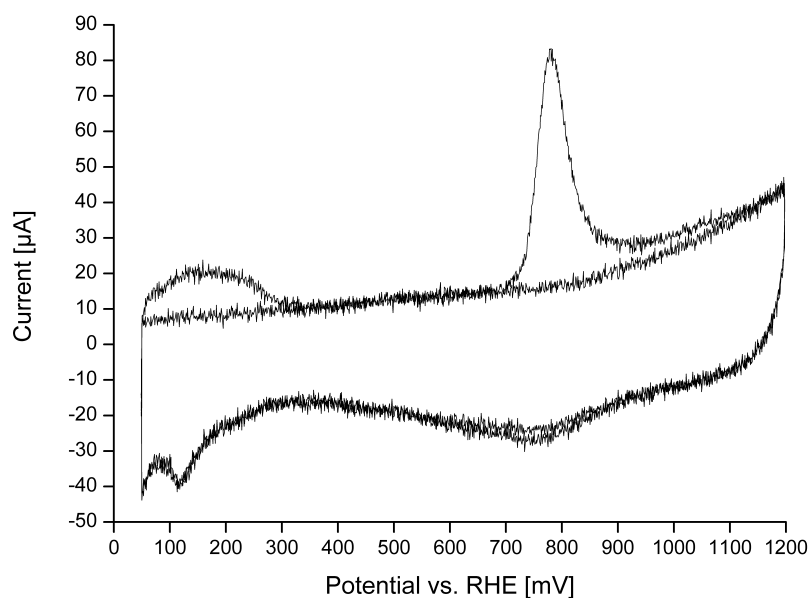


Figure 4.7: CO stripping voltammogram showing CV of the 2% Pt/Vulcan catalyst. Two cycles are shown. Conditions:  $v=10\ \text{mV/s}$ , adsorption at 50 mV, 0.5 M  $\text{H}_2\text{SO}_4$  electrolyte.

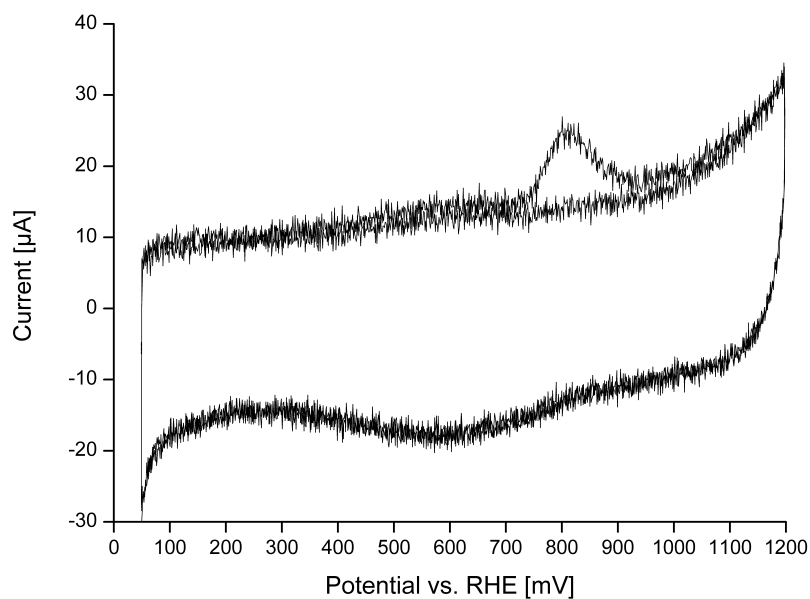


Figure 4.8: CO stripping voltammogram showing CV of the 0.5% Pt/Vulcan catalyst. Two cycles are shown. Conditions:  $v=10$  mV/s, adsorption at 50 mV, 0.5 M  $H_2SO_4$  electrolyte.

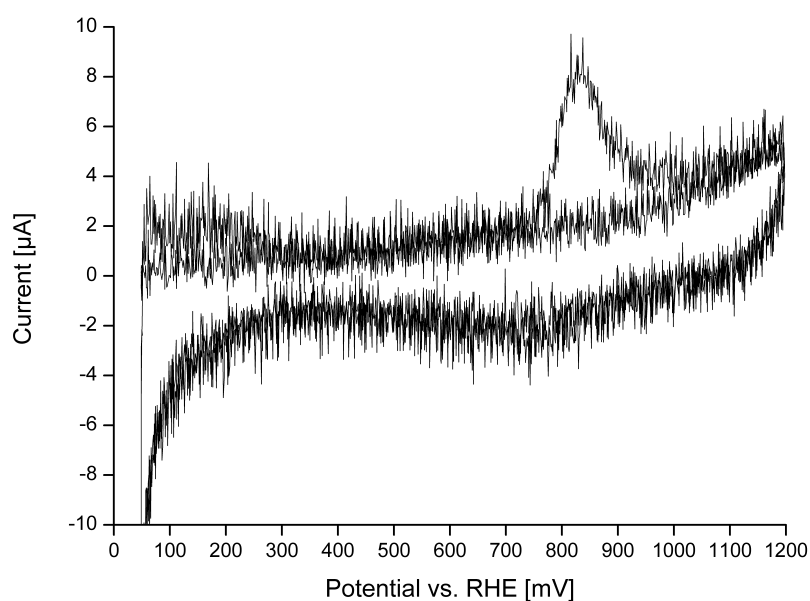


Figure 4.9: CO stripping voltammogram showing CV of the 0.5% Pt/Graphite catalyst. Two cycles are shown. Conditions:  $v=10$  mV/s, adsorption at 50 mV, 0.5 M  $H_2SO_4$  electrolyte.

By subtracting the second cycle baseline from the first cycle peaks at approximately 800 mV and integrating, dispersions are determined and shown in Table 4.3. Details and calculated values are shown in Appendix F.

Table 4.3: CO Stripping Voltammetry Determined Dispersions

Catalyst	$D$ [%]
2% Pt/Vulcan	49
0.5% Pt/Vulcan	40
0.5% Pt/Graphite	28

## 4.3 Catalyst Activity Measurements

### 4.3.1 Optimization

The results of the catalyst optimization tests are shown in Figs. 4.10 to 4.13. For experimental details, see Appendix G.1. Without catalyst dilution, the pressure drop across the catalyst bed was found too high to produce usable results. One test was successfully performed on the 2% Pt/Vulcan catalyst with results shown in Fig. 4.10a. Here the pressure drop was reported at 1.8 bar. Another trial resulted in a pressure drop of  $>2$  bar exceeding the safety limits of the testing apparatus.

With catalyst dilution, the pressure drop was found to decrease to between 0.2 and 0.7 bar between parallel runs. Three parallel tests were successfully performed on the 2% Pt/Vulcan catalyst, with results shown in Fig. 4.10b.

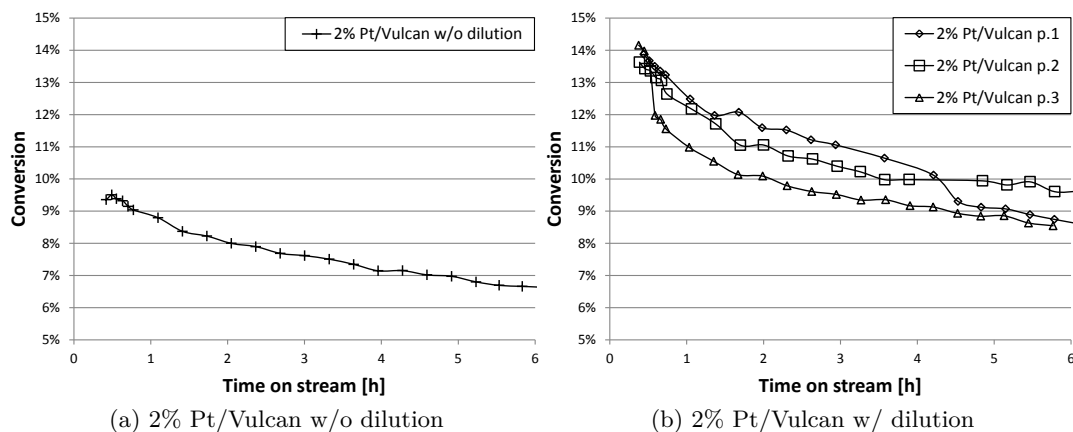


Figure 4.10: Time dependent conversion levels for the 2% Pt/Vulcan catalyst measured without (a) and with (b) catalyst dilution. Test conditions:  $T = 500^{\circ}\text{C}$ , Outlet pressure = 1 bar, Flow rate = 50 mL/min, Feed composition: 10/40/50 v/v/v  $\text{H}_2/\text{C}_3\text{H}_8/\text{N}_2$ .

For the temperature variation experiments, tests were performed on the 2% Pt/Vulcan catalyst at 475 and at 525  $^{\circ}\text{C}$ . The results are presented in Fig. 4.11 along with the 2<sup>nd</sup> parallel from Fig. 4.10b tested at 500  $^{\circ}\text{C}$ .

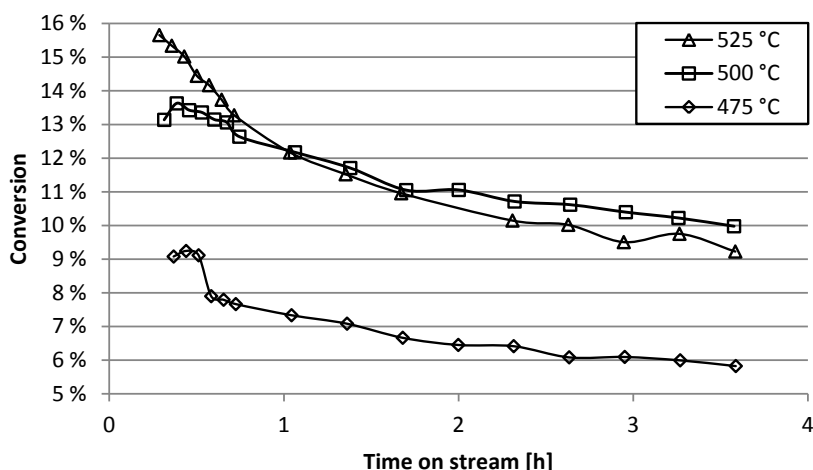


Figure 4.11: Time dependent conversion for the 2% Pt/Vulcan catalyst tested at 475, 500 and 525 °C. Test conditions: Outlet pressure = 1 bar, Flow rate = 50 mL/min, Feed composition: 10/40/50 v/v/v H<sub>2</sub>/C<sub>3</sub>H<sub>8</sub>/N<sub>2</sub>.

To determine the catalyst metal load's effect on the catalytic activity, tests were performed on the 0.5% Pt/Vulcan catalyst. The results from two parallel tests are presented in Fig. 4.12a with a comparison with the 2% Pt/Vulcan catalyst shown in Fig. 4.12b.

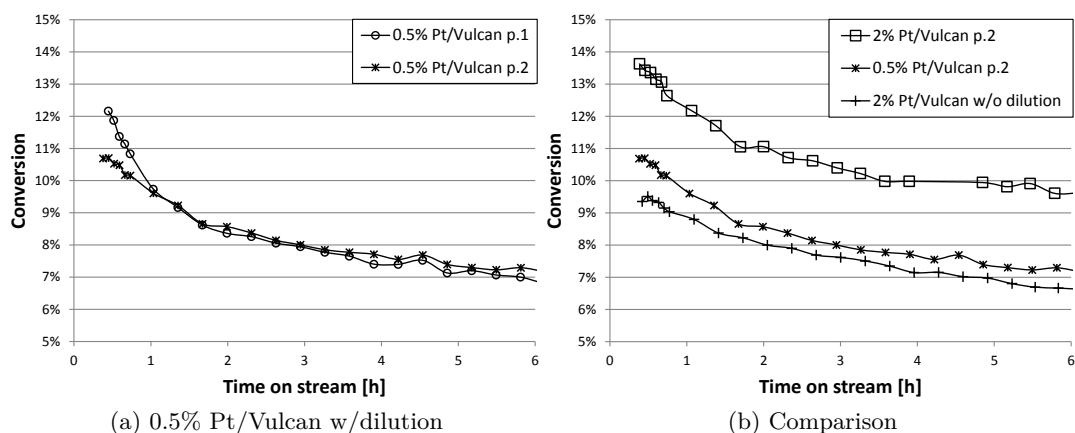


Figure 4.12: Time dependent conversion levels for the 0.5% Pt/Vulcan catalyst (a) and comparison between the 2% and 0.5% Pt/Vulcan catalysts (b). Test conditions: T = 500 °C, Outlet pressure = 1 bar, Flow rate = 50 mL/min, Feed composition: 10/40/50 v/v/v H<sub>2</sub>/C<sub>3</sub>H<sub>8</sub>/N<sub>2</sub>.

In the flow rate varying experiments, two parallel runs were successfully completed, each using one of the transition methods described in chapter 3.3.2. The first parallel changed the feed flow with the reactor on stream, and changed the flow at 2 h intervals. The second parallel employed the intermediate flushing and feed analysis technique and changed the flow at 1 h intervals. Results for the former are shown in Figs. 4.13a and 4.13b. Results for the latter are shown in Figs. 4.13c and 4.13d.

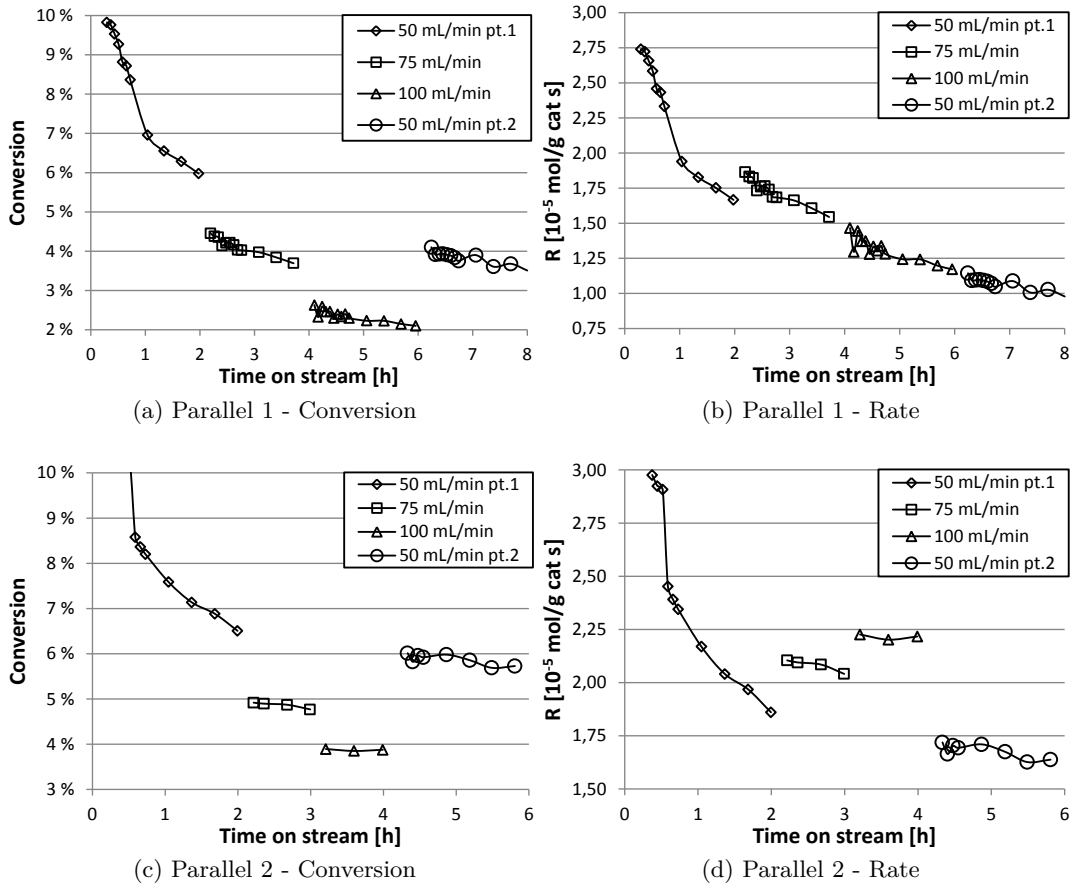


Figure 4.13: Time dependent conversion levels and rates of propane consumption under varying flow rate for the 0.5% Pt/Vulcan catalyst. Two parallels are shown. Test conditions:  $T = 500^{\circ}\text{C}$ , Outlet pressure = 1 bar, Feed composition: 10/40/50 v/v/v  $\text{H}_2/\text{C}_3\text{H}_8/\text{N}_2$ .

### 4.3.2 Deactivation Model

The results from the 0.5% Pt/Vulcan catalyst activity measurements are shown in Fig. 4.14 as rates of propane consumption. Geometric regression curves are added to serve as mathematical models for predicting, and correcting for catalyst deactivation.

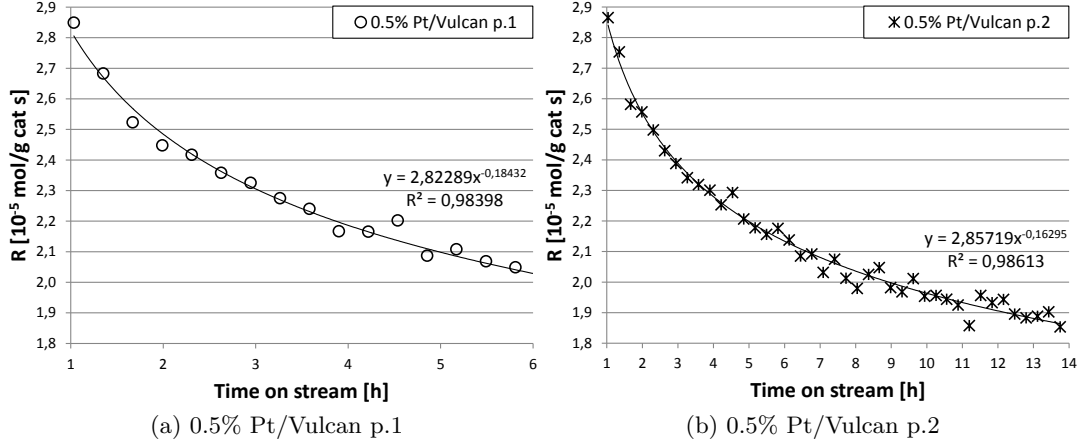


Figure 4.14: Time dependent rate of propane consumption for the 0.5% Pt/Vulcan catalyst. Two parallels are shown, each with a geometric regression line. Test conditions:  $T = 500^{\circ}\text{C}$ , Outlet pressure = 1 bar, Flow rate = 50 mL/min, Feed composition: 10/40/50 v/v/v  $\text{H}_2/\text{C}_3\text{H}_8/\text{N}_2$

From the regression formulas shown in Fig. 4.14,  $R_A(t) = 2.82t^{-0.18}$  from parallel 1 and  $R_A(t) = 2.86t^{-0.16}$  from parallel 2. By setting  $t_0 = 1$  h, and  $R_A^0 = R(t_0)$ , the deactivation models shown in equation (4.1) and (4.2) are derived.

$$\varphi_{A,1}(t) = \frac{R_A}{R_A^0} = t^{-0.18} \quad t \in [1, 6] \quad (4.1)$$

$$\varphi_{A,2}(t) = \frac{R_A}{R_A^0} = t^{-0.16} \quad t \in [1, 14] \quad (4.2)$$

### 4.3.3 Kinetic Study

For the kinetic study, two experiments were successfully completed, one investigating the  $\text{C}_3\text{H}_8$  order and one the  $\text{H}_2$  order. Both experiments employed the on-stream feed change technique described in chapter 3.3.2.

The results were derived by monitoring the conversion over time. Between each change in feed composition, the conversion was monitored until 3 stable measurements had been made. These measurements were subsequently converted to reaction rates using equation (2.15), corrected for deactivation using equation (4.2) and averaged. The measurement with the lowest flow rate of the monitored reactant was then defined as the reference flow rate,  $F_{Ref}$ , and its respective reaction rate  $R_{Ref}$ . The other measurements were then converted to relative reaction rates,  $R/R_{Ref}$ , and relative flow rates,  $F/F_{Ref}$ , assumed equal to relative partial pressures  $p/p_{Ref}$  of the monitored reactants. Log-log plots of  $R/R_{Ref}$  versus  $p/p_{Ref}$  were then produced and presented in Fig. 4.15. For experimental details see Appendix G.3.



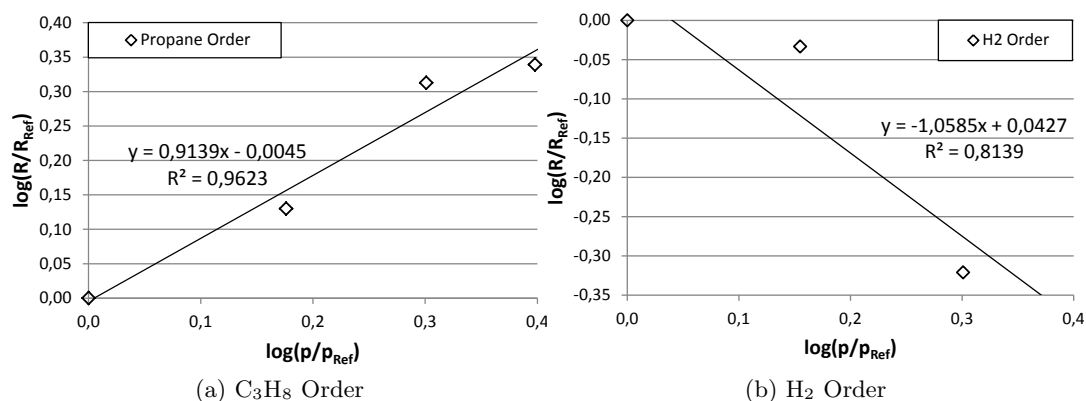


Figure 4.15: Log-log plots of relative reaction rates versus relative partial pressure of C<sub>3</sub>H<sub>8</sub> and H<sub>2</sub> for the 0.5% Pt/Vulcan catalyst. Linear regression lines and formulas are added. Test conditions:  $T = 500^{\circ}\text{C}$ , Outlet pressure = 1 bar, Flow rate = 50 mL/min.

From the regression formulas shown in Fig. 4.15 the following reaction orders are determined:

$$a = 0.9$$

$$b = - 1.1$$

#### 4.3.4 Blank Tests

When testing the supports, some dehydrogenation activity were detected, but not enough to calculate conversion levels with reportable accuracy. Some selected chromatograms from the GC analyses are shown in Appendix G.4. They show that vulcan is the most active support, with a detectable propylene peak at up to approximately 50 min time on stream. The CNF is the second most active, with a detectable propylene peak at up to approximately 25 min time on stream. The graphite is the least active, with no detectable propylene peak across all measurements. No side products were detected at any time during the tests.

#### 4.3.5 Catalyst Support Comparison

The results for the catalyst support comparison are shown in Figs. 4.16 to 4.17. The conversion levels and reaction rates displayed by the catalysts are shown in Fig. 4.16.

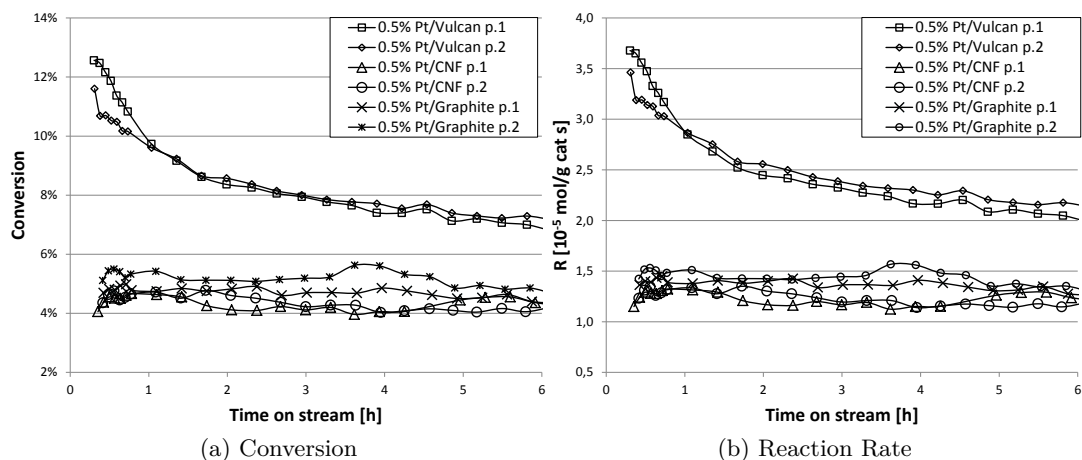


Figure 4.16: Plots comparing the conversion levels (a) and reaction rates (b) of the 0.5% Pt/Vulcan, CNF and graphite catalysts. Two parallels are shown for each catalyst. Test conditions:  $T = 500^{\circ}\text{C}$ , Outlet pressure = 1 bar, Flow rate = 50 mL/min. Feed composition: 10/40/50 v/v/v  $\text{H}_2/\text{C}_3\text{H}_8/\text{N}_2$

Using the results from Fig. 4.16, and the dispersions from Table 4.3, turnover frequencies were determined and presented in Fig. 4.17.

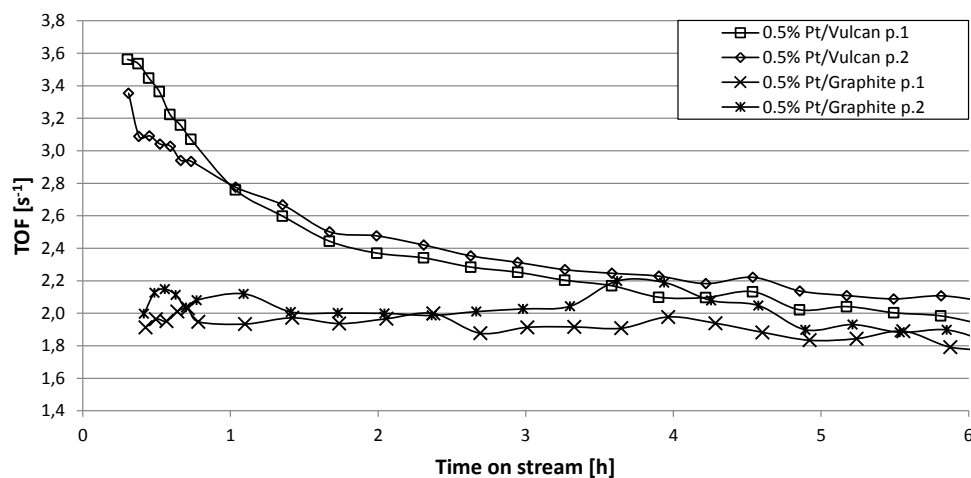


Figure 4.17: Plots comparing the turnover frequencies of the 0.5% Pt/Vulcan, and graphite catalysts. Two parallels are shown for each catalyst. Test conditions:  $T = 500^{\circ}\text{C}$ , Outlet pressure = 1 bar, Flow rate = 50 mL/min. Feed composition: 10/40/50 v/v/v  $\text{H}_2/\text{C}_3\text{H}_8/\text{N}_2$

#### 4.3.6 Vulcan Supported Catalysts Comparison

The results for the investigation of the Pt-colloid stock suspension's stability are presented in Fig. 4.18, showing an activity comparison between the 0.5% Pt/Vulcan, and the 0.5% Pt/VulcanB catalysts.

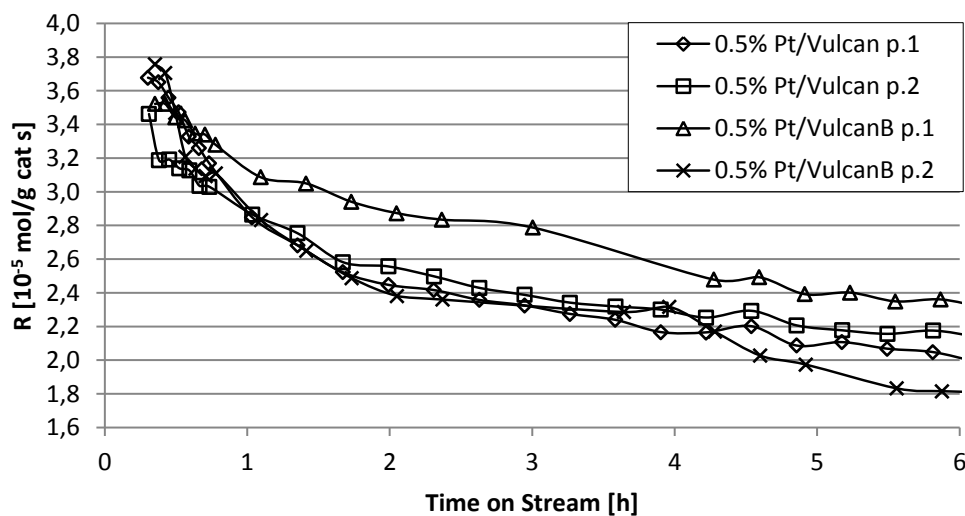


Figure 4.18: Plot comparing the reaction rates displayed by the 0.5% Pt/Vulcan and 0.5% Pt/VulcanB catalysts prepared 2 months apart. Two parallels are shown for each catalyst. Test conditions:  $T = 500^{\circ}\text{C}$ , Outlet pressure = 1 bar, Flow rate = 50 mL/min. Feed composition: 10/40/50 v/v/v  $\text{H}_2/\text{C}_3\text{H}_8/\text{N}_2$

The results for the investigation of the acid concentrations effect on the synthesis procedure are presented in Fig. 4.19, showing an activity comparison between the 0.5% Pt/VulcanC, the 0.5% Pt/VulcanD and the 0.5% Pt/VulcanE catalysts.

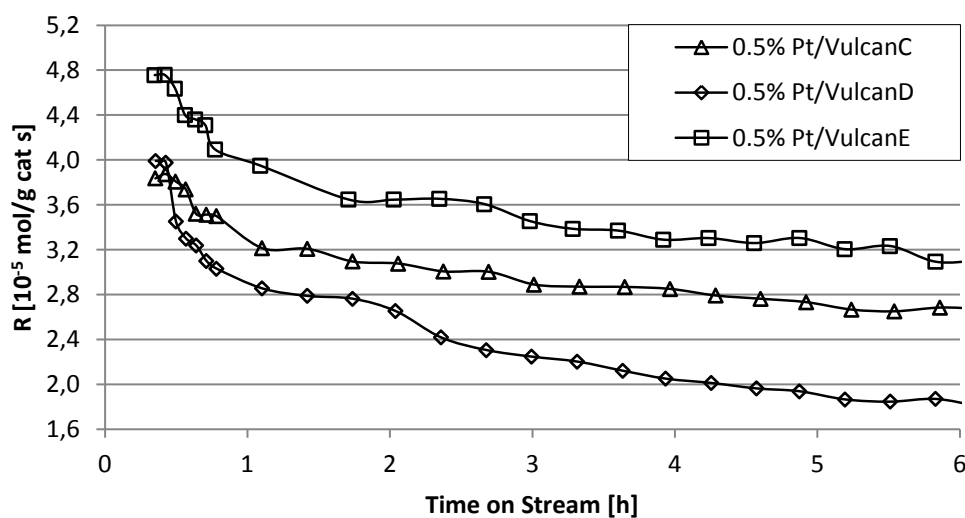


Figure 4.19: Plot comparing the reaction rates displayed by the 0.5% Pt/VulcanC, 0.5% Pt/VulcanD and 0.5% Pt/VulcanE catalysts prepared with different amount of HCl added. Test conditions:  $T = 500^{\circ}\text{C}$ , Outlet pressure = 1 bar, Flow rate = 50 mL/min. Feed composition: 10/40/50 v/v/v  $\text{H}_2/\text{C}_3\text{H}_8/\text{N}_2$

# 5. Discussion

## 5.1 Catalyst Synthesis Results

The catalyst synthesis route followed was proved to successfully prepare Pt/Carbon catalysts. Since the TGA measurements proved inefficient in determining the catalysts' Pt content (discussed in more detail in chapter 5.2.2), the Pt deposition yield of this method is undetermined. Results from the activity tests of the 0.5% Pt/Vulcan catalysts where the HCl addition was varied, did however indicate that the HCl addition used was enough to ensure 100 % deposition yield (discussed in more detail in chapter 5.3.6).

When changing the target metal load, the method required slight alteration in that the stock suspension was diluted before heating to 170 °C. Dilution was performed using the same EG to 1M NaOH(EG) volume ratio as when preparing the stock suspension, aimed at keeping a similar pH during the heating when preparing the 0.5 %wt. catalysts as when preparing the 2 %wt. catalyst. Since it is known that the pH of the stock affects the Pt particle size[25] and consequently catalyst dispersion, measurement error during the dilution could affect the resulting dispersions of the catalyst, providing a possible source of uncertainty. As the effect of pH during the heating period was not investigated, the level of uncertainty is unknown.

The preparation of Pt/CNF catalysts required an increased amount of liquids in the reactor. It is possible that this disturbed the pH at different stages in the synthesis, possibly affecting dispersion and/or Pt deposition. It was therefore aimed at maintaining the same pH as with the 2% Pt/Vulcan synthesis at all stages, by keeping the same HCl to volume and NaOH to volume ratios. As the effect of volume during the synthesis procedure was not investigated, the level of uncertainty is unknown.

The stability of the Pt colloidal stock suspension was investigated by activity measurements, (discussed in more detail in chapter 5.3.6), and the results indicated that the suspension is stable, and can be used to prepare catalysts with reproducible results over 2 months apart.

## 5.2 Catalyst Characterization Results

### 5.2.1 BET Measurements

The surface area measurements for the catalysts determined using BET nitrogen adsorption are shown in Table 4.2. Reproducibility is shown to be reasonably good, showing less than 10 % difference in results between most parallel tests.

The BET isotherms shown in Figs 4.1 to 4.3 show adsorption with very good linear fits with the BET equation (2.5), with  $R^2$  values in excess of 0.99 across all measurements.

The differences between the parallel measurements are therefore likely caused by weighing error. Carbon, especially vulcan and CNF, has throughout the experimental work proven difficult to weigh due to its low density and sensitivity to static electricity.

The adsorption-desorption isotherms produced are shown in Appendix C, Fig. C.1. From the IUPAC classification of adsorption isotherms[42], it can be seen that the vulcan supported samples closely resemble Type II isotherms showing only mild desorption hysteresis at high pressures. Type II isotherms are known to be suitable for BET isotherms[27], and since the hysteresis is well outside the pressure range used for the BET plot, the measurement can be assumed to be quite accurate. The results for second vulcan parallel was also found to be very similar to those found in the literature[43, 44].

The adsorption-desorption isotherms for the CNF supported samples are less resembling of Type II isotherms, with a kink in the isotherm indicating the stepwise multilayer growth of a Type VI isotherm, known to be less suitable for BET surface area measurements than Type II. Desorption hysteresis is virtually undetected. The mentioned kink is however not sharp, and while the BET isotherms shown in Fig. 4.2 show some curvature, indicating that one or more of the BET requirements are unsatisfied, the curvature is not very pronounced and the linear fit is still good. It is therefore chosen to report the surface areas, but they are likely of less accuracy than the other reported results. Compared to the manufacturer data[45], reported surface areas for the untreated support are slightly lower.

The adsorption-desorption isotherms for the graphite supported samples also resemble Type II isotherms, though with a much stronger desorption hysteresis than vulcan, visible down to  $P/P_0$  ratios of approximately 0.45. This is however outside of the measurement range of the BET plot, and the measurements can be assumed to be reasonable accurate. Graphite also has a higher density than vulcan and CNF, allowing for a larger sample size and consequently better weighing accuracy. This is reflected by the consistent results between parallels.

It is shown from the results that the surface area decreases with Pt-deposition. The effect is especially clear for the vulcan supported samples. A possible cause for this is Pt-blockage of the porous structure. This is supported by the fact that the 2% Pt/Vulcan catalyst has lower surface area than the 0.5% Pt/Vulcan catalyst. The effect is less apparent, or undetectable for the other supports likely due to a larger pored structure less susceptible to blockage by Pt nanoparticles. Another possible cause is particle agglomeration caused by the synthesis treatment with various liquids and heat. This is supported by the fact that 0.5% Pt/Vulcan catalyst is closer in surface area to the 2% catalyst than the untreated support, counterintuitive to what their relative metal loads would suggest. The two causes are however not mutually exclusive, and it is possible the the observed results may be explained by a combination of both causes.

## 5.2.2 TGA Measurements

Results from the TGA measurements are not reported, but the thermograms produced are shown in Appendix D. Based on the comparative plot shown in Fig. D.1, it is clear that this method is not suitable for determining metal loads at such low

loads, with some TGA measurements showing negative ash content, and displaying very poor reproducibility between measurements. This is because the measurement target value is very small, and the uncertainty associated with the measurement appears to be larger than the target value. This effect is amplified by the small sample mass capacity available to the TGA apparatus. Due to carbon's low density, sample masses in the range of 10 mg per analysis were used. For reasons mentioned in the previous section, this could be subject to significant weighing error.

It was planned to repeat the TGA measurements using a technique increasing the sample weight capacity of the apparatus. This was not performed due to instrumental failure.

As the TGA measurements proved unusable, it was chosen to assume a metal content equal to the nominal value for all catalysts when determining dispersion. This is likely not a bad assumption as Oh et al.[25] reported TG metal contents for Pt/Carbon catalysts prepared with a polyol method, equal to the nominal value for metal contents of 20 %wt, only registering Pt loss at metal contents above 20 %wt. Since the synthesis procedure used was similar, assuming 100 % Pt deposition yield is likely not a major source of uncertainty.

### 5.2.3 Hydrogen Chemisorption - Volumetric Method

Results from the volumetric hydrogen chemisorption experiments are not reported. Adsorption isotherms and calculated dispersions are shown in Appendix E.1. The adsorption isotherms generally give poor linear fits, and are not monotonically increasing as would be expected. The resulting calculated dispersions vary greatly and some are even negative. The best isotherms produced proved to be irreproducible, and it was therefore chosen to not report the results of the volumetric chemisorption experiments.

The cause of the poor measurements may be poor vacuum conditions. Air leaking into the system may disturb the measurements. This is unlikely to be the only disturbance as leak test are performed as part of the experimental procedure. Some of the measurements passed their leak tests with good margins, and it did not appear to improve the measurements. A more likely cause is hydrogen-support interactions like the spillover effect, known to affect hydrogen chemisorption experiments on Pt[46]. Various carbons have also been reported to have hydrogen storage properties[5], suggesting hydrogen may be absorbed by the support. Whatever the cause, it seems safe to conclude that the method is unsuited for determining dispersion of Pt/Carbon catalysts. Similar experiments have been performed on Pt/Carbon catalysts earlier, producing linear isotherms[47], so it is possible better results may be obtained by changing experimental parameters like pretreatment temperatures.

### 5.2.4 Hydrogen Chemisorption - Pulse Method

Based on the results, it is clear that optimal chemisorption conditions were not met. Pulse data for three selected experiments are shown in Figs. 4.4 to 4.6, the rest are shown in Appendix E.2. The figures in Appendix E.2 show pulse data gathered at

35 °C. The sizes of the saturated peaks shows when compared to the blank experiment, shown in Fig. E.4, that the desorption between pulses is significant, leading to the cooled experiments performed shown in Figs. 4.4 to 4.6.

The 0 °C experiment shows better results than the 35 °C experiment with peaks visibly building up in size, but when compared to the blank experiment it is apparent that desorption is still significant. The saturated peaks of an experiment without significant desorption would be expected to appear much like those of the blank experiment, with adsorption peaks at roughly 3/4 the height of the calibration peaks, and comparable integrated peak areas (not shown).

The -72 °C experiment, shows on the other hand to be at too low temperature, as the first peak is equal to all the other peaks, indicating an inhibited rate of adsorption.

This led to the experiment at -46 °C, shown in Fig. 4.6. The results for this experiment are somewhat better than for the 0 °C experiment, but still not close to the blank experiment. Interestingly, the pulse peaks appear to diminish in size towards the end of the experiment. In this experiment, the reactor was kept in a cooling bath consisting of dry ice in a 30/70 v/v Ethanol/Ethylene Glycol mixture. This resulted in a temperature of -46 °C, which increased to about -41 °C over the course of the experiment. This is colder than what is reported by Jensen & Lee[48]. Coupled with the unstable temperature, the likely cause of this is use of too much dry ice. The results show that even at this low temperature, the desorption rate is significantly temperature dependent, indicating that significant desorption takes place at -46 °C. The optimal adsorption temperature, if it exists, is therefore believed to lie between -72 and -46 °C.

### 5.2.5 CO Stripping Voltammetry

The voltammograms for the 2% Pt/Vulcan, 0.5% Pt/Vulcan and the 0.5% Pt/Graphite samples are shown in Fig. 4.7 to 4.9. It was also attempted to determine the dispersion of the 0.5% Pt/CNF catalyst, but sonication in water proved inefficient in dispersing the catalyst. Attempt was also made, without significant improvement, by grinding the catalyst pre-sonication, and using ethanol instead of water. As seen in the voltammograms, the CO desorption peak appears at approximately 800 mV, similar to previously reported results[33].

Detailed calculations including peak areas are shown in Appendix F. As the signal to noise ratio was less than optimal, especially for the 0.5 % samples, a smoothing filter was applied to the data set before integrating.

There are several possible sources of uncertainty associated with this experiment. As the sample size is only 60 µg, the analysis is very sensitive to perfect mixing during the dispersion. This is especially true for the 0.5 % samples, and since no repeat experiments were performed, the reproducibility of the experiment is unknown. Repeat experiments were planned, but were not carried out due to time limitations.

The relation shown in equation (2.11), assumes a 1:1 adsorption stoichiometry between Pt and CO. This stoichiometry ratio is debated, and has previously been reported as between 1:0.65 and 1:0.8 for various systems[49]. This makes the calculated dispersions somewhat uncertain as this assumption could lead to underestimation.

An interesting result is that the 2% Pt/Vulcan catalyst displays a higher dispersion than the 0.5% Pt/Vulcan catalyst. Based on their relative loads, this is somewhat counterintuitive as increasing the load would be more likely to decrease than increase dispersion. The activity measurements supports this, since the 0.5% catalyst displays about 3/4 of the activity of the 2% catalyst, shown in Fig. 4.12b, not less than 1/4 as their relative loads and determined dispersions would suggest, and there is little reason for the 0.5% Pt/Vulcan catalyst to have a significantly higher specific activity than its 2 %wt. counterpart. It is therefore possible that the metal load affects the voltammetric measurements, possibly by influencing the mass transfer across the nafion membrane. The voltammogram of the 2% Pt/Vulcan catalyst shows a clear H<sub>2</sub> desorption peak between 50 and 300 mV that is absent in the 0.5% Pt/Vulcan catalyst's voltammogram and small and noise obscured in the 0.5% Pt/Graphite catalyst's voltammogram, suggesting the load influences the system in some way.

Adding the assumption of the area per Pt atom, the uncertainty of the results may be significant, and the determined dispersions may be better suited for internal comparison than as accurate measurements of dispersion.

## 5.3 Catalyst Activity Results

### 5.3.1 Optimization

The results comparing the undiluted and diluted tests are shown in Fig. 4.10. While the undiluted test shows the lower conversion and is seemingly closer to differential reactor conditions than the diluted tests, it was chosen to employ dilution for all subsequent testing. Not using dilution caused pressure drops approaching and exceeding the safety limits of the apparatus and could therefore not be counted on to produce reproducible results. Having a high pressure drop also increases the pressure in the catalyst bed which in turn decreases the equilibrium conversion level, as shown in Appendix I. A lowered equilibrium conversion averaged over the catalyst bed is likely the cause of the lowered conversion level observed in the undiluted sample. If the reaction rate is lowered due to closeness to equilibrium, then differential conditions are not fulfilled, and the use of undiluted samples is further discouraged. The three parallel diluted runs also show decent reproducibility being within 1.5 % points of each other throughout most of the measurements.

The results comparing the various reaction temperatures are shown in Fig. 4.11. While the test at 475 °C shows the lowest conversion level as expected, the equilibrium conversion at 475 °C and 1 bar is only approximately 11 %, see Appendix I. The initial conversion level for this run is at over 9 %, i.e. quite close to equilibrium and therefore not showing differential conditions. The conversion level drops to about 6 % over the time scale investigated. This is still about 55 % of the equilibrium level and differential reactor conditions are consequently not reached.

The equilibrium conversion at 500 °C and 1 bar is 17.3 %. The initial conversion at these conditions is about 13.5 %, which is too high to be considered differential conditions. The conversion level drops to about 10 % over the time period investigated, still too high for differential conditions.



The equilibrium conversion at 525 °C and 1 bar is 25.3 %. The initial conversion at these conditions is about 15.5 %, but drops to about 12 % within 1 h on stream which may be considered differential conditions at less than half of the equilibrium level. The rate of deactivation is however notably higher than for the other temperatures, and after about 1 h on stream the activity is lower than for the 500 °C test.

Based on the results, it is hard to conclude with an optimal reaction temperature. The absence of repeat experiments also makes the results somewhat inconclusive. While the 525 °C test was the only test that reached differential conditions, its high deactivation rate makes it unsuitable for testing on a larger time scale. It was therefore chosen to proceed using 500 °C and decrease the catalysts metal load to 0.5 %wt. instead, more similar to the commercial standard[8].

In Fig. 4.12, a comparison between the 0.5% and 2% Pt/Vulcan catalysts are shown. The 0.5% catalyst exhibited very good reproducibility after about 1 h on stream, and reached differential conditions after about 2 h. Comparison between the two show that the 0.5% catalyst is less active, but not as much as their respective metal loads would suggest, showing nearly 3/4 the conversion level at 1/4 the load. The reason for this is the 2% catalyst's closeness to equilibrium, inhibiting the reaction rate. Another possible reason is differences in the synthesis procedure. The two catalysts were synthesized some time apart and used different stock suspensions. Excepting this and that the stock suspension was diluted during the synthesis of the 0.5% catalyst, the synthesis procedures were identical. It is possible that the 0.5% catalyst has a higher dispersion than the 2% catalyst. This is however contradicted by the dispersion measurements, and metal loads differing from their nominal values may be the cause. Since this was not successfully determined, this remains a subject of investigation.

In Fig. 4.13, the results for the flow variation experiments are shown. In the first experiment, the conversion is shown to decrease with increased flow, as would be expected when decreasing space time. When going from 100 to 50 mL/min the conversion increases back to the level expected following the initial 50 mL/min data, suggesting that the deactivation rate is independent of flow rate. Observing the rate of reaction, it is shown to slightly increase going from 50 to 75 mL/min but remain reasonably unchanged for the subsequent flow rate transitions. This suggests that for the first transition, differential conditions are not reached, but are reached at the time of the subsequent transitions as indicated by the activity's independence of the flow rate. The cause is the lowered conversion level brought on by both deactivation and increase in flow rate.

In the second experiment, like the first, the conversion is shown to decrease with increased flow rate and increase again upon its reversal. Unlike the first experiment though, the increase in flow rate appear to decrease the rate of deactivation as the initial conversion level of the second 50 mL/min part is higher than would be expected at only 0.5 % lower than the last measure point of the first part at 2 h apart. For comparison, the first experiment exhibited a 2 % drop over 4 h, i.e. twice the deactivation rate. This is reflected by the reported rates, showing significant increase with increasing flow rate, as well as decrease upon reversal, indicating that differential reactor conditions were never reached during the course of this experiment. A reaction rate that is affected by the flow rate may also be caused by external mass

transfer limitations[13]. This is however an unlikely scenario, as it would be expected to see differences in both experiments had external mass transfer limitations been present.

The two experiments yielded somewhat contradictory results. The reasons for this probably lies in the different methods used. The first experiment changed the feed flow with the reactor on stream, and therefore had to make the assumption that the feed gas analysis for the initial flow rate applied for the subsequent flow rates, thus making it a potential source of error. The second experiment eliminated this by flushing the reactor and analysing the feed gas between each flow rate transition. It did however introduce another error source with the flushing treatment. Before settling on the flushing treatment reported, attempt was made using 75mL/min N<sub>2</sub> flow for 45 min as the flushing treatment. Results are shown in Appendix G.1, showing significant deactivation between flow rates, likely caused by coking of residual propane in the system while the reactor was offline during feed analysis. It was therefore chosen to increase the flushing flow rate, increase the flushing time and to introduce hydrogen, known to adsorb competitively with propane and propylene[14], to more efficiently remove propane from the system and diminish any deactivation.

It is possible that the hydrogen flushing treatment resulted in some activity recovery. Depending on the reaction system and the type of coke formed, hydrogen is known to be able to restore lost activity by coke removal [50]. However, in a study by Larsson et al.[16], hydrogen treatment at 789 K of a coked dehydrogenation Pt/Al<sub>2</sub>O<sub>3</sub> catalyst was found to have no effect on the coke. While this indicates that hydrogen flushing could not have restored any activity, it is not conclusive as different supports were used, possibly forming other types of coke more susceptible to hydrogen treatment. Any activity recovery caused by hydrogen treatment does however not explain the drop in activity from the 100 mL/min to the second 50 mL/min measurement. It is therefore possible that this method simply introduces more sources of error than it removes and since no repeat experiment were successfully performed, the results from this experiments are too uncertain to rely on. The first experiment was not repeated either, but since the results were more like expected the optimization decision was based on this experiment. To make a better informed decision however, repeat experiments should have been performed employing both methods. An experiment investigating the hydrogen treatment's effect on the activity should also have been performed. The experiment performed is not conclusive as any increase in conversion due to the hydrogen treatment is negated by the decrease caused by the higher flow rate.

From the results it is difficult to conclude with an optimal flow rate, while the first experiment indicated that differential conditions were achieved at 75 and 100 mL/min, the pressure drop gained at these higher flow rates were significant. As the 50 mL/min appeared to reach differential conditions after a only a few hours on stream, it was chosen to proceed using 50 mL/min. It is worth mentioning that the initial deactivation could cause the catalyst bed to coke unevenly. This could mean that the reaction rate is not constant throughout the catalyst bed even at seemingly differential conversion levels. To proceed with 50 mL/min, even coking has to be assumed for the initial period on stream. It is unknown how good this assumption is, and it should be noted that 50 mL/min was chosen for reasons of necessity regarding the pressure drop, not for optimal conversion levels.

It was considered to also vary the composition of the feed gas as part of the optimization experiments. As the propane was already quite diluted for the baseline case, it was shown by simulation that further dilution of propane would have little effect on the equilibrium conversion levels, see Appendix I, Table I.1. It was therefore chosen to not perform such experiments.

### 5.3.2 Deactivation Model

Based on the results from the optimization experiments, it was chosen to base a deactivation model on the data collected at 500 °C, 50 mL/min flow rate, using the 0.5% Pt/Vulcan catalyst with dilution. As the purpose of this exercise was to achieve a mathematical expression that could be used to correct data for deactivation, no extensive modeling was performed, and a mathematical expression was simply fitted to the experimental data. Across two parallels, geometric regression curves were found to fit well with the experimental data, with  $R^2$  values in excess of 0.98 for both parallels. Residual plots, shown in Appendix G.2, Fig. G.1, were produced and show randomly distributed residual functions suggesting the models are well suited for predicting activity data.

A weakness with the geometric regression curve is that it is not extrapolatable to  $t = 0$  since  $R_A \rightarrow \infty$  as  $t \rightarrow 0$ . It was therefore chosen to define a reference time,  $t_0$ , and rate,  $R_A^0$  at  $t = 1$  h. This time was chosen since the two parallels showed good reproducibility from about 1 h time on stream and onwards. This means that when using the model for correction, it corrects the activity to 1 h on stream level, instead of initial level. This was deemed acceptable since the purpose was not to determine initial activity, but to compare measurements taken at different times on stream to each other.

### 5.3.3 Kinetic Study

The results of the kinetic study are shown in Fig. 4.15. A detailed description of its production is shown in Appendix G.3.

A few assumptions had to be made to produce the plots shown. First, since the method where the feed was changed with the reactor on stream was the only one that produced viable results, no intermediate feed analyses were made, and the MFC settings had to be used as a baseline for the GC measurements. Based on the reported results, this does not seem to be a source of great uncertainty. However, at the measurements with the highest concentrations of the monitored reactants (60 %  $C_3H_8$  and 20 %  $H_2$ ), the  $N_2$  flow was too low for the MFC settings to be reliable. This resulted in an unexpected low conversion level (negative for the  $H_2$  experiment), and these measurements were consequently discarded.

When correcting for deactivation, it was chosen to use equation (4.2) and not (4.1) as it had a slightly better fit with experimental data and was produced from a larger sample size. Using the model assumes that the rate of deactivation is the same for all feed compositions. This is obviously not the case since it is known that propylene is the main coke precursor[14]. The rate of deactivation is therefore, to some extent,

proportional to  $R_{C_3H_8}$  which, as shown by this experiment's results, depends on the feed composition. It was therefore chosen to deactivate the catalyst for 3 h on stream at the same conditions used when making the deactivation model before taking measurements. The deactivation was shown to be much slower after 3 h, and the error introduced by using the deactivation model is minimized.

Since a pressure drop was observed across the catalyst bed throughout all measurements, there was a pressure gradient across the catalyst bed, making the partial pressure of the monitored reactants not directly measurable. It was therefore chosen to make the measurements relative to the lowest flow rate measurements, and assume  $F/F_{Ref} = p/p_{Ref}$ . The method requires that  $F$  is constant, or negligibly changed across the catalyst bed. This is likely to be fulfilled for the propane experiment since the conversion is low and the propane feed is relatively high. This is more uncertain for the hydrogen experiment since the hydrogen feed is much lower and may be significantly disturbed by the hydrogen produced. This is reflected by the linear fits produced, which is better for propane than for hydrogen.

It is also a possibility that the measurements with the lowest conversion levels were disturbed by closeness to equilibrium. Simulation data shown in Appendix I, Table I.1 suggests however that this is not the case.

The results indicate that propane dehydrogenation follows power law kinetics at low conversion levels on Pt/Vulcan catalysts. The propane order was found to be approximately 0.9, fairly close to 1 which is previously reported for alkane dehydrogenations[51]. The linear fit produced is fairly good, but with several assumptions made and no repeat experiment successfully performed, the uncertainty of the experiment is unknown. The closeness to the previously reported results is however an indication of the experiment's validity.

The hydrogen order was found to be approximately  $-1.1$ , outside the  $0$  to  $-0.5$  range usually reported for alkane dehydrogenations[51]. As only 3 measurement points were produced, the linear fit is not particularly good. Removal of the last measurement point brings the order to approximately  $-0.2$ , which is within the usually reported range. Since no repeat experiment was successfully performed, the uncertainty associated with the results is significant.

### 5.3.4 Blank Tests

The results showed some dehydrogenation activity for the supports with vulcan > CNF > graphite, which displayed no detectable activity. For both vulcan and cnf, any detected activity was gone after less than 1 h on stream. It is possible that some of the activity shown came from Pt deposits on the reactor walls stemming from previous experiments. Whether or not this was the case is however not important, as the purpose of the experiments was to determine if the supports or homogeneous effects could disturb the measurements. Since any activity observed was undetectable before 1 h on stream, it is safe to conclude that the Pt deposited on the catalysts is the main source of dehydrogenation activity in the reported experiments.

It was also planned to perform experiments with quartz wool, SiC and an empty reactor. This was deemed unnecessary since the graphite sample displayed no activity,

while held in place with quartz wool and diluted with SiC. This experiment effectively ruled out any catalytic activity caused by graphite, quartz wool and SiC as well as any homogeneous activity. No repeat experiments were deemed necessary.

### 5.3.5 Support Comparison

From the results shown in Fig. 4.16, it is clear that the vulcan supported catalyst is far more active than the CNF and graphite supported catalysts, with graphite possibly being slightly more active than CNF. The reasons for this is likely a lower dispersion for the CNF and graphite supported catalysts. The graphite and CNF supported catalysts activity appear to be much more stable than for the vulcan supported catalyst. This is likely to be an effect of the lowered activity than a catalyst property, since the deactivation rate is known to be related to the propene production rate[14]. It also seems to appear that the activity for the CNF and graphite supported catalyst is not monotonically decreasing as would be expected. It therefore appears that the GC measurement accuracy is lowered at low conversion levels, creating the waved activity curves observed in Fig. 4.16. Conversion curves more to scale are shown in Appendix G.1, empasizing the measurement inaccuracy. Disregarding the middle portion of the plot, it is however visible that the later measurements are lower in activity than the earlier measurements.

The CO stripping voltammetry experiments reveal that the differences in activity is at least partially due to lower dispersion in the graphite sample, and the turnover frequencies shown in Fig. 4.17 shows that the specific activity displayed by the catalysts is significantly closer than activity per unit mass, though the vulcan catalyst is still the more active. It is worth mentioning that the graphite catalyst's turnover frequencies are based on the conversion levels shown in Fig. 4.16a and therefore subject to the same measurement inaccuracy. The uncertainty associated with the dispersion measurements could also be significant, as discussed in chapter 5.2.5. As the dispersion of the 0.5% Pt/CNF catalyst was not determined, no turnover frequencies are reported. Considering the mass specific activity, it is likely that the CNF catalyst also has a lower dispersion than the vulcan catalyst. Since the synthesis procedure had to be changed for the CNF catalyst, the Pt content of the CNF catalyst is more uncertain than for the vulcan catalyst. This is discussed in more detail in chapter 5.3.6. As the graphite catalyst synthesis procedure was identical to the vulcan catalyst synthesis, this is likely not the case for the graphite catalyst.

Based on the combined results of the support comparison, BET measurements, and the dispersion measurements, it seems likely that the lowered dispersions displayed by the graphite catalyst and indicated by the CNF catalyst are caused by the low surface areas measured for the graphite and CNF catalysts. A low support surface is more likely to cause Pt agglomeration upon deposition, lowering the dispersion[52]. Contradicting this is the lower activity displayed by the CNF catalyst relative to that of the graphite catalyst. Considering that the the BET surface areas displayed by the CNF catalyst was higher than for the graphite catalyst, it would be expected that the dispersion and likely the activity would be higher as well. As neither dispersion or Pt content measurements were successfully performed on the CNF catalyst, there is no guarantee that the difference in activity is caused by BET surface area alone, and the changed synthesis procedure is a source of uncertainty. There are also other

factors than surface area that could affect the dispersion, like the surface chemistry of the supports[53]. Oxygen groups on the carbon surface have been shown to cause Pt-agglomeration by changing the electrostatic forces between Pt and support during the polyol process[34, 53] and decreasing dispersion. As the supports were not characterized for oxygen content, the surface chemistry's role in making the low dispersion is unknown, but assuming 100 % Pt deposition yield in the synthesis of the CNF catalyst, it is not unlikely that the CNF surface chemistry is at least partially the cause of the low dispersion indicated by the results.

### 5.3.6 Vulcan Supported Catalyst Comparison

The investigation of the Pt-colloid stock suspension's stability was deemed necessary based on the support comparison results shown in Fig. 4.16. The results for the CNF supported catalyst indicated a low catalyst dispersion. Since the Pt-stock is a colloidal suspension, it would be thermodynamically unstable by nature[54] and Pt-particle agglomeration leading to lowered dispersion could be significant, depending on the suspension's kinetic stability. Since the 0.5% Pt/CNF catalyst was prepared over 2 months after the 0.5% Pt/Vulcan catalyst to which it was compared, it was unknown if the lowered dispersion was caused by the support or the aging of the stock suspension.

The results of the experiment is shown in Fig. 4.18, where it can be seen that the 0.5% Pt/VulcanB catalyst's activity is quite similar to that of the 0.5% Pt/Vulcan catalyst, with parallel 2 showing very similar activity, and parallel 1 slightly higher. For the second parallel, the amount of catalyst tested was decreased to 30 mg for practical reasons. This decreased the weighing accuracy, and is likely the cause of the poorer reproducibility displayed by the vulcanB catalyst. The results indicate that the vulcanB catalyst has a similar dispersion to the vulcan catalyst, which again indicate that the stock suspension is kinetically stable over the timeframe investigated. The lowered dispersion of the 0.5% Pt/CNF is therefore not caused by aging of the stock suspension.

Another possible reason for the results could be the dilution of the synthesis mixture required for the 0.5% Pt/CNF catalyst synthesis. The fraction of Pt deposited on the support is known to be dependant on the pH in the mixture[25], and since the dilution possibly disturbed this, it was chosen to investigate wether or not the HCl addition during the synthesis procedure was enough to guarantee close to 100 % Pt deposition.

The results of the experiment is shown in Fig. 4.19, where it can be seen that the activity follows vulcanE > vulcanC > vulcan D. As with the previous experiment, the amount of catalyst tested was decreased to 30 mg for practical reasons. The lowering of the weighing accuracy coupled with the lack of repeat experiments makes the accuracy of the displayed results somewhat questionable. However, no clear correlation between HCl amount added and activity is shown, since the vulcanE catalyst is shown to be more active than the vulcanC catalyst, while the vulcanD catalyst is shown to be less active than the vulcanC catalyst, counterintuitive to the first result. While inconclusive, this could indicate that the HCl addition first used is sufficient to cause 100 % Pt deposition. Since all liquid additions for the 0.5% Pt/CNF

synthesis were increased by a factor of 1.5 relative to the 0.5% Pt/Vulcan synthesis, the concentration of all components except Pt and CNF should be the same, and differences in pH is not likely to be the cause of the low activity displayed by the 0.5% Pt/CNF catalyst.

### 5.3.7 Selectivity

No selectivity results are reported, but calculated selectivity measurements are shown in Appendix G.1. It can be seen that the selectivity measurements vary greatly, some showing  $> 100\%$ . The reason for this is that the propylene GC calibration was performed using a calibration gas only containing 1000 ppmv of propylene, see Appendix H, requiring significant extrapolation from the calibrated area to experimental conditions. This resulted in a poor measurement accuracy, as shown by the figures in Appendix G.1. It was also attempted to use the same relative response factor for propylene as propane, as suggested by Dietz[55], but results were not improved.

The raw data do however indicate that the catalyst is highly selective at the conversion levels investigated. For the vulcan supported catalyst, side products were detected by GC for conversion levels above about 10 %, but undetected below. This was symptomatic of all 0.5% Pt/Vulcan tests conducted at 500 °C. Two chromatograms from the 0.5% Pt/Vulcan experiment at 500 °C, parallel 1, are shown in Appendix G.4, Fig. G.7, showing the methane peak disappearing after about 1 h on stream, at between 9 and 10 % conversion. The tests for the graphite and CNF supported catalysts showed no side products throughout the measurements, likely due to the lower conversion levels displayed.

## 6. Future Work

As the synthesis procedure proved effective, it can be used to produce other carbon supported Pt catalysts. A variety of carbon allotropes remain to be tested, particularly in the CNF and CNT categories. Based on the results it may be favourable to focus on carbon types with high specific surface areas, as they would be more likely to achieve comparable dispersions.

The TG analyses should be performed as planned with an increase of the sample mass to more accurately determine the metal content of the catalysts. The uncertainty associated with the synthesis procedure makes the TGA vital in determining the metal content and consequently the dispersions of the prepared catalysts.

Further optimization is required for the dispersion measurements. The pulse chemisorption may be optimized for adsorption temperature, aiming at between  $-70$  and  $-50$  °C, possibly achieving a manageable desorption rate while maintaining an acceptable high rate of adsorption. The adsorption temperature can be adjusted by keeping the reactor in a dry ice in ethanol/ethylene glycol bath at various mix ratios[48]. An interesting option is to use CO as an adsorption gas instead of hydrogen. This could eliminate any disturbance caused by hydrogen-carbon interactions and possibly improve on the desorption rate. This could be attempted both with volumetric and with pulse chemisorption.

The CO voltammetric method was the most promising technique used for the determination of dispersion. While results were obtained, the signal to noise ratio was less than optimal for the low loaded catalysts. This could possibly be improved on by investigating the possibility of increasing the sample mass. It is also necessary to test the CNF supported catalyst. Since a dispersed ink was not obtained, using a different solvent might yield better results. The solvent would have to be inert with the electrode and easily dried. Since only polar solvents were used and found inefficient, a non-polar solvent like hexane should be attempted first.

While the results indicated that BET surface area was an important factor for the dispersion of the prepared catalysts, the surface chemistry of the supports may also be a significant factor. To investigate this, the supports may be characterized by e.g. temperature programmed desorption as performed by Zhou et al.[56].

To further optimize the activity measurement conditions, it would be favourable to make the system accept higher flow rates without increasing the pressure drop. This could be achieved by increasing the reactor diameter allowing for a larger gas flow and leading to a decrease in linear bed length and gas velocity which will generate a lower pressure drop. Increasing the flow rate could lead to differential reactor conditions upon start-up. The linear bed length, as stated by Chorkendorff & Niemantsverdriet[27], should be at least 50 times the catalyst particle diameter to ensure an ideal flow pattern. Considering the fine particled nature of the carbons tested, this should not pose an issue even with decreasing the bed length.



The graphite and CNF supported catalysts tested displayed low conversion levels, and the GC apparatus displayed poor measurement accuracy at these levels. To increase the accuracy, it would be favorable to test these catalysts at higher conversion levels at lower space velocity. This could be achieved by decreasing the gas flow or increasing the sample mass. The former would compromise the MFC accuracy as the N<sub>2</sub> flow is already at a low setting. The latter would exceed the size of the current reactor when testing the CNF catalyst, but could be achieved by increasing the reactor diameter. Consequently, increasing the reactor diameter allows for more flexibility in the setup and should be performed for continued catalyst testing.

## 7. Conclusion

The synthesis method used was proved efficient in producing Pt on vulcan, CNF and graphite catalysts that were found active for propane dehydrogenation. Experimental testing indicated that the stock suspension's stability was sufficient to produce catalysts with reproducible properties for more than 2 months apart.

BET surface area measurements found surface areas for the prepared catalysts in the order vulcan > CNF > graphite. Good linear fits with the BET equation indicated a high measurement accuracy for vulcan and graphite, but the CNF was found to deviate from linearity, making the measurement less certain. The measurements found that the surface areas of the catalysts were less than those of the supports. This is attributed to Pt blockage of the porous structure and/or carbon agglomeration stemming from the synthesis procedure.

TGA was found inefficient in determining the Pt content of the prepared catalysts. This is attributed to a high measurement inaccuracy stemming from a combination of a small measurement target value and small sample sizes.

Hydrogen chemisorption was found inefficient in determining catalyst dispersion. The volumetric experiments were unable to produce linear isotherms, likely caused by hydrogen-carbon interactions. The pulse experiments were unable to achieve an adsorption temperature obtaining a manageable desorption rate while maintaining a high adsorption rate.

Using CO stripping voltammetry, dispersion measurements were obtained for the vulcan and graphite supported catalysts was found in the order vulcan > graphite with some measurement uncertainty. The CNF catalyst was found unable to produce the catalyst ink needed to perform the experiment. The results indicated that the metal load may affect the voltammetric experiment.

For the activity measurements, an optimal set of operation conditions was found providing an acceptable trade-off between pressure drop, rate of deactivation and closeness to differential reactor conditions.

The propane dehydrogenation reaction was found to follow power law kinetics on a Pt/Vulcan catalyst with a propane order of 0.9 and hydrogen order of  $-1.1$ . The propane order investigation gave a good linear fit, while the hydrogen order investigation gave less accurate results.

A comparison of the three supports found that the activity of the catalysts followed the order vulcan > graphite > CNF. Vulcans superior activity to graphite was attributed its higher dispersion. The specific activity was closer, but inaccurate measurements for the graphite catalyst made the comparison inconclusive. The low CNF activity was also likely to result from low dispersion, but this was not successfully measured. The lower dispersions displayed by the graphite catalyst and indicated by the CNF supported catalysts were attributed to the low surface areas and surface chemistries of the support materials.

# Bibliography

- [1] A. M. Aitani, "Propylene production," in *Encyclopedia of Chemical Processing* (S. Lee, ed.), Taylor & Francis, 2006.
- [2] J. S. Plotkin, "The changing dynamics of olefin supply/demand," *Catalysis Today*, vol. 106, pp. 10–14, 2005.
- [3] J. Moulijn, M. Makkee, and A. van Diepen, *Chemical Process Technology*. Chichester: John Wiley & Sons, 1<sup>st</sup> ed., 2001.
- [4] J. Blas, "Shale gas byproducts fall to a 10-year low." Financial Times <http://www.ft.com/intl/cms/s/0/afe2958e-ba24-11e1-84dc-00144feabdc0.html#axzz2BjQ8LGX2>, 05.06.2013.
- [5] K. P. D. Jong and J. W. Geus, "Carbon nanofibers: Catalytic synthesis and applications," *Catalysis Reviews - Science and Engineering*, vol. 42, pp. 481–510, 2000.
- [6] P. Serp, M. Corrias, and P. Kalck, "Carbon nanotubes and nanofibers in catalysis," *Applied Catalysis A: General*, vol. 253, pp. 337–358, 2003.
- [7] S. Sahebdehfar, M. T. Ravanchi, F. T. Zangeneh, S. Mehrazma, and S. Rajabi, "Kinetic Study of Propane Dehydrogenation and Side Reactions over Pt-Sn/Al<sub>2</sub>O<sub>3</sub> Catalyst," *Chemical Engineering Research and Design*, vol. 90, pp. 1090–1097, 2012.
- [8] O. A. Bariås, *Transient Kinetic Investigation of the Catalytic Dehydrogenation of Propane*. PhD thesis, Norwegian University of Science and Technology, 1993.
- [9] G. Aylward and T. Findlay, *SI Chemical Data*. Milton: John Wiley & Sons, 6<sup>th</sup> ed., 2006.
- [10] M. P. Lobera, C. Téllez, J. Herguido, and M. Menéndez, "Transient kinetic modelling of propane dehydrogenation over a Pt-Sn-K/Al<sub>2</sub>O<sub>3</sub> catalyst," *Applied Catalysis A: General*, vol. 349, pp. 156–164, 2008.
- [11] Q. Li, Z. Sui, X. Zhou, and D. Chen, "Kinetics of propane dehydrogenation over Pt-Sn/Al<sub>2</sub>O<sub>3</sub> catalyst," *Applied Catalysis A: General*, vol. 398, pp. 18–26, 2011.
- [12] A. Siahvashi, D. Chesterfield, and A. A. Adesina, "Nonoxidative and Oxidative Propane Dehydrogenation over Bimetallic Mo-Ni/Al<sub>2</sub>O<sub>3</sub> Catalyst," *Industrial & Engineering Chemistry Research*, vol. 52, pp. 4017–4026, 2013.

- [13] H. S. Fogler, *Elements of Chemical Reaction Engineering*. Upper Saddle River: Pearson Education, 4<sup>th</sup> ed., 2006.
- [14] M. van Sint Annaland, J. A. M. Kuipers, and W. P. M. van Swaaij, “A kinetic rate expression for the time-dependent coke formation rate during propane dehydrogenation over a platinum alumina monolithic catalyst,” *Catalysis Today*, vol. 66, pp. 427–436, 2001.
- [15] O. A. Bariås, A. Holmen, and E. A. Blekkan, “Propane Dehydrogenation over Supported Pt and Pt-Sn Catalysts: Catalyst Preparation, Characterization, and Activity Measurements,” *Journal of Catalysis*, vol. 158, pp. 1–12, 1996.
- [16] M. Larsson, M. Hultén, E. A. Blekkan, and B. Andersson, “The effect of reaction conditions and time on stream on the coke formed during propane dehydrogenation,” *Journal of Catalysis*, vol. 164, pp. 44–53, 1996.
- [17] I. Kvande, *Carbon nanofiber supported platinum catalysts*. PhD thesis, Norwegian University of Science and Technology, 2007.
- [18] “Carbon Black User’s Guide.” Cancarb  
[http://www.cancarb.com/pdf/carbon\\_black\\_user\\_guide.pdf](http://www.cancarb.com/pdf/carbon_black_user_guide.pdf), 05.06.2013.
- [19] H. Liu, C. Song, L. Zhang, J. Zhang, H. Wang, and D. P. Wilkinson, “A review of anode catalysis in the direct methanol fuel cell,” *Journal of Power Sources*, vol. 155, pp. 95–110, 2006.
- [20] P. Ferreira-Aparicio, M. Folgado, and L. Daza, “High surface area graphite as alternative support for proton exchange membrane fuel cell catalysts,” *Journal of Power Sources*, vol. 192, pp. 57–62, 2009.
- [21] A. Mastalir, Z. Király, I. Dékány, and M. Bartók, “Microcalorimetric and catalytic investigations of transition metal nanoparticles intercalated in graphite,” *Colloids and Surfaces A: Physicochemical and Engineering Aspects*, vol. 141, pp. 397–403, 1998.
- [22] “Hot Electrons in Carbon - Graphite behaves like a semiconductor.” Max Born Institut Berlin  
[http://www.mbi-berlin.de/en/research/highlights/highlight\\_graphite.html](http://www.mbi-berlin.de/en/research/highlights/highlight_graphite.html), 05.06.2013.
- [23] I. Martin-Gullon, J. Vera, J. A. Conesa, J. L. González, and C. Merino, “Differences between carbon nanofibers produced using Fe and Ni in a floating catalyst reactor,” *Carbon*, vol. 44, pp. 1572–1580, 2006.
- [24] A. S. Volynkin, *In Preparation*. PhD thesis, Norwegian University of Science and Technology.
- [25] H.-S. Oh, J.-G. Oh, and H. Kim, “Modification of polyol process for synthesis of highly platinum loaded platinum carbon catalysts for fuel cells,” *Journal of Power Sources*, vol. 183, pp. 600–603, 2008.
- [26] F. Fievet, J. Lagier, B. Blin, B. Beaudoin, and M. Figlarz, “Homogeneous and heterogeneous nucleations in the polyol process for the preparation of micron and submicron size metal particles,” *Solid State Ionics*, vol. 32-33, pp. 198–205, 1989.

- [27] I. Chorkendorff and J. Niemantsverdriet, *Concepts of Modern Catalysis and Kinetics*. Weinheim: John Wiley & Sons, 2<sup>nd</sup> ed., 2007.
- [28] “Thermogravimetric analysis: A beginners guide.” PerkinElmer, Inc. [http://www.perkinelmer.com/CMSResources/Images/44-74556GDE\\_TGABeginnersGuide.pdf](http://www.perkinelmer.com/CMSResources/Images/44-74556GDE_TGABeginnersGuide.pdf), 05.06.2012.
- [29] A. Gervasini and C. Flego, “Hydrogen adsorption and desorption on alumina supported platinum-multicomponent catalysts with a gas chromatographic pulse technique,” *Applied Catalysis*, vol. 72, pp. 153–163, 1991.
- [30] A. J. Bard and L. R. Faulkner, *Electrochemical Methods: Fundamentals and Applications*. New York: John Wiley & Sons, 2<sup>nd</sup> ed., 2001.
- [31] C. H. Hamann, A. Hamnett, and W. Vielstich, *Electrochemistry*. Weinheim: John Wiley & Sons, 2<sup>nd</sup> ed., 2007.
- [32] T. Vidaković, M. Christov, and K. Sundmacher, “The use of CO stripping for in situ fuel cell catalyst characterization,” *Electrochimica Acta*, vol. 52, pp. 5606–5613, 2007.
- [33] P. Ochal, J. L. Gomez de la Fuente, M. Tsypkin, F. Seland, S. Sunde, N. Muthuswamy, M. Rønning, D. Chen, S. Garcia, S. Alayoglu, and B. Eichhorn, “CO stripping as an electrochemical tool for characterization of Ru@Pt core shell catalysts,” *Journal of Electroanalytical Chemistry*, vol. 665, pp. 140–146, 2011.
- [34] N. Muthuswamy, *Platinum based Catalysts for Methanol Fuel Cells: Metal Clusters and Carbon Supports*. PhD thesis, Norwegian University of Science and Technology, 2011.
- [35] F. G. Will, “Hydrogen Adsorption on Platinum Single Crystal Electrodes - Isotherms and Heats of Adsorption,” *Journal of the Electrochemical Society*, vol. 112, pp. 451–455, 1965.
- [36] J. Pérez-Ramírez, R. J. Berger, G. Mul, F. Kapteijn, and J. A. Moulijn, “The six-flow reactor technology: A review on fast catalyst screening and kinetic studies,” *Catalysis Today*, vol. 60, pp. 93–109, 2000.
- [37] B. S. Richardson, J. F. Birdwell, F. G. Pin, J. F. Jansen, and R. F. Lind, “Sodium borohydride based hybrid power system,” *Journal of Power Sources*, vol. 145, pp. 21–29, 2005.
- [38] A. Holmen, *Heterogen Katalyse*. Institutt for kjemisk prosesssteknologi, NTNU.
- [39] J. T. Richardson, *Principles of Catalyst Development*. New York: Springer, 1989.
- [40] H. M. Nair and J. M. Miller, *Basic Gas Chromatography*. Hoboken: John Wiley & Sons, 2<sup>nd</sup> ed., 2009.
- [41] R. L. Grob and E. F. Barry, *Modern Practice of Gas Chromatography*. Hoboken: John Wiley & Sons, 4<sup>th</sup> ed., 2004.

- [42] K. S. W. Sing, D. H. Everett, R. A. W. Haul, L. Moscou, R. A. Pierotti, J. Rouquérol, and T. Siemieniewska, "Reporting Physisorption Data for Gas/Solid Systems," *Pure and Applied Chemistry*, vol. 57, pp. 603–619, 1985.
- [43] M. Carmo, A. R. dos Santos, J. G. R. Poco, and M. Linardi, "Physical and electrochemical evaluation of commercial carbon black as electrocatalysts supports for DMFC applications," *Journal of Power Sources*, vol. 173, pp. 860–866, 2007.
- [44] Y. Takasu, T. Kawaguchi, W. Sugimoto, and Y. Murakami, "Effect of the surface area of carbon support on the characteristics of highly-dispersed Pt-Ru particles as catalysts for methanol oxidation," *Electrochimica Acta*, vol. 48, pp. 3861–3868, 2003.
- [45] "CNF Manufacturer Data." Sigma-Aldrich  
<http://www.sigmaaldrich.com/catalog/product/aldrich/719781>, 05.06.13.
- [46] V. V. Rosanov and O. V. Krylov, "Hydrogen spillover in heterogeneous catalysis," *Russian Chemical Reviews*, vol. 66, pp. 107–119, 1997.
- [47] C. Prado-Burguete, A. Linares-Solano, F. Rodríguez-Reinoso, and C. Salinas-Martínez de Lecea, "Effect of Carbon Support and Mean Pt Particle Size on Hydrogen Chemisorption by Carbon Supported Pt Catalysts," *Journal of Catalysis*, vol. 128, pp. 397–404, 1991.
- [48] C. M. Jensen and D. W. Lee, "Dry-Ice Bath Based on Ethylene Glycol Mixtures," *Journal of Chemical Education*, vol. 77, p. 629, 2000.
- [49] D. Chen, Q. Tao, L. W. Liao, S. X. Liu, Y. X. Chen, and S. Ye, "Determining the Active Surface Area for Various Platinum Electrodes," *Electrocatalysis*, vol. 2, pp. 207–219, 2011.
- [50] C. H. Bartholomew and R. J. Farrauto, *Fundamentals of Industrial Catalytic Processes*. Hoboken: John Wiley & Sons Inc., 2<sup>nd</sup> ed., 2012.
- [51] D. E. Resasco, "Dehydrogenation by heterogeneous catalysts," in *Encyclopedia of Catalysis* (I. T. Horváth, ed.), Hoboken: John Wiley & Sons, 2003.
- [52] J. H. Sinfelt, "Highly Dispersed Catalytic Materials," *Annual Review of Materials Science*, vol. 2, pp. 641–662, 1972.
- [53] A. Guerrero-Ruiz, P. Badenes, and I. Rodríguez-Ramos, "Study of some factors affecting the Ru and Pt dispersions over high surface area graphite-supported catalysts," *Applied Catalysis A: General*, vol. 173, pp. 313–321, 1998.
- [54] P. C. Hiemenz and R. Rajagopalan, *Principles of Colloid and Surface Chemistry*. New York: Marcel Dekker, 3<sup>rd</sup> ed., 1997.
- [55] W. A. Dietz, "Response factors for gas chromatographic analyses," *Journal of Gas Chromatography*, vol. 5, pp. 68–71, 1967.
- [56] J.-H. Zhou, Z.-J. Sui, J. Zhu, P. Li, D. Chen, Y.-C. Dai, and W.-K. Yuan, "Characterization of surface oxygen complexes on carbon nanofibers by TPD, XPS and FT-IR," *Carbon*, vol. 45, pp. 785–796, 2007.

# A. Chemicals

Chemical	Formula	State	Purity	Distributor
Acetone	C <sub>3</sub> H <sub>6</sub> O	l	Technical	VWR
Air	O <sub>2</sub> /N <sub>2</sub>	g	(5.0)	Yara
Argon	Ar	g	(5.0)	Yara
Carbon Black	C	s		Fuel Cell Store
Carbon Monoxide	CO	g		Yara
Carbon nanofibers	C	s	>99.9 %	Sigma-Aldrich
Chloroplatinic acid	H <sub>2</sub> PtCl <sub>6</sub> ·6H <sub>2</sub> O	s	ACS Reagent	Sigma-Aldrich
Dry Ice	CO <sub>2</sub>	s		Yara
Ethanol	C <sub>2</sub> H <sub>5</sub> OH	l	96 vol%	VWR
Ethylene Glycol	C <sub>2</sub> H <sub>4</sub> (OH) <sub>2</sub>	l	>99.5 %	Sigma-Aldrich
Graphite	C	s		Sigma-Aldrich
Sodium Hydroxide	NaOH	s	Analytical	VWR
Helium	He	g	(4.6)	Yara
Hydrochloric Acid	HCl	aq	37 %	Merck KGaA
Hydrogen	H <sub>2</sub>	g	(5.0)	Yara
Hydrogen in Argon	H <sub>2</sub> /Ar	g		Yara
Nafion	*	aq		
Nitrogen	N <sub>2</sub>	g	(5.0)	Yara
Nitrogen	N <sub>2</sub>	l		Yara
Propane	C <sub>3</sub> H <sub>8</sub>	g	(3.5)	Air Liquide
Sulfuric Acid	H <sub>2</sub> SO <sub>4</sub>	aq	95-97%	Sigma-Aldrich

\* Nafion is a sulfonated tetrafluoroethylene based fluoropolymer-copolymer with monomer formulas: C<sub>7</sub>HF<sub>13</sub>O<sub>5</sub>S·C<sub>2</sub>F<sub>4</sub>.

## B. Catalyst Synthesis Details

### Constants

Mass fraction of Pt in  $\text{H}_2\text{PtCl}_6 \cdot 6\text{H}_2\text{O} = 37.5 \text{ wt}\%$

### Stock Suspension 1

$$m_{\text{H}_2\text{PtCl}_6 \cdot 6\text{H}_2\text{O}} = 0.9366 \text{ g}$$

$$V_{EG} = 277 \text{ mL}$$

$$V_{\text{NaOH}(EG)} = 46 \text{ mL}$$

$$V_{Tot} = 319 \text{ mL (Measured)}$$

$$C_{Pt,Stock} = \frac{0.375 \cdot 0.9366 \text{ g}}{319 \text{ mL}} = 0.001101 \text{ g/mL}$$

### Stock Suspension 2

$$m_{\text{H}_2\text{PtCl}_6 \cdot 6\text{H}_2\text{O}} = 0.9249 \text{ g}$$

$$V_{EG} = 277 \text{ mL}$$

$$V_{\text{NaOH}(EG)} = 46 \text{ mL}$$

$$V_{Tot} = 308 \text{ mL (Measured)}$$

$$C_{Pt,Stock} = 0.001126 \text{ g/mL}$$

### 2% Pt/Vulcan

Stock: 1

$$V_{Stock} = 38.4 \text{ mL}$$

$$m_{Vulcan} = 2.0725 \text{ g}$$

$$V_{Ethanol,1} = 40 \text{ mL}$$

$$V_{Ethanol,2} = 20 \text{ mL}$$

$$V_{0.54\text{M}\text{HCl}} = 11.1 \text{ mL}$$

Assuming 100 % Pt deposition yield and no loss of support.

$$m_{Pt} = 0.001101 \text{ g/mL} \cdot 38.4 \text{ mL} = 0.04228 \text{ g}$$

$$x_{Pt} = \frac{0.04228 \text{ g}}{0.04228 \text{ g} + 2.0725 \text{ g}} = \underline{0.0200}$$

**Note:** Reported as the 2% Pt/Vulcan catalyst.



### 0.5% Pt/Vulcan - Attempt 1

Stock: 2

$$V_{Stock} = 10 \text{ mL}$$

$$m_{Vulcan} = 2.2441 \text{ g}$$

$$V_{Ethanol,1} = 40 \text{ mL}$$

$$V_{Ethanol,2} = 20 \text{ mL}$$

$$V_{0.54M HCl} = 11.1 \text{ mL}$$

$$x_{Pt} = 0.0050$$

**Note:** Stock suspension notably smaller in volume after heating. Unknown consequences. Discarded.

### 0.5% Pt/Vulcan - Attempt 2

Stock: 2

$$V_{Stock} = 10 \text{ mL}$$

$$V_{EG} = 24.4 \text{ mL}$$

$$V_{NaOH(EG)} = 4 \text{ mL}$$

$$m_{Vulcan} = 2.2449 \text{ g}$$

$$V_{Ethanol,1} = 40 \text{ mL}$$

$$V_{Ethanol,2} = 20 \text{ mL}$$

$$V_{0.54M HCl} = 11.1 \text{ mL}$$

$$x_{Pt} = 0.0050$$

**Note:** Reported as the 0.5% Pt/Vulcan catalyst.

### 0.5% Pt/CNF - Attempt 1

Stock: 2

$$V_{Stock} = 10 \text{ mL}$$

$$V_{EG} = 24.4 \text{ mL}$$

$$V_{NaOH(EG)} = 4 \text{ mL}$$

$$m_{CNF} = 2.2437 \text{ g}$$

$$V_{Ethanol,1} = 40 \text{ mL}$$

$$V_{Ethanol,2} = 20 \text{ mL}$$

$$V_{0.54M HCl} = 11.1 \text{ mL}$$

$$x_{Pt} = 0.0050$$

**Note:** Catalyst bed has noticeable dry spots after heating. Sample discarded.

### 0.5% Pt/Graphite

Stock: 2

$$V_{Stock} = 10 \text{ mL}$$

$$V_{EG} = 24.4 \text{ mL}$$

$$V_{NaOH(EG)} = 4 \text{ mL}$$

$$m_{Graphite} = 2.2434 \text{ g}$$

$$V_{Ethanol,1} = 40 \text{ mL}$$

$$V_{Ethanol,2} = 20 \text{ mL}$$

$$V_{0.54M HCl} = 11.1 \text{ mL}$$

$$x_{Pt} = 0.0050$$

**Note:** Reported as the 0.5% Pt/Graphite catalyst.

### 0.5% Pt/CNF - Attempt 2

Stock: 2

$$V_{Stock} = 10 \text{ mL}$$

$$V_{EG} = 40.8 \text{ mL}$$

$$V_{NaOH(EG)} = 6.8 \text{ mL}$$

$$m_{CNF} = 2.2428 \text{ g}$$

$$V_{Ethanol,1} = 60 \text{ mL}$$

$$V_{Ethanol,2} = 30 \text{ mL}$$

$$V_{0.54M HCl} = 16.7 \text{ mL}$$

$$x_{Pt} = \underline{0.0050}$$

**Note:** Instrumental failure. Sample discarded.

### 0.5% Pt/CNF - Attempt 3

Stock: 2

$$V_{Stock} = 10 \text{ mL}$$

$$V_{EG} = 40.8 \text{ mL}$$

$$V_{NaOH(EG)} = 6.8 \text{ mL}$$

$$m_{CNF} = 2.2405 \text{ g}$$

$$V_{Ethanol,1} = 60 \text{ mL}$$

$$V_{Ethanol,2} = 30 \text{ mL}$$

$$V_{0.54M HCl} = 16.7 \text{ mL}$$

$$x_{Pt} = \underline{0.0050}$$

**Note:** Instrumental failure. Sample discarded.

### 0.5% Pt/CNF - Attempt 4

Stock: 2

$$V_{Stock} = 10 \text{ mL}$$

$$V_{EG} = 40.8 \text{ mL}$$

$$V_{NaOH(EG)} = 6.8 \text{ mL}$$

$$m_{CNF} = 2.2456 \text{ g}$$

$$V_{Ethanol,1} = 60 \text{ mL}$$

$$V_{Ethanol,2} = 30 \text{ mL}$$

$$V_{0.54M HCl} = 16.7 \text{ mL}$$

$$x_{Pt} = \underline{0.0050}$$

**Note:** Reported as the 0.5% Pt/CNF catalyst.

### 0.5% Pt/Vulcan - Aged Suspension

Stock: 2

$$V_{Stock} = 10 \text{ mL}$$

$$V_{EG} = 24.4 \text{ mL}$$

$$V_{NaOH(EG)} = 4 \text{ mL}$$

$$m_{Vulcan} = 2.2438 \text{ g}$$

$$V_{Ethanol,1} = 40 \text{ mL}$$

$$V_{Ethanol,2} = 20 \text{ mL}$$

$$V_{0.54M HCl} = 11.1 \text{ mL}$$

$$x_{Pt} = \underline{0.0050}$$

**Note:** Reported as the 0.5% Pt/VulcanB catalyst.

### **0.5% Pt/Vulcan - HCl Effect 1**

Stock: 2

$$V_{Stock} = 10 \text{ mL}$$

$$V_{EG} = 24.4 \text{ mL}$$

$$V_{NaOH(EG)} = 4 \text{ mL}$$

$$m_{Vulcan} = 2.2419 \text{ g}$$

$$V_{Ethanol,1} = 40 \text{ mL}$$

$$V_{Ethanol,2} = 20 \text{ mL}$$

$$V_{0.54M HCl} = 11.1 \text{ mL}$$

$$x_{Pt} = 0.0050$$

**Note:** Reported as the 0.5% Pt/VulcanC catalyst.

### **0.5% Pt/Vulcan - HCl Effect 2**

Stock: 2

$$V_{Stock} = 10 \text{ mL}$$

$$V_{EG} = 24.4 \text{ mL}$$

$$V_{NaOH(EG)} = 4 \text{ mL}$$

$$m_{Vulcan} = 2.2451 \text{ g}$$

$$V_{Ethanol,1} = 40 \text{ mL}$$

$$V_{Ethanol,2} = 20 \text{ mL}$$

$$V_{0.54M HCl} = 16.7 \text{ mL}$$

$$x_{Pt} = 0.0050$$

**Note:** Reported as the 0.5% Pt/VulcanD catalyst.

### **0.5% Pt/Vulcan - HCl Effect 3**

Stock: 2

$$V_{Stock} = 10 \text{ mL}$$

$$V_{EG} = 24.4 \text{ mL}$$

$$V_{NaOH(EG)} = 4 \text{ mL}$$

$$m_{Vulcan} = 2.2419 \text{ g}$$

$$V_{Ethanol,1} = 40 \text{ mL}$$

$$V_{Ethanol,2} = 20 \text{ mL}$$

$$V_{0.54M HCl} = 22.2 \text{ mL}$$

$$x_{Pt} = 0.0050$$

**Note:** Reported as the 0.5% Pt/VulcanE catalyst.

## C. BET Measurements

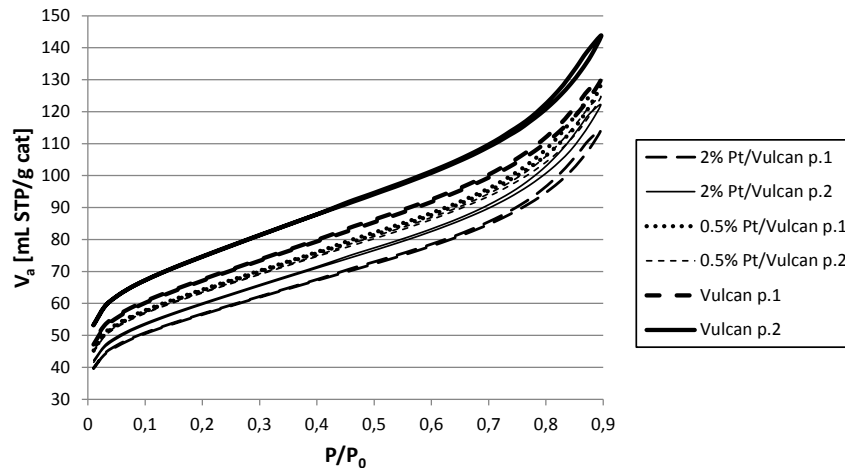
Weighed sample masses for the BET experiments are shown in Table C.1, calculated BET results are shown in Table C.2 and adsorption-desorption isotherms are shown in Fig. C.1.

Table C.1: BET Sample Masses

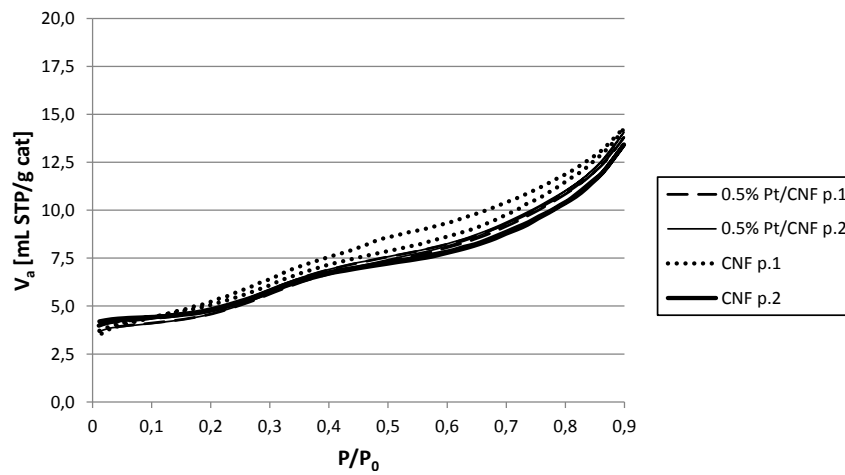
Sample	$m$ [mg]	
	Parallel 1	Parallel 2
2% Pt/Vulcan	131.9	144.8
0.5% Pt/Vulcan	194.1	173.3
Vulcan	108.2	60.3
0.5% Pt/CNF	73.8	65.6
CNF	39.6	42.9
0.5% Pt/Graphite	103.2	232.8
Graphite	270.3	321.3

Table C.2: BET Surface Area Results

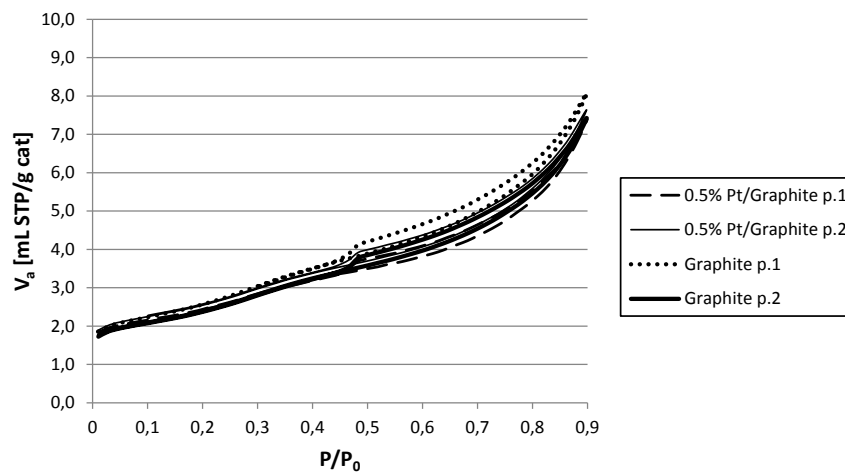
Sample	$\alpha$ [g/mL STP]	$\eta$ [g/mL STP]	$V_0$ [mL STP/g]	$S_{BET}$ [m <sup>2</sup> /g]
2% Pt/Vulcan p.1	0.0237	-0.0002	42.5375	185.1742
2% Pt/Vulcan p.2	0.0224	-0.0002	45.0005	195.8962
0.5% Pt/Vulcan p.1	0.0211	-0.0002	47.9374	208.6809
0.5% Pt/Vulcan p.2	0.0214	-0.0002	47.2921	205.8720
Vulcan p.1	0.0201	-0.0002	50.2805	218.8812
Vulcan p.2	0.0182	-0.0002	55.6791	242.3822
0.5% Pt/CNF p.1	0.2386	0.0027	4.1446	18.0423
0.5% Pt/CNF p.2	0.2373	0.0028	4.1652	18.1318
CNF p.1	0.2257	0.0031	4.3696	19.0217
CNF p.2	0.2482	0.0012	5.1415	22.3821
0.5% Pt/Graphite p.1	0.4975	0.0022	2.0014	8.7124
0.5% Pt/Graphite p.2	0.4752	0.0023	2.0943	9.1171
Graphite p.1	0.4567	0.0047	2.1670	9.4336
Graphite p.2	0.4956	0.0042	2.0010	8.7109



(a) Vulcan



(b) CNF



(c) Graphite

Figure C.1: Adsorption-desorption isotherms showing nitrogen adsorption-desorption on the vulcan supported catalysts and the untreated vulcan support (a), the 0.5% Pt/CNF catalyst and the untreated CNF support (b) and the 0.5% Pt/Graphite catalyst and the graphite support (c). Two parallels are shown for each sample.

## D. TGA Measurements

The thermograms produced by the TGA of the 2% Pt/Vulcan and the 0.5% Pt/Vulcan catalysts and the untreated vulcan support are shown in Figs. D.2 to D.8. A comparative plot of the thermograms is shown in Fig. D.1.

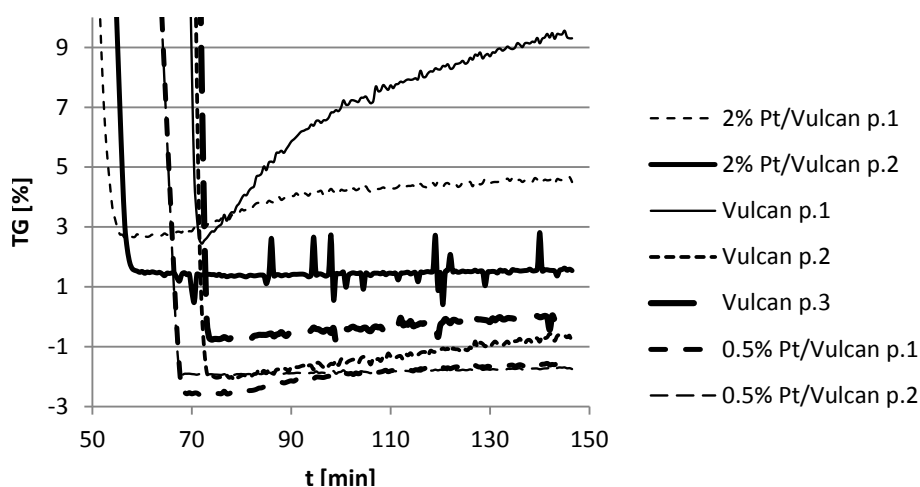


Figure D.1: Comparative thermograms for all TGA measurements, showing relative sample weight versus time. Atmosphere: 20 mL/min 20/80 O<sub>2</sub>/N<sub>2</sub> + 10 mL/min Ar. Temperature program: Roomtemperature to 900°C at 10°C/min.

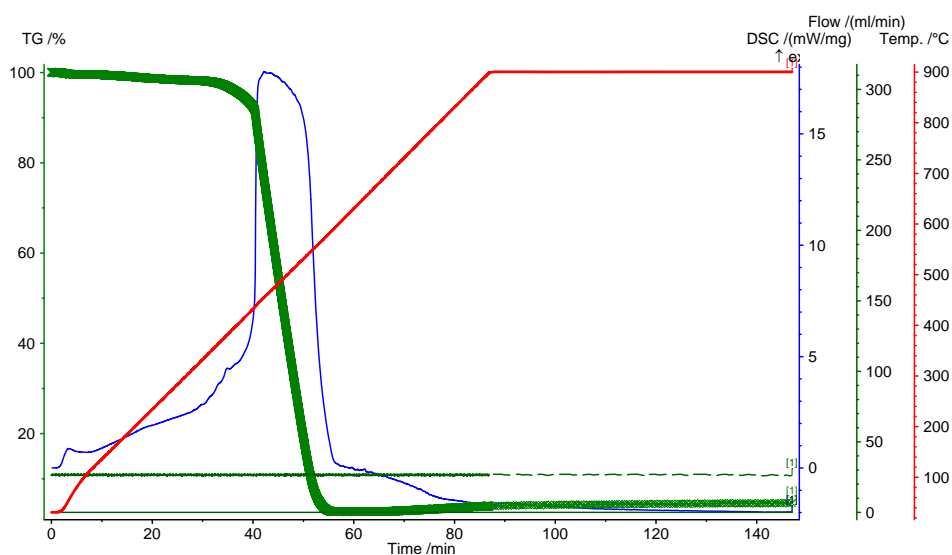


Figure D.2: Thermogram of the 2% Pt/Vulcan catalyst, parallel 1, showing relative sample weight, temperature, differential scanning calorimetry and gas flow as a function of time. Atmosphere: 20 mL/min 20/80 O<sub>2</sub>/N<sub>2</sub> + 10 mL/min Ar.

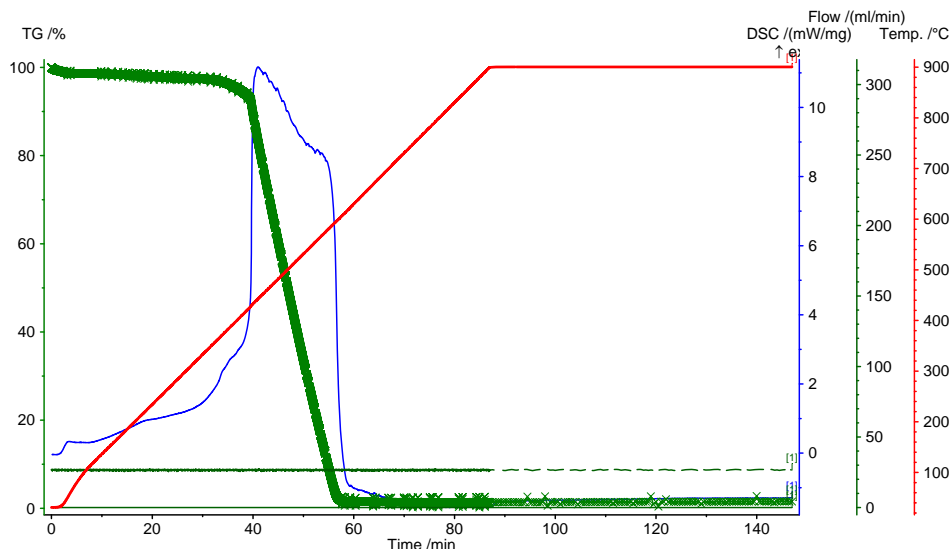


Figure D.3: Thermogram of the 2% Pt/Vulcan catalyst, parallel 2, showing relative sample weight, temperature, differential scanning calorimetry and gas flow as a function of time. Atmosphere: 20 mL/min 20/80 O<sub>2</sub>/N<sub>2</sub> + 10 mL/min Ar.

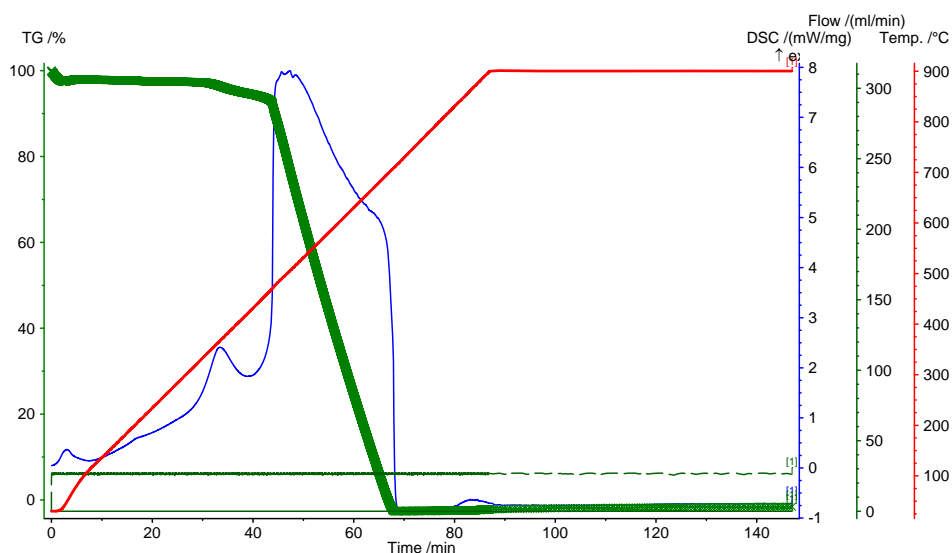


Figure D.4: Thermogram of the 0.5% Pt/Vulcan catalyst, parallel 1, showing relative sample weight, temperature, differential scanning calorimetry and gas flow as a function of time. Atmosphere: 20 mL/min 20/80 O<sub>2</sub>/N<sub>2</sub> + 10 mL/min Ar.

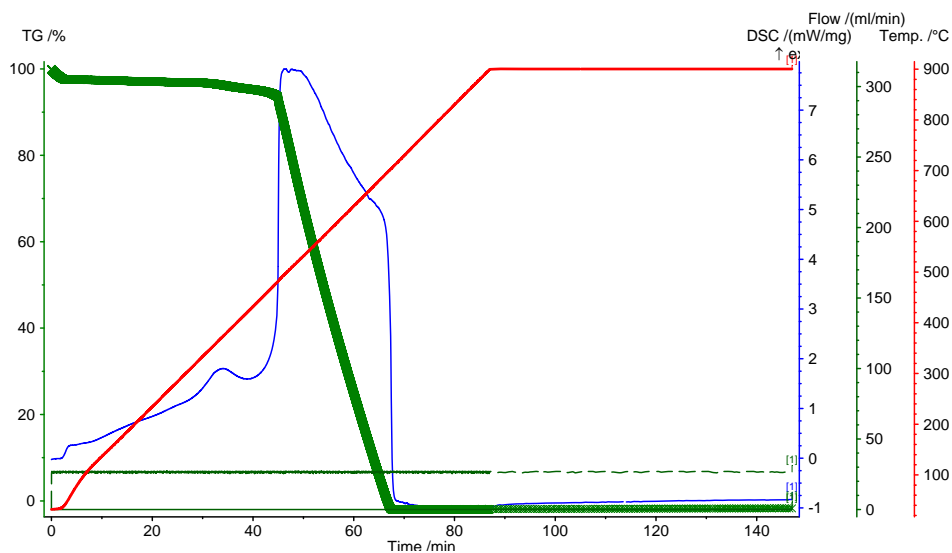


Figure D.5: Thermogram of the 0.5% Pt/Vulcan catalyst, parallel 2, showing relative sample weight, temperature, differential scanning calorimetry and gas flow as a function of time. Atmosphere: 20 mL/min 20/80 O<sub>2</sub>/N<sub>2</sub> + 10 mL/min Ar.

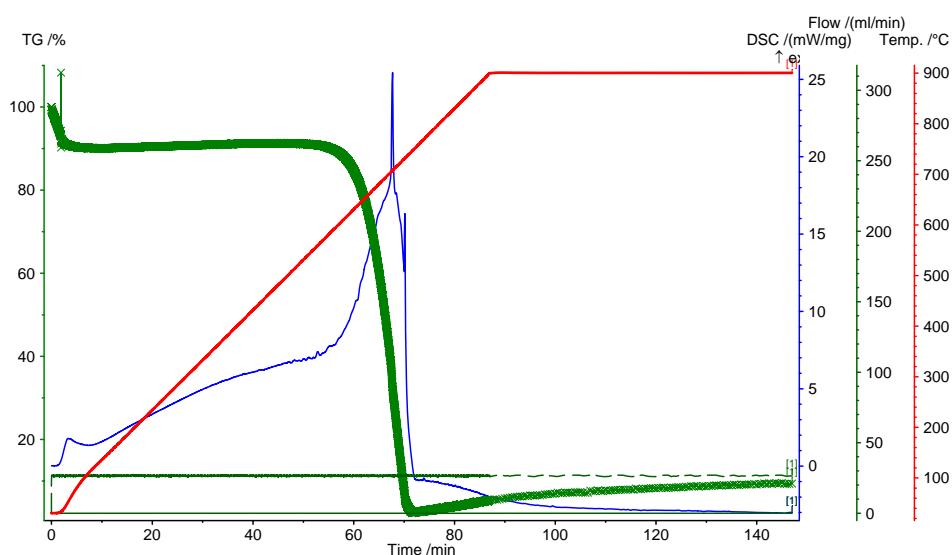


Figure D.6: Thermogram of the untreated vulcan support, parallel 1, showing relative sample weight, temperature, differential scanning calorimetry and gas flow as a function of time. Atmosphere: 20 mL/min 20/80 O<sub>2</sub>/N<sub>2</sub> + 10 mL/min Ar.



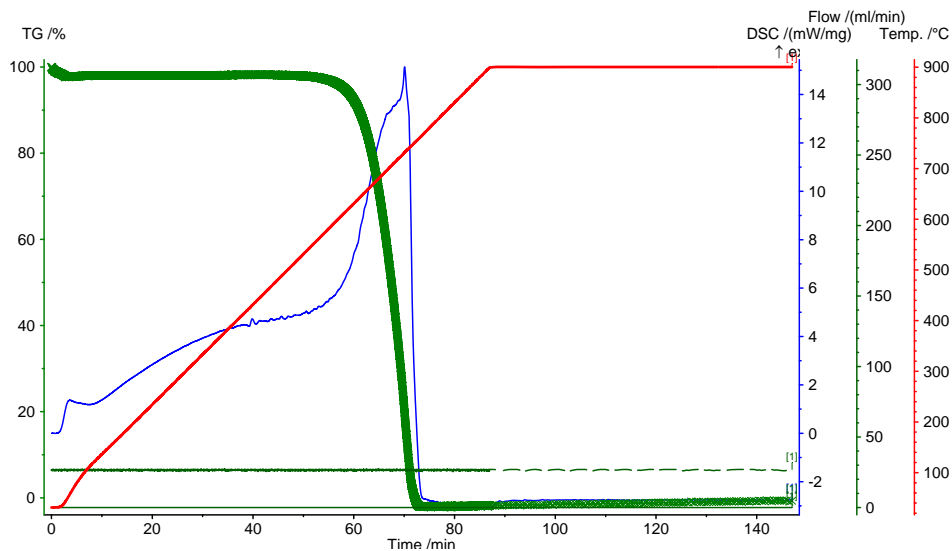


Figure D.7: Thermogram of the untreated vulcan support, parallel 2, showing relative sample weight, temperature, differential scanning calorimetry and gas flow as a function of time. Atmosphere: 20 mL/min 20/80 O<sub>2</sub>/N<sub>2</sub> + 10 mL/min Ar.

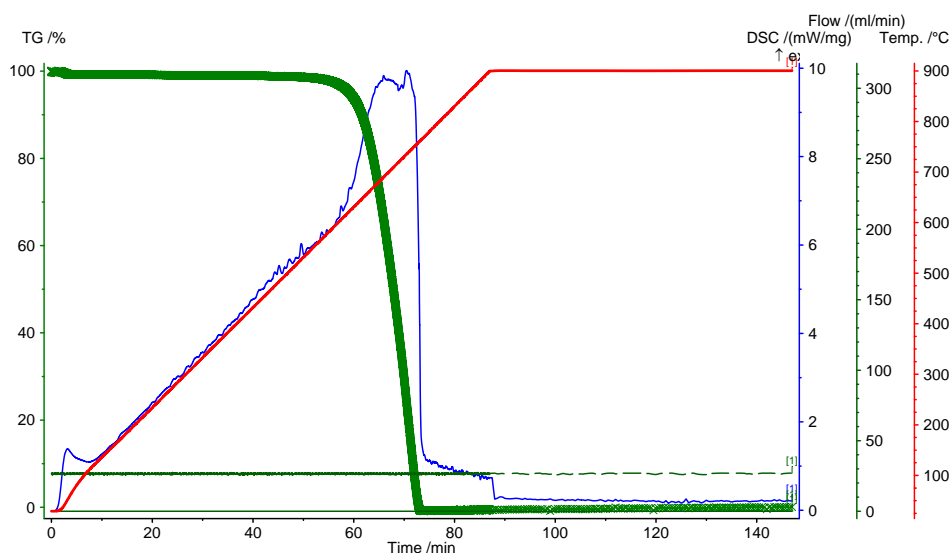


Figure D.8: Thermogram of the untreated vulcan support, parallel 3, showing relative sample weight, temperature, differential scanning calorimetry and gas flow as a function of time. Atmosphere: 20 mL/min 20/80 O<sub>2</sub>/N<sub>2</sub> + 10 mL/min Ar.

# E. Hydrogen Chemisorption Measurements

## E.1 Volumetric Method

Weighed sample masses for the volumetric chemisorption experiments are shown in Table E.1. The isotherms produced by the volumetric hydrogen chemisorption on the 2% Pt/Vulcan, 0.5% Pt/Vulcan and 0.5% Pt/CNF catalysts are shown in Fig. E.1. Calculated dispersions are shown in Table E.2.

*Table E.1: Volumetric Hydrogen Chemisorption Sample Masses*

Sample	$m$ [mg]
2% Pt/Vulcan p.1	203.3
2% Pt/Vulcan p.2	242.2
2% Pt/Vulcan p.3	200.0
0.5% Pt/Vulcan p.1	76.0
0.5% Pt/Vulcan p.2	77.5
0.5% Pt/CNF	65.1

*Table E.2: Calculated Monolayer Coverages and Dispersions*

Catalyst	$V_0$ [mL STP/g cat]		$D$ [%]	
	1 <sup>st</sup> Isotherm	Difference	1 <sup>st</sup> Isotherm	Difference
2% Pt/Vulcan p.1	0.2269	0.0119	19.7494	1.0322
2% Pt/Vulcan p.2	0.0627	-0.0049	5.4566	-0.4294
2% Pt/Vulcan p.3	0.4744	0.0601	41.2896	5.2313
0.5% Pt/Vulcan p.1	0.0011	-0.0239	0.0260	9.0639
0.5% Pt/Vulcan p.2	-0.0473	-0.0094	-16.4808	-3.2977
0.5% Pt/CNF	-0.0525	0.0784	18.2660	27.3266

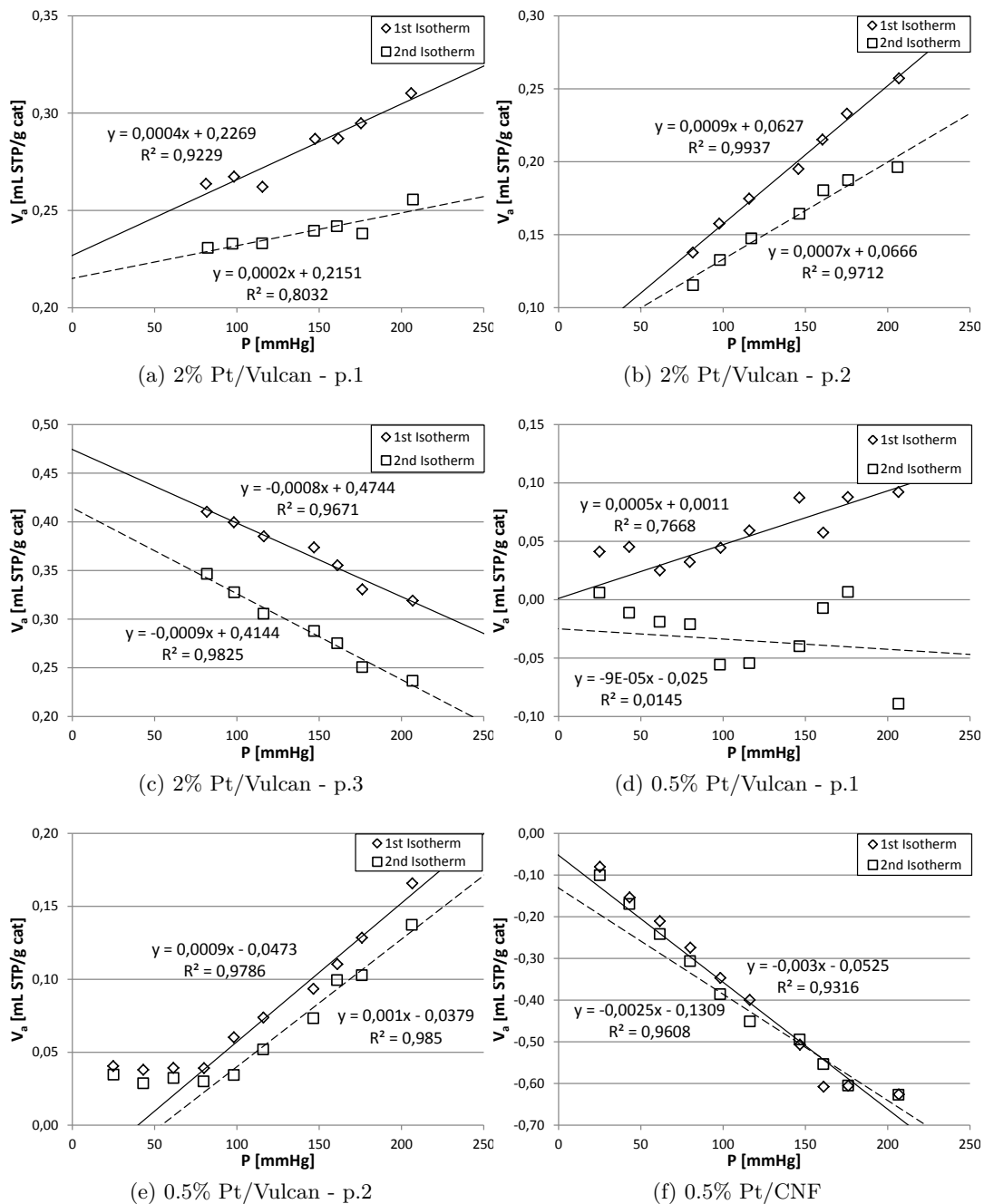


Figure E.1: Adsorption isotherms for volumetric chemisorption of  $H_2$  on the 2% Pt/Vulcan (a-c), 0.5% Pt/Vulcan and 0.5% Pt/CNF catalysts. Shown are both the first and second adsorption isotherms, both with linear regression lines, solid for the first, dashed for the second.

## E.2 Pulse Method

Pulse chemisorption data showing TCD responses versus pulse number for the various measurements are shown in Figs E.2 to E.4. Varied parameters are the pulse loop size (PLS), time between pulses ( $\Delta t$ ) and adsorption temperature ( $T$ ).

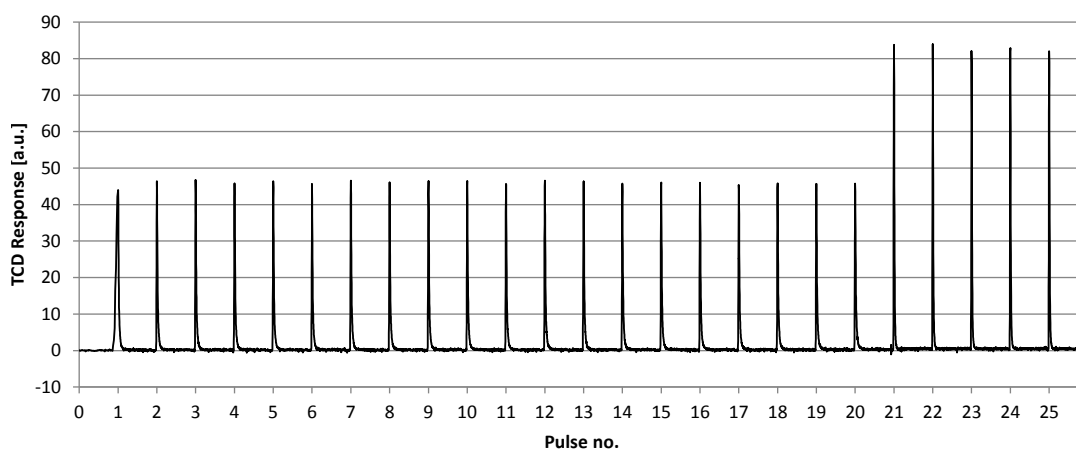


Figure E.2: Pulse data showing hydrogen pulse chemisorption on the 0.5% Pt/Vulcan catalyst. 20 adsorption pulses (left) and 5 calibration pulses (right) are shown.  $PLS = 500 \mu L$ ,  $\Delta t = 200 s$ ,  $T = 35^\circ C$ .

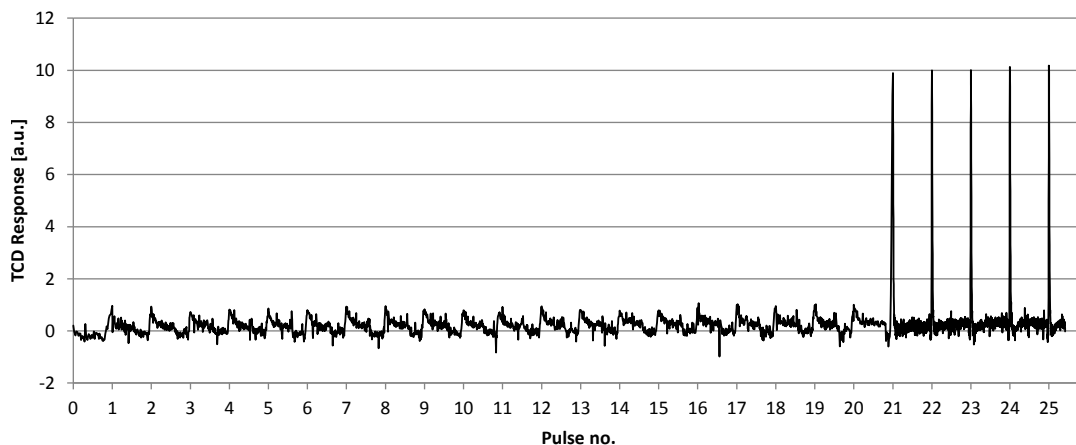


Figure E.3: Pulse data showing hydrogen pulse chemisorption on the 0.5% Pt/Vulcan catalyst. 20 adsorption pulses (left) and 5 calibration pulses (right) are shown.  $PLS = 50 \mu L$ ,  $\Delta t = 80 s$ ,  $T = 35^\circ C$ .

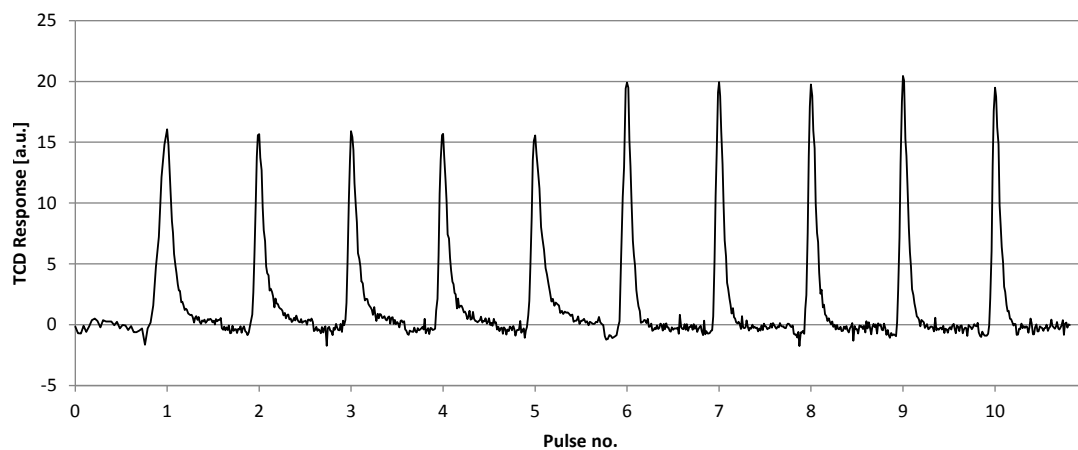


Figure E.4: Pulse data showing hydrogen pulse chemisorption on the a blank quartz wool sample. 5 adsorption pulses (left) and 5 calibration pulses (right) are shown.  $PLS = 50 \mu L$ ,  $\Delta t = 80 s$ ,  $T = 35^\circ C$ .

# F. CO Stripping Voltammetry Measurements

For all measurements, the catalyst was dispersed in water at 1 mg/mL concentration, and 30  $\mu\text{L}$  of ink was twice deposited on the electrode, making the sample mass 60  $\mu\text{g}$ . CO stripping peaks subtracted the second cycle baselines are shown in Figs. F.1 to F.3 with raw signal in black and smoothed signal in red. Calculated values are shown in Table F.1.

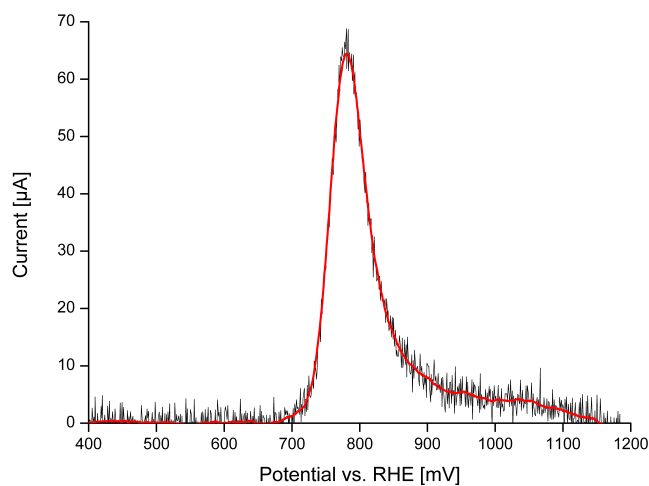


Figure F.1: CO stripping voltammetric peak of the 2% Pt/Vulcan catalyst. Conditions:  $v=10$  mV/s, adsorption at 50 mV, 0.5 M  $\text{H}_2\text{SO}_4$  electrolyte.

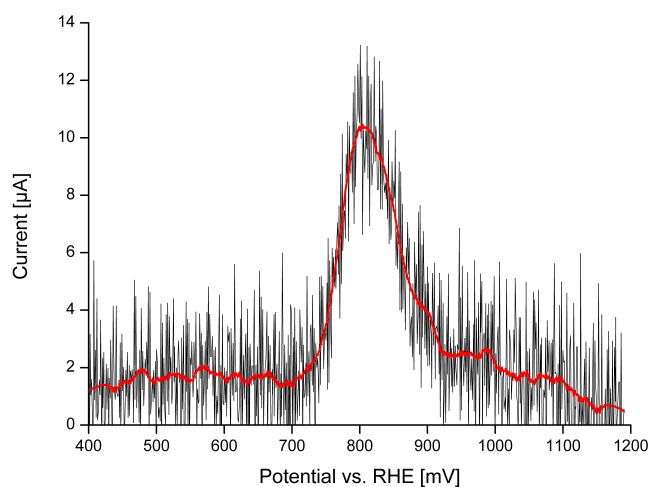


Figure F.2: CO stripping voltammetric peak of the 0.5% Pt/Vulcan catalyst. Conditions:  $v=10$  mV/s, adsorption at 50 mV, 0.5 M  $\text{H}_2\text{SO}_4$  electrolyte.

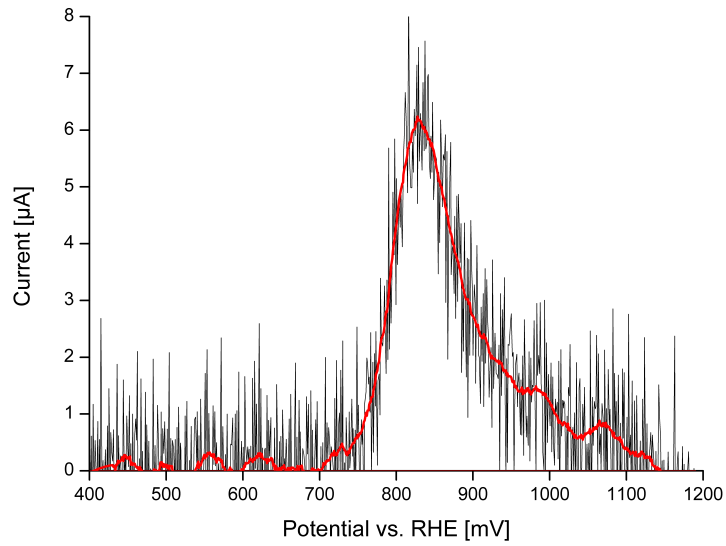


Figure F.3: CO stripping voltammetric peak of the 0.5% Pt/Graphite catalyst. Conditions:  $v=10$  mV/s, adsorption at 50 mV, 0.5 M  $H_2SO_4$  electrolyte.

Table F.1: CO Stripping Voltammetry Calculations

Catalyst	Area [ $\mu W$ ]	$Q_{CO}$ [ $\mu C$ ]	$S_{CO}$ [ $cm^2$ ]	$n_s$ [nmol]	$D$ [%]
2% Pt/Vulcan	6.0805	608.05	1.4477	3.0051	48.85
0.5% Pt/Vulcan	1.2533	125.33	0.2984	0.6193	40.28
0.5% Pt/Graphite	0.8654	86.54	0.2060	0.4277	27.81

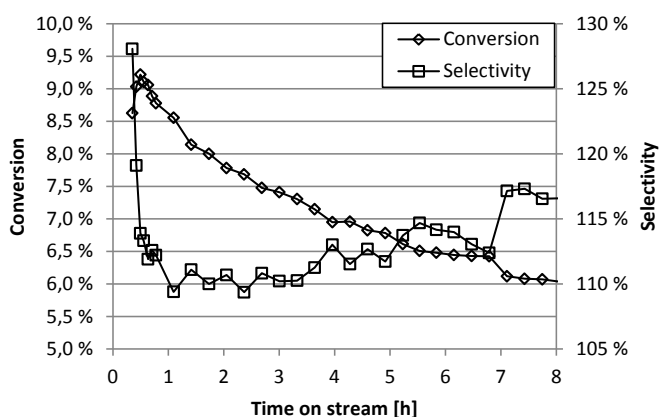
# G. Activity Measurements

## G.1 Experimental Raw Data

The following is conversion and selectivity data as well as experimental conditions for every activity measurement performed.

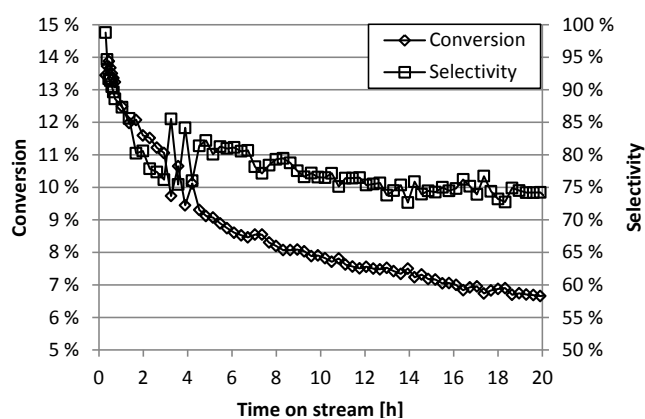
2% Pt/Vulcan w/o dilution

Conditions	
$m_{Cat}$ [mg]	55.2
$m_{SiC}$ [mg]	0
$P_{Drop}$ [bar]	1.8
$t_{Total}$ [h]	8
$T$ [°C]	500
$F_0$ [mL STP/min]	
H <sub>2</sub>	5
C <sub>3</sub> H <sub>8</sub>	20
N <sub>2</sub>	25



2% Pt/Vulcan w/ dilution - Parallel 1

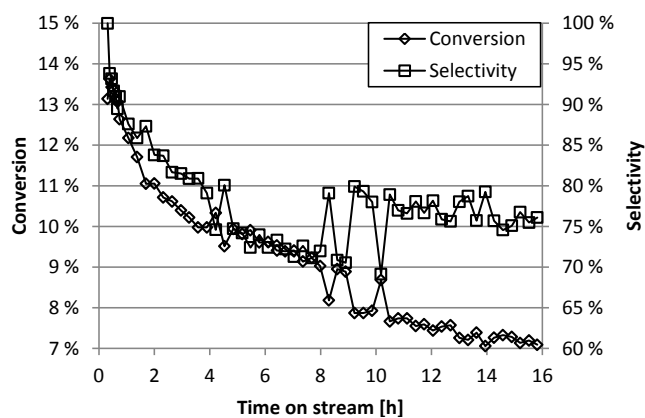
Conditions	
$m_{Cat}$ [mg]	46.7
$m_{SiC}$ [mg]	199.3
$P_{Drop}$ [bar]	0.25
$t_{Total}$ [h]	20
$T$ [°C]	500
$F_0$ [mL STP/min]	
H <sub>2</sub>	5
C <sub>3</sub> H <sub>8</sub>	20
N <sub>2</sub>	25





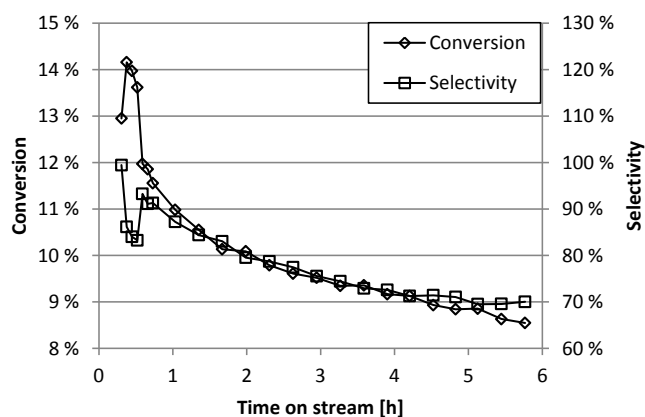
### 2% Pt/Vulcan w/ dilution - Parallel 2

Conditions	
$m_{Cat}$ [mg]	49.1
$m_{SiC}$ [mg]	198.3
$P_{Drop}$ [bar]	0.45
$t_{Total}$ [h]	16
$T$ [°C]	500
$F_0$ [mL STP/min]	
H <sub>2</sub>	5
C <sub>3</sub> H <sub>8</sub>	20
N <sub>2</sub>	25



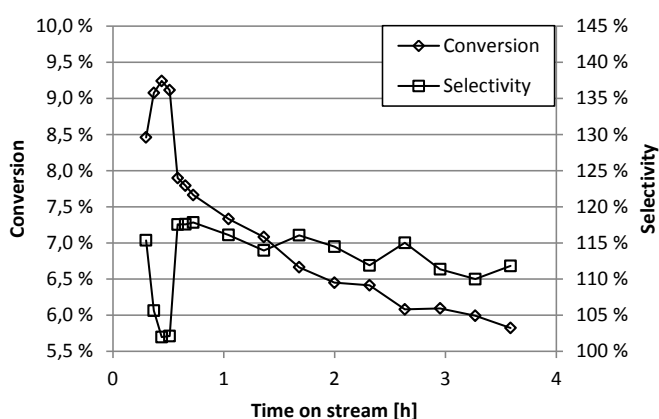
### 2% Pt/Vulcan w/ dilution - Parallel 3

Conditions	
$m_{Cat}$ [mg]	48.2
$m_{SiC}$ [mg]	204.1
$P_{Drop}$ [bar]	0.25
$t_{Total}$ [h]	6
$T$ [°C]	500
$F_0$ [mL STP/min]	
H <sub>2</sub>	5
C <sub>3</sub> H <sub>8</sub>	20
N <sub>2</sub>	25



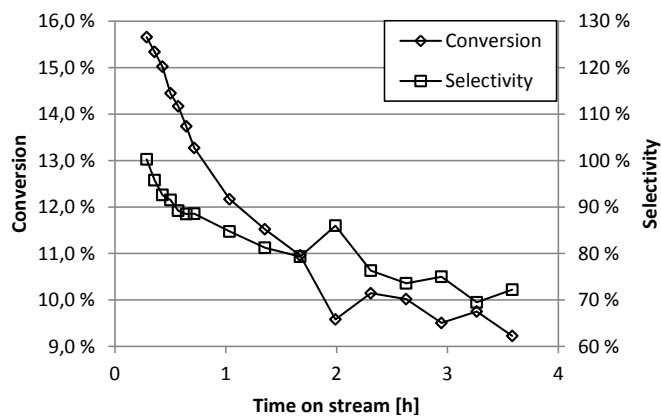
### 2% Pt/Vulcan w/ dilution - 475 °C

Conditions	
$m_{Cat}$ [mg]	51.1
$m_{SiC}$ [mg]	232.8
$P_{Drop}$ [bar]	0.55
$t_{Total}$ [h]	4
$T$ [°C]	475
$F_0$ [mL STP/min]	
H <sub>2</sub>	5
C <sub>3</sub> H <sub>8</sub>	20
N <sub>2</sub>	25



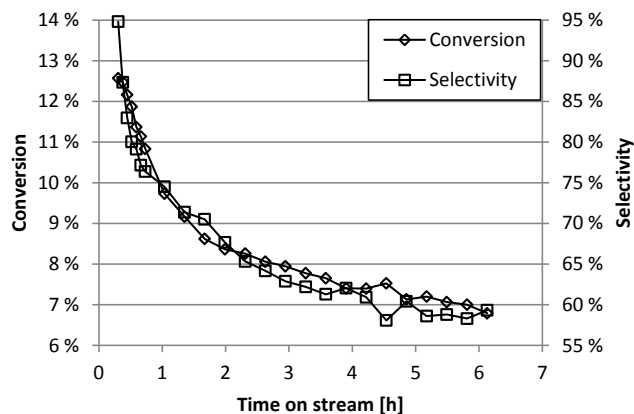
2% Pt/Vulcan w/ dilution - 525 °C

Conditions	
$m_{Cat}$ [mg]	52.4
$m_{SiC}$ [mg]	201.5
$P_{Drop}$ [bar]	0.45
$t_{Total}$ [h]	4
$T$ [°C]	525
$F_0$ [mL STP/min]	
H <sub>2</sub>	5
C <sub>3</sub> H <sub>8</sub>	20
N <sub>2</sub>	25



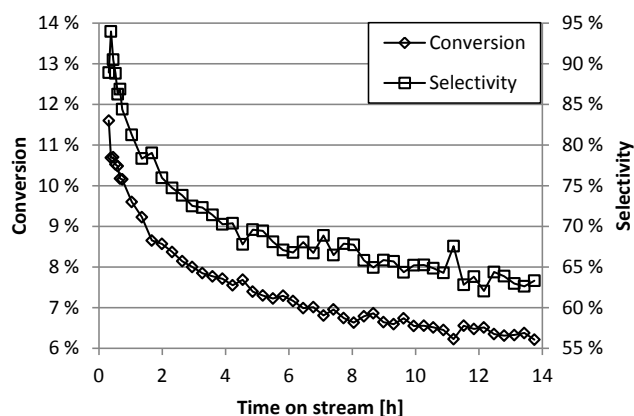
0.5% Pt/Vulcan - Parallel 1

Conditions	
$m_{Cat}$ [mg]	51.6
$m_{SiC}$ [mg]	199.5
$P_{Drop}$ [bar]	0.25
$t_{Total}$ [h]	7
$T$ [°C]	500
$F_0$ [mL STP/min]	
H <sub>2</sub>	5
C <sub>3</sub> H <sub>8</sub>	20
N <sub>2</sub>	25



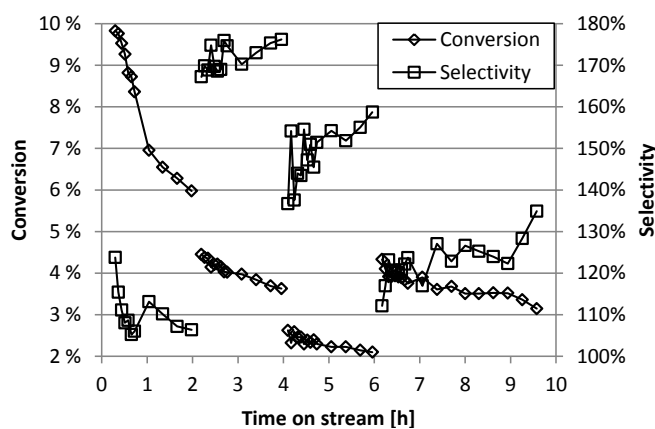
0.5% Pt/Vulcan - Parallel 2

Conditions	
$m_{Cat}$ [mg]	50.5
$m_{SiC}$ [mg]	198.3
$P_{Drop}$ [bar]	0.25
$t_{Total}$ [h]	14
$T$ [°C]	500
$F_0$ [mL STP/min]	
H <sub>2</sub>	5
C <sub>3</sub> H <sub>8</sub>	20
N <sub>2</sub>	25



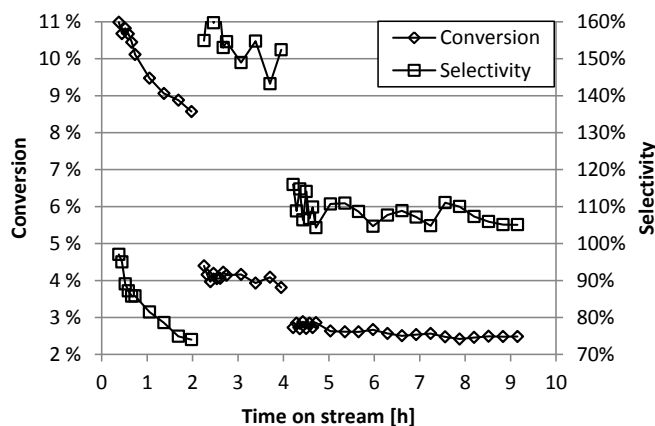
### 0.5% Pt/Vulcan - Flow, w/o intermediate flushing

Conditions	
$m_{Cat}$ [mg]	52.9
$m_{SiC}$ [mg]	199.8
$P_{Drop}$ [bar]	0.2, 0.25, 0.3
$t_{Total}$ [h]	10
$T$ [°C]	500
$F_0$ [mL STP/min]	
H <sub>2</sub>	5, 7.5, 10
C <sub>3</sub> H <sub>8</sub>	20, 30, 40
N <sub>2</sub>	25, 37.5, 50



### 0.5% Pt/Vulcan - Flow, w/75 mL/min N<sub>2</sub> flushing

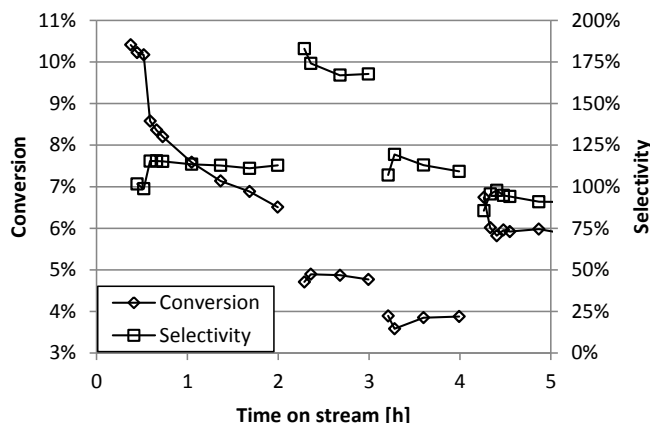
Conditions	
$m_{Cat}$ [mg]	49.8
$m_{SiC}$ [mg]	207.2
$P_{Drop}$ [bar]	0.2, 0.3, 0.4
$t_{Total}$ [h]	10
$T$ [°C]	500
$F_0$ [mL STP/min]	
H <sub>2</sub>	5, 7.5, 10
C <sub>3</sub> H <sub>8</sub>	20, 30, 40
N <sub>2</sub>	25, 37.5, 50



**Note:** Clear deactivation between 50 and 75 mL/min. Experiment aborted and discarded. Flushing technique changed.

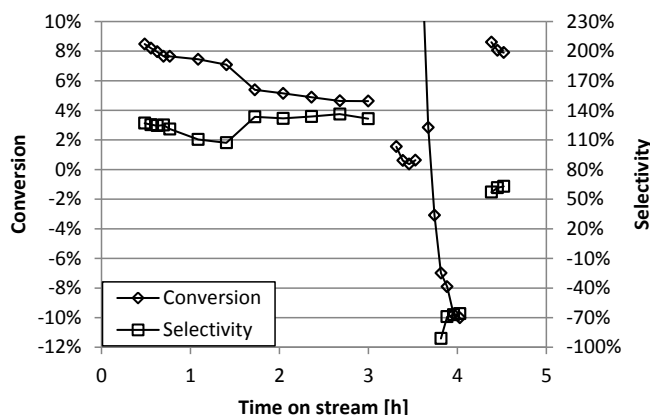
### 0.5% Pt/Vulcan - Flow, w/100 mL/min 35/65 v/v H<sub>2</sub>/N<sub>2</sub> flushing

Conditions	
$m_{Cat}$ [mg]	52.1
$m_{SiC}$ [mg]	211.8
$P_{Drop}$ [bar]	0.4, 0.6, 0.8
$t_{Total}$ [h]	6
$T$ [°C]	500
$F_0$ [mL STP/min]	
H <sub>2</sub>	5, 7.5, 10
C <sub>3</sub> H <sub>8</sub>	20, 30, 40
N <sub>2</sub>	25, 37.5, 50



### 0.5% Pt/Vulcan - H<sub>2</sub> Power - w/o intermediate flushing

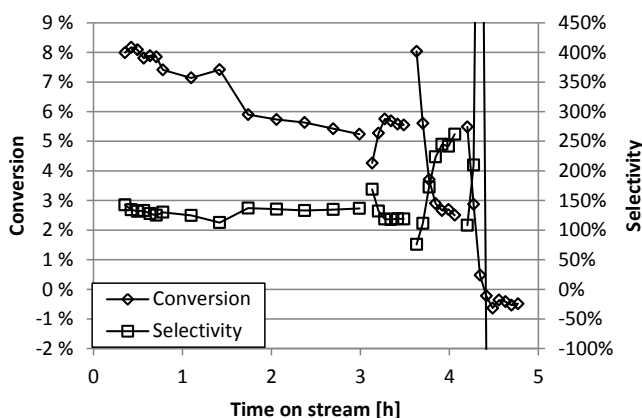
Conditions	
$m_{Cat}$ [mg]	50.3
$m_{SiC}$ [mg]	211.6
$P_{Drop}$ [bar]	0.3
$t_{Total}$ [h]	5
$T$ [°C]	500
$F_0$ [mL STP/min]	
H <sub>2</sub>	5, 10, 15, 20
C <sub>3</sub> H <sub>8</sub>	20
N <sub>2</sub>	25, 20, 15, 10



**Note:** Unusable results. Experiment discarded. Concentrations and time between transitions changed.

### 0.5% Pt/Vulcan - H<sub>2</sub> Power - w/o intermediate flushing

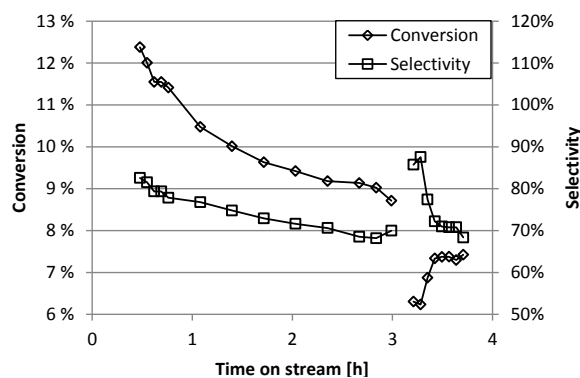
Conditions	
$m_{Cat}$ [mg]	53.3
$m_{SiC}$ [mg]	203.0
$P_{Drop}$ [bar]	0.6
$t_{Total}$ [h]	5
$T$ [°C]	500
$F_0$ [mL STP/min]	
H <sub>2</sub>	5, 3.5, 7, 10
C <sub>3</sub> H <sub>8</sub>	20
N <sub>2</sub>	25, 26.5, 23, 20



**Note:** Last data set discarded. Rest reported.

### 0.5% Pt/Vulcan - H<sub>2</sub> Power - w/50 mL/min 70/30 v/v H<sub>2</sub>/N<sub>2</sub> flushing

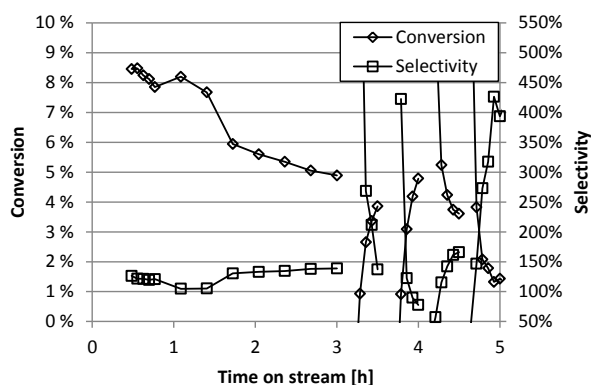
Conditions	
$m_{Cat}$ [mg]	50.4
$m_{SiC}$ [mg]	202.5
$P_{Drop}$ [bar]	0.3
$t_{Total}$ [h]	4
$T$ [°C]	500
$F_0$ [mL STP/min]	
H <sub>2</sub>	5, 3.5
C <sub>3</sub> H <sub>8</sub>	20
N <sub>2</sub>	25, 26.5



**Note:** Visible deactivation during transition. Experiment aborted and discarded.

### 0.5% Pt/Vulcan - C<sub>3</sub>H<sub>8</sub> Power - w/o intermediate flushing

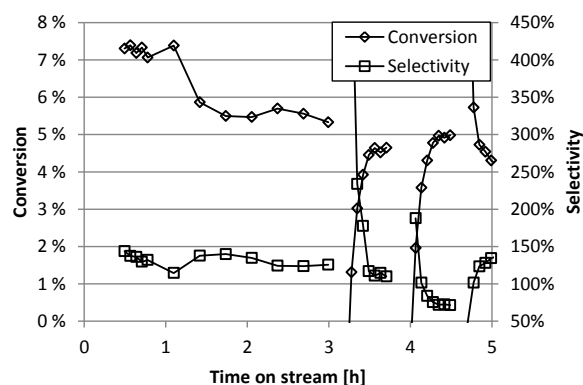
Conditions	
$m_{Cat}$ [mg]	51.4
$m_{SiC}$ [mg]	204.0
$P_{Drop}$ [bar]	0.6
$t_{Total}$ [h]	5
$T$ [°C]	500
$F_0$ [mL STP/min]	
H <sub>2</sub>	5
C <sub>3</sub> H <sub>8</sub>	20, 15, 10, 25, 30
N <sub>2</sub>	25, 30, 35, 20, 15



**Note:** Steady states not reached. Experiment discarded. Time between transitions changed.

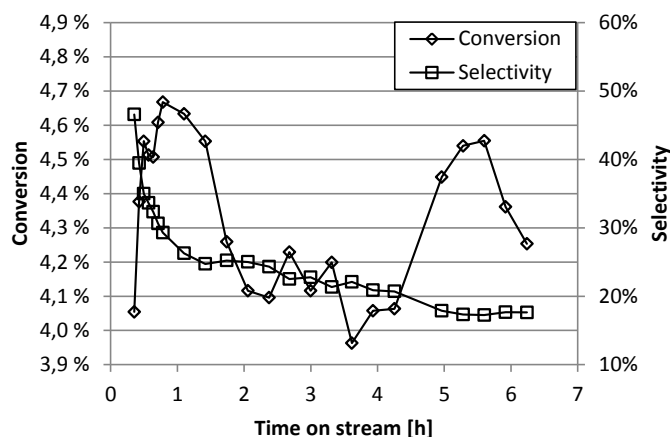
### 0.5% Pt/Vulcan - C<sub>3</sub>H<sub>8</sub> Power - w/o intermediate flushing

Conditions	
$m_{Cat}$ [mg]	51.8
$m_{SiC}$ [mg]	199.7
$P_{Drop}$ [bar]	0.6
$t_{Total}$ [h]	6
$T$ [°C]	500
$F_0$ [mL STP/min]	
H <sub>2</sub>	5
C <sub>3</sub> H <sub>8</sub>	20, 15, 10, 25, 30
N <sub>2</sub>	25, 30, 35, 20, 15



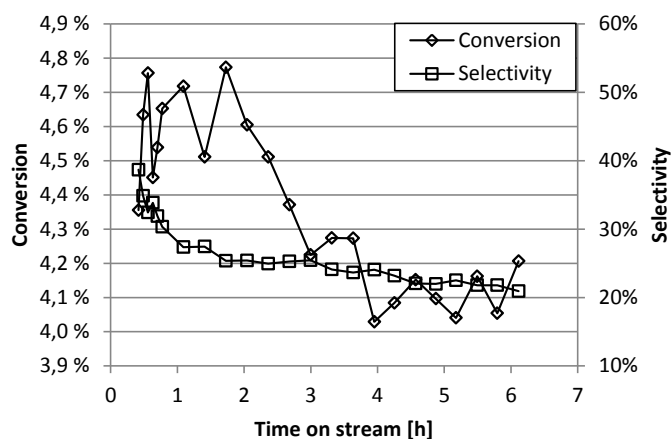
### 0.5% Pt/CNF - Parallel 1

Conditions	
$m_{Cat}$ [mg]	52.3
$m_{SiC}$ [mg]	218.2
$P_{Drop}$ [bar]	<0.2
$t_{Total}$ [h]	7
$T$ [°C]	500
$F_0$ [mL STP/min]	
H <sub>2</sub>	5
C <sub>3</sub> H <sub>8</sub>	20
N <sub>2</sub>	25



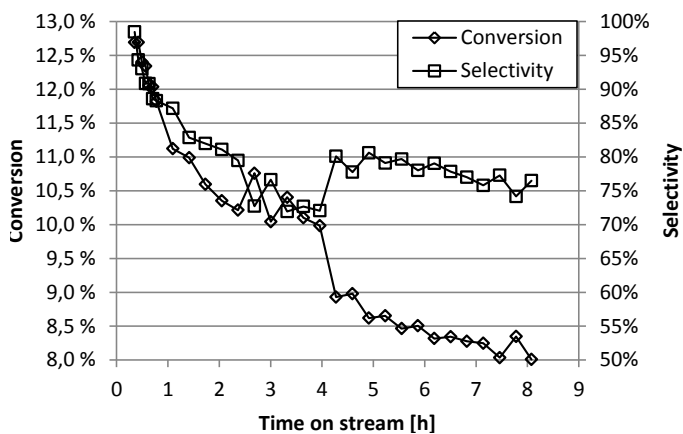
### 0.5% Pt/CNF - Parallel 2

Conditions	
$m_{Cat}$ [mg]	52.3
$m_{SiC}$ [mg]	0
$P_{Drop}$ [bar]	<0.2
$t_{Total}$ [h]	7
$T$ [°C]	500
$F_0$ [mL STP/min]	
H <sub>2</sub>	5
C <sub>3</sub> H <sub>8</sub>	20
N <sub>2</sub>	25



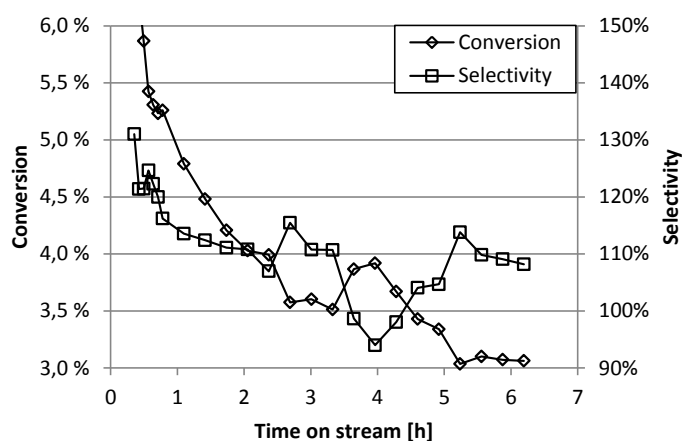
### 0.5% Pt/VulcanB - Parallel 1

Conditions	
$m_{Cat}$ [mg]	53.1
$m_{SiC}$ [mg]	487.0
$P_{Drop}$ [bar]	1.2
$t_{Total}$ [h]	9
$T$ [°C]	500
$F_0$ [mL STP/min]	
H <sub>2</sub>	5
C <sub>3</sub> H <sub>8</sub>	20
N <sub>2</sub>	25



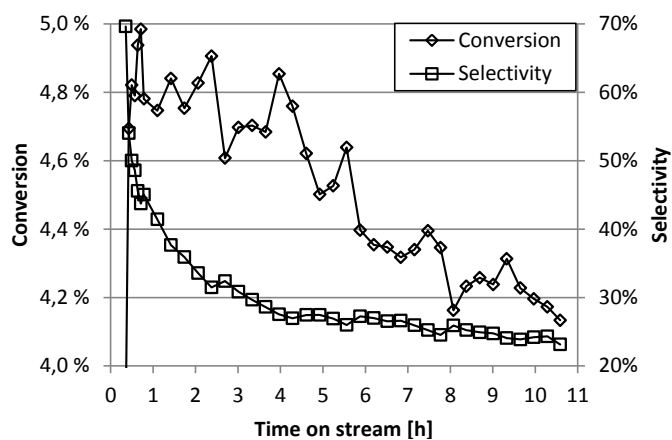
### 0.5% Pt/VulcanB - Parallel 2

Conditions	
$m_{Cat}$ [mg]	25.2
$m_{SiC}$ [mg]	228.3
$P_{Drop}$ [bar]	0.25
$t_{Total}$ [h]	7
$T$ [°C]	500
$F_0$ [mL STP/min]	
H <sub>2</sub>	5
C <sub>3</sub> H <sub>8</sub>	20
N <sub>2</sub>	25



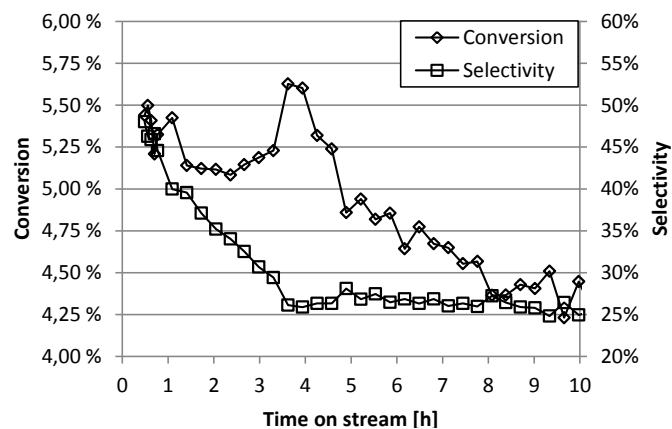
### 0.5% Pt/Graphite - Parallel 1

Conditions	
$m_{Cat}$ [mg]	51.1
$m_{SiC}$ [mg]	212.8
$P_{Drop}$ [bar]	0.5
$t_{Total}$ [h]	11
$T$ [°C]	500
$F_0$ [mL STP/min]	
H <sub>2</sub>	5
C <sub>3</sub> H <sub>8</sub>	20
N <sub>2</sub>	25



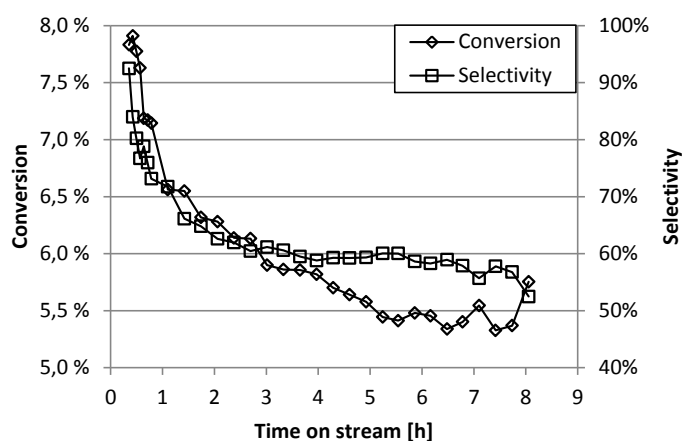
### 0.5% Pt/Graphite - Parallel 2

Conditions	
$m_{Cat}$ [mg]	53.3
$m_{SiC}$ [mg]	257.6
$P_{Drop}$ [bar]	0.5
$t_{Total}$ [h]	11
$T$ [°C]	500
$F_0$ [mL STP/min]	
H <sub>2</sub>	5
C <sub>3</sub> H <sub>8</sub>	20
N <sub>2</sub>	25



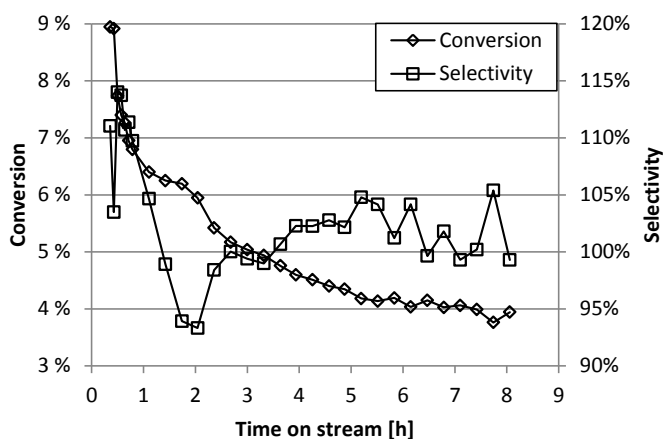
### 0.5% Pt/VulcanC

Conditions	
$m_{Cat}$ [mg]	30.2
$m_{SiC}$ [mg]	265.2
$P_{Drop}$ [bar]	<0.2
$t_{Total}$ [h]	8
$T$ [°C]	500
$F_0$ [mL STP/min]	
H <sub>2</sub>	5
C <sub>3</sub> H <sub>8</sub>	20
N <sub>2</sub>	25



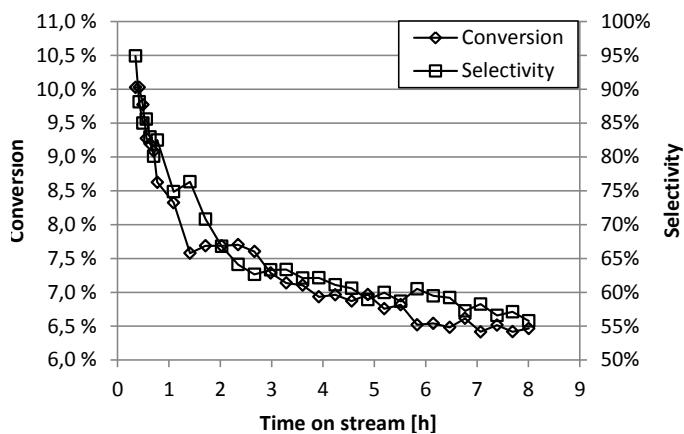
### 0.5% Pt/VulcanD

Conditions	
$m_{Cat}$ [mg]	32.6
$m_{SiC}$ [mg]	268.7
$P_{Drop}$ [bar]	0.5
$t_{Total}$ [h]	8
$T$ [°C]	500
$F_0$ [mL STP/min]	
H <sub>2</sub>	5
C <sub>3</sub> H <sub>8</sub>	20
N <sub>2</sub>	25



### 0.5% Pt/VulcanE

Conditions	
$m_{Cat}$ [mg]	31.2
$m_{SiC}$ [mg]	311.1
$P_{Drop}$ [bar]	0.3
$t_{Total}$ [h]	8
$T$ [°C]	500
$F_0$ [mL STP/min]	
H <sub>2</sub>	5
C <sub>3</sub> H <sub>8</sub>	20
N <sub>2</sub>	25



### Supports

Vulcan Conditions	
$m_{Cat}$ [mg]	10.5
$m_{SiC}$ [mg]	213.6
$P_{Drop}$ [bar]	0.25
$t_{Total}$ [h]	2
$T$ [°C]	500
$F_0$ [mL STP/min]	
H <sub>2</sub>	5
C <sub>3</sub> H <sub>8</sub>	20
N <sub>2</sub>	25

CNF Conditions	
$m_{Cat}$ [mg]	17.2
$m_{SiC}$ [mg]	178.5
$P_{Drop}$ [bar]	<0.2
$t_{Total}$ [h]	2
$T$ [°C]	500
$F_0$ [mL STP/min]	
H <sub>2</sub>	5
C <sub>3</sub> H <sub>8</sub>	20
N <sub>2</sub>	25

Graphite Conditions	
$m_{Cat}$ [mg]	33.2
$m_{SiC}$ [mg]	273.2
$P_{Drop}$ [bar]	0.35
$t_{Total}$ [h]	2
$T$ [°C]	500
$F_0$ [mL STP/min]	
H <sub>2</sub>	5
C <sub>3</sub> H <sub>8</sub>	20
N <sub>2</sub>	25



## G.2 Deactivation Model

Using the reaction rate data for the 0.5% Pt/Vulcan catalyst shown in Fig. 4.14 and subtracting the values from the regression curves, residual plots are formed and shown in Fig. G.1.

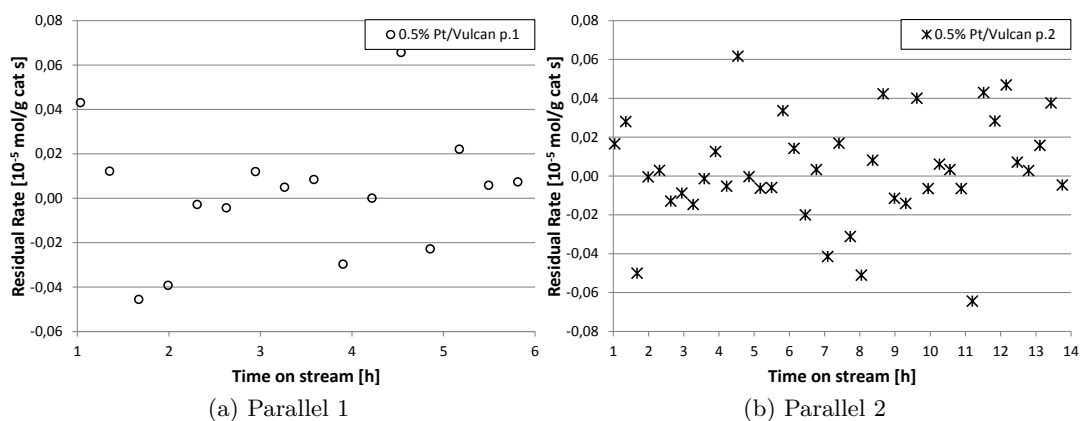


Figure G.1: Residual plots from the deactivation models for the 0.5% Pt/Vulcan catalyst. Two parallels are shown.

### G.3 Kinetic Study

The power law plots are generated with the following procedure. 1.) Measure the conversion at various compositions. 2.) Remove non-steady-state data. 3.) Convert to reaction rate and correct for deactivation. 4.) Average the measurements, make relative to the lowest partial pressure, and plot on a log-log scale. Progressive plots are shown for  $H_2$  in Fig. G.2 and  $C_3H_8$  in Fig. G.3.

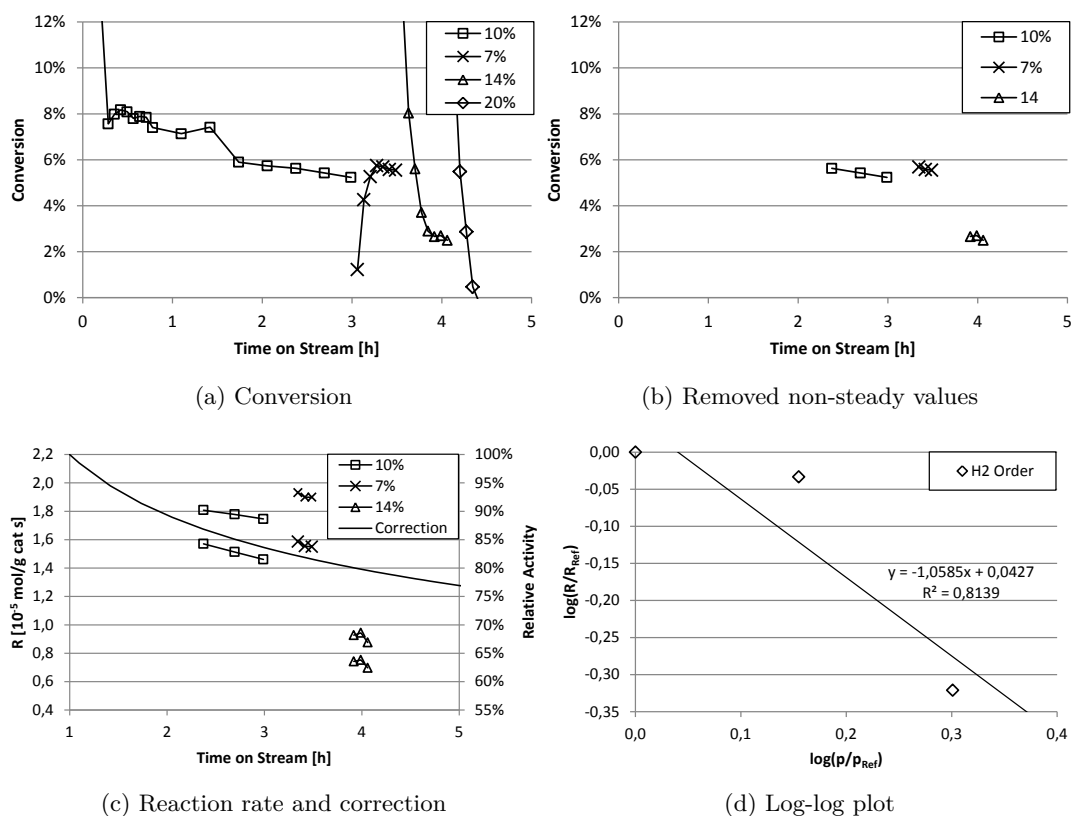


Figure G.2: Progressive plots for the  $H_2$  kinetic study on the 0.5% Pt/Vulcan catalyst.

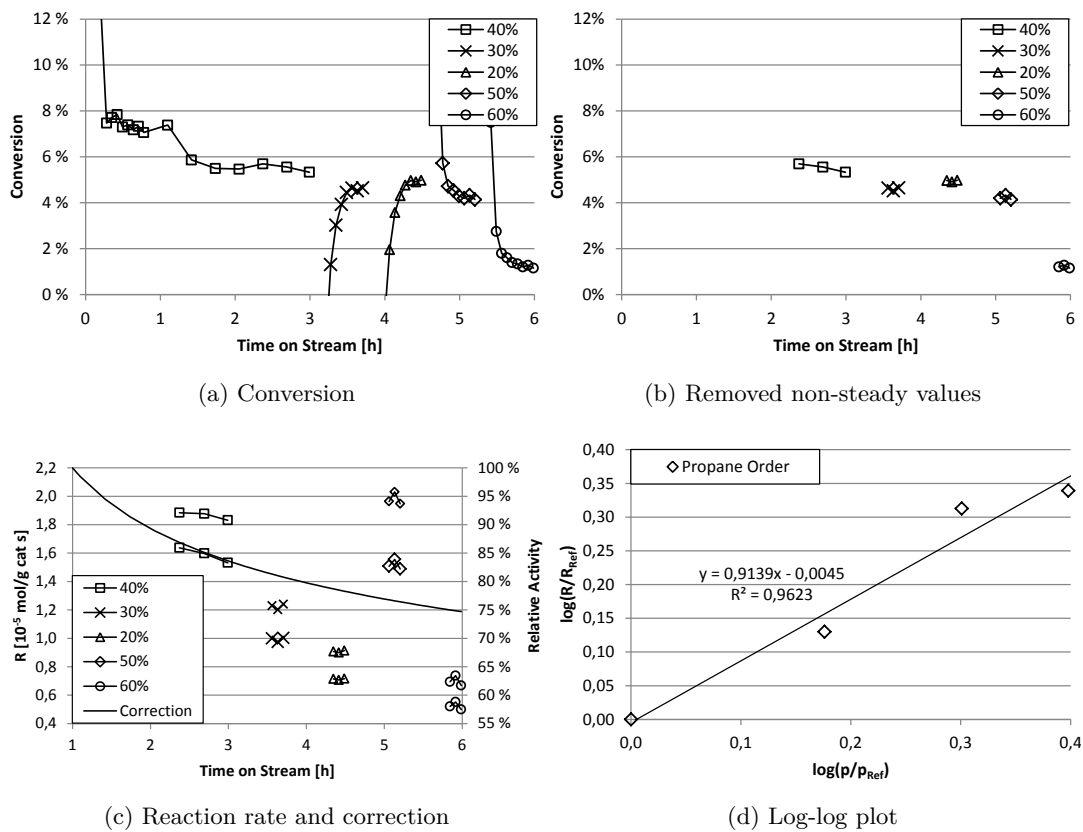
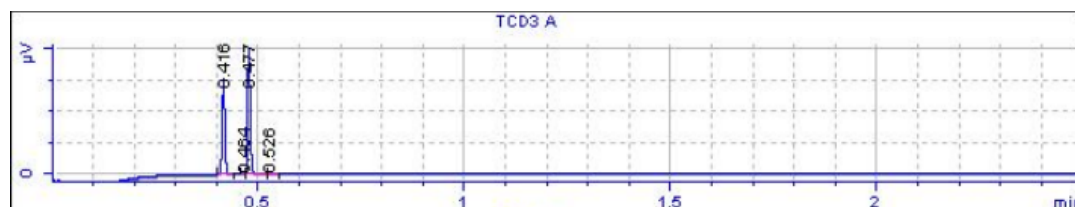


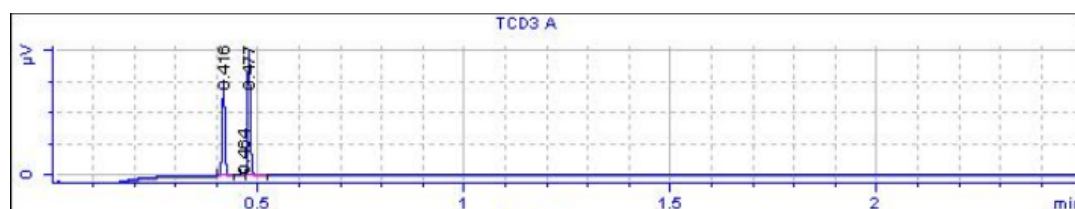
Figure G.3: Progressive plots for the  $C_3H_8$  kinetic study on the 0.5% Pt/Vulcan catalyst.

## G.4 Selected Chromatograms

To illustrate the catalyst support activities and the selectivity, a few selected GC chromatograms are shown in Figs. G.4 to G.7 showing TCD response in  $\mu\text{V}$  versus elution time in min.

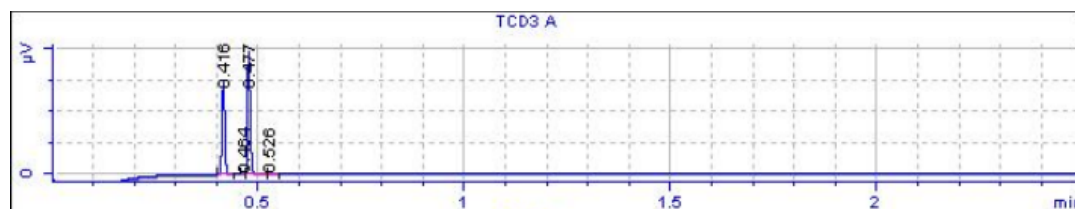


(a) Time on stream = 0.55 h

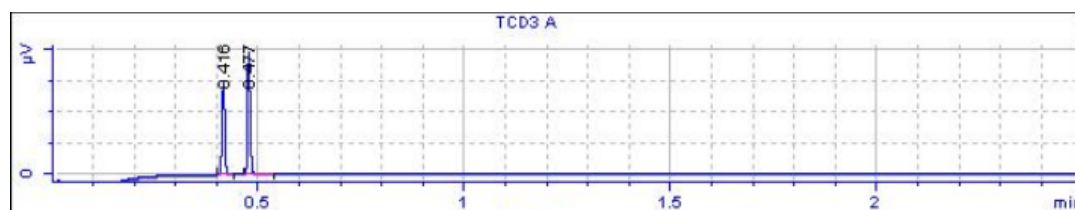


(b) Time on stream = 0.62 h

Figure G.4: Selected chromatograms from the catalytic test of the vulcan support showing  $\text{N}_2$  at  $t = 0.416$ ,  $\text{C}_3\text{H}_8$  at 0.477 and  $\text{C}_3\text{H}_6$  at 0.526. The peak detected at 0.464 is an impurity detected in all almost measurements.



(a) Time on stream = 0.34 h



(b) Time on stream = 0.41 h

Figure G.5: Selected chromatograms from the catalytic test of the CNF support showing  $\text{N}_2$  at  $t = 0.416$ ,  $\text{C}_3\text{H}_8$  at 0.477 and  $\text{C}_3\text{H}_6$  at 0.526. The peak detected at 0.464 is an impurity detected in almost all measurements.

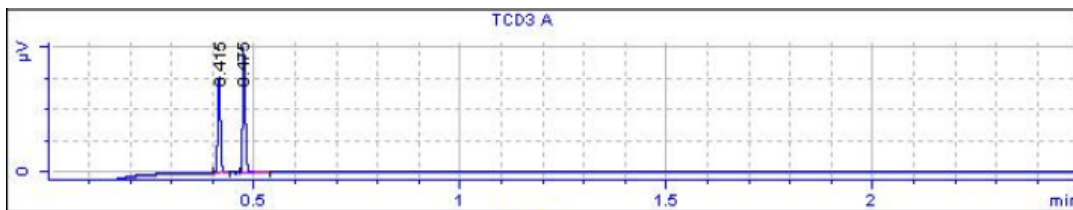
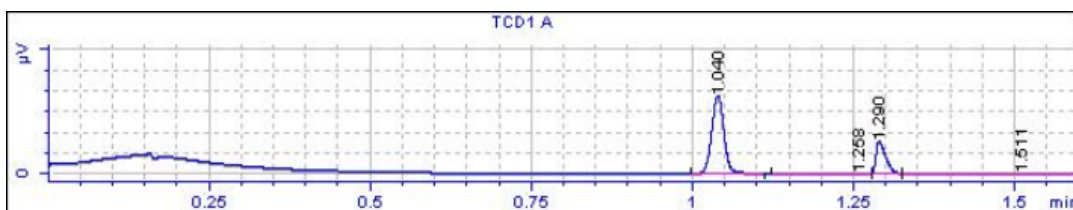
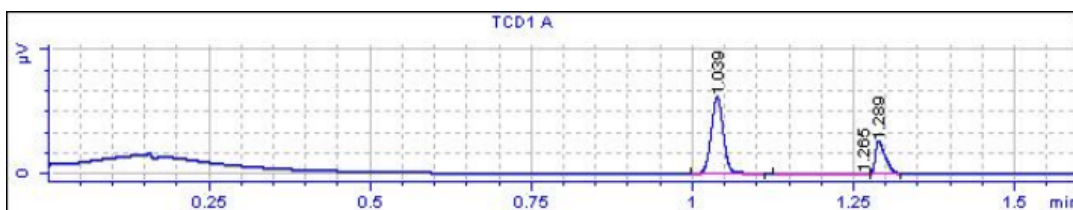


Figure G.6: Selected chromatogram from the catalytic test of the graphite support showing  $N_2$  at  $t = 0.416$ ,  $C_3H_8$  at  $0.477$  and no detected  $C_3H_6$  peak.



(a) Time on stream = 1.03 h,  $X = 9.73\%$



(b) Time on stream = 1.35 h,  $X = 9.17\%$

Figure G.7: Selected chromatograms from the activity test of the 0.5% Pt/Vulcan catalyst, parallel 1, showing  $H_2$  at  $t = 1.04$ ,  $N_2$  at 1.29 and  $CH_4$  at 1.511. The peak detected at 1.26 is an impurity detected in almost all measurements.

## H. Micro GC Calibration Data

The micro GC apparatus was calibrated using the internal standard calibration method, using nitrogen as the internal standard. Results are shown below in Table H.1 and Fig. H.1.

Table H.1: Internal Standard GC Calibration Data

$Y_{N_2}$	$A_{N_2}$ [ $\mu\text{V s}$ ]
0.1	6204.2
0.3	20008.8
0.5	33773.9
0.7	47623.4
0.9	60318.3

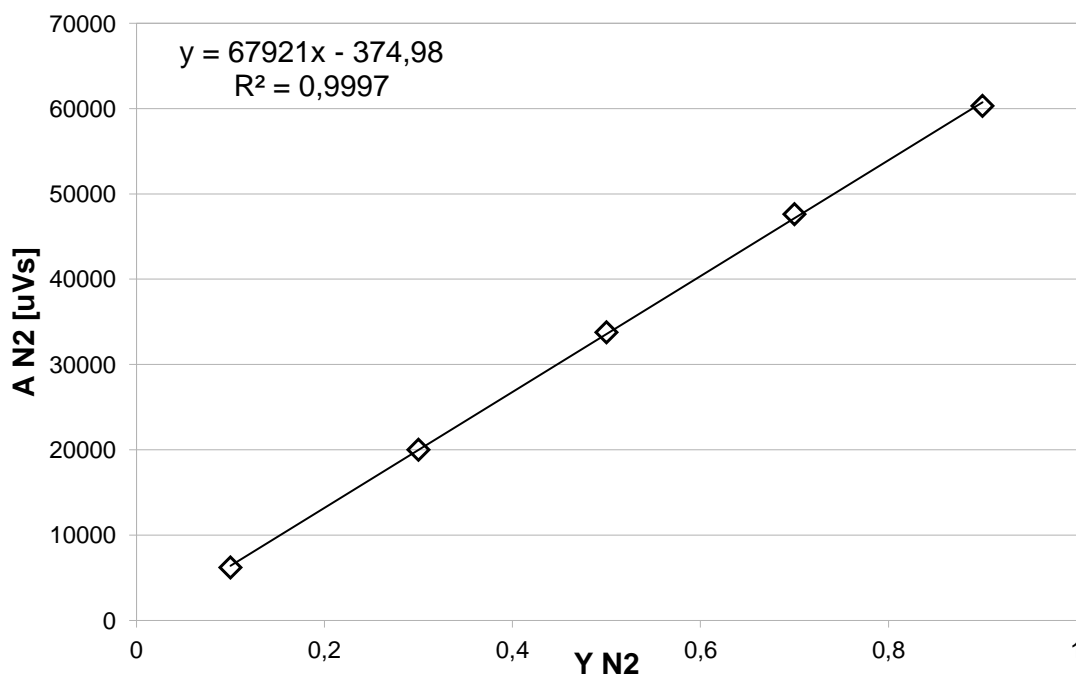


Figure H.1: Internal standard GC calibration data showing response as a function of nitrogen fraction. A regression curve is added.

Feed gas calibrations are shown in Table H.2 and product gas calibrations are shown in Table H.3.

Table H.2: Feed Gas GC Calibration Data

$Y_i$			$A_i$ [ $\mu\text{V s}$ ]			$RRF_i$	
$\text{C}_3\text{H}_8$	$\text{H}_2$	$\text{N}_2$	$\text{C}_3\text{H}_8$	$\text{H}_2$	$\text{N}_2$	$\text{C}_3\text{H}_8$	$\text{H}_2$
0	0.1	0.9	0	77079	60831	-	11.4039
0	0.2	0.8	0	155808	52530	-	11.8643
0	0.3	0.7	0	235801	44255	-	12.4325
0	0.4	0.6	0	318126	41411	-	11.5232
0	0.5	0.5	0	395620	34681	-	11.4074
0.1	0.4	0.5	22525	317240	34462	3.2681	11.5069
0.2	0.3	0.5	43881	235852	30886	3.5519	12.7270
0.3	0.2	0.5	66070	155856	32060	3.4347	12.1533
0.4	0.1	0.5	88056	76276	33336	3.3018	11.4404
0.5	0	0.5	109154	0	34488	3.1650	-
0.4	0	0.6	87762	0	41460	3.1752	-
0.3	0	0.7	66645	0	48171	3.2282	-
0.2	0	0.8	44574	0	55105	3.2355	-
0.1	0	0.9	22572	0	61903	3.2818	-
<b>Average:</b>						<b>3.2936</b>	<b>11.8288</b>

Table H.3: Product Gas GC Calibration Data

$Y_i$		$A_i$ [ $\mu\text{V s}$ ]		$RRF_i$
$\text{C}_3\text{H}_6$	$\text{N}_2$	$\text{C}_3\text{H}_6$	$\text{N}_2$	$\text{C}_3\text{H}_6$
0.001	0.995	216	68820	<b>3.1239</b>
$\text{CH}_4$	$\text{N}_2$	$\text{CH}_4$	$\text{N}_2$	$\text{CH}_4$
0.04	0.48	6690	32410	2.4770
0.10	0.45	15602	30595	2.2948
0.14	0.43	22206	29295	2.3281
0.20	0.40	31895	27210	2.3443
0.32	0.34	51006	23265	2.3294
<b>Average:</b>				<b>2.3547</b>
$\text{C}_2\text{H}_4$	$\text{N}_2$	$\text{C}_2\text{H}_4$	$\text{N}_2$	$\text{C}_2\text{H}_4$
0.000994	0.995	3630	68820	<b>52.7979</b>
$\text{C}_2\text{H}_6$	$\text{N}_2$	$\text{C}_2\text{H}_6$	$\text{N}_2$	$\text{C}_2\text{H}_6$
0.04	0.48	44996	230548	2.3420
0.10	0.45	118237	217867	2.4422
0.14	0.43	168374	209598	2.4673
0.20	0.40	247310	194528	2.5427
0.32	0.34	419473	164326	2.7122
<b>Average:</b>				<b>2.5013</b>

# I. Simulation Data

The equilibrium conversion ( $X_{eq}$ ) for the reaction  $C_3H_8 \rightleftharpoons C_3H_6 + H_2$  was determined by simulating the reaction with Unisim Design using the Peng-Robinson fluid package and an equilibrium reactor. The equilibrium conversion was simulated without any side reactions, at various pressures and temperatures and simulation results are shown in Fig. I.1 and results are shown in Table I.2 and simulations were also performed with varying composition, with results shown I.1.

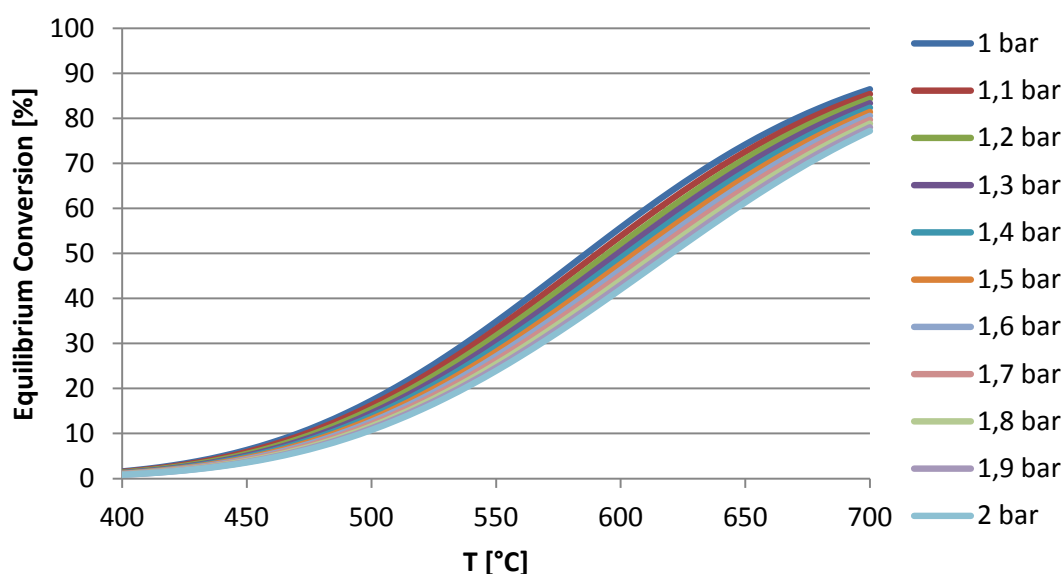


Figure I.1: Simulated equilibrium conversion for the propane dehydrogenation reaction as a function of temperature for a 40/50/10 v/v/v  $C_3H_8/N_2/H_2$  feed. Multiple total pressures are shown. Side reactions are not accounted for.

Table I.1: Simulated Equilibrium Conversions - Composition

Conditions: $T = 500\text{ }^\circ\text{C}$ , $p = 1\text{ bar}$			
$Y_{C_3H_8} = 40\text{ \%vol.}$ , $N_2\text{ rest}$		$Y_{H_2} = 10\text{ \%vol.}$ , $N_2\text{ rest}$	
$Y_{H_2}$ [%vol.]	$X_{eq}$ [%]	$Y_{C_3H_8}$ [%vol.]	$X_{eq}$ [%]
7	19.5	20	19.8
10	17.3	30	18.4
14	15.0	40	17.3
20	12.2	50	16.4
		60	15.7




Table I.2: Simulated Equilibrium Conversions - Temperature and Pressure

$T$ [°C]	$p$ [bar]										
	1	1.1	1.2	1.3	1.4	1.5	1.6	1.7	1.8	1.9	2
	$X_{eq}$ [%]										
400	1.6	1.4	1.3	1.2	1.2	1.1	1.0	1.0	0.9	0.9	0.8
410	2.2	2.0	1.8	1.7	1.6	1.5	1.4	1.3	1.2	1.2	1.1
420	2.9	2.7	2.5	2.3	2.1	2.0	1.9	1.8	1.7	1.6	1.5
430	3.8	3.5	3.3	3.0	2.8	2.7	2.5	2.4	2.3	2.2	2.1
440	5.0	4.6	4.3	4.0	3.7	3.5	3.3	3.1	3.0	2.9	2.7
450	6.4	5.9	5.5	5.1	4.8	4.5	4.3	4.1	3.9	3.7	3.6
460	8.0	7.4	6.9	6.5	6.1	5.8	5.5	5.2	5.0	4.8	4.6
470	9.9	9.2	8.6	8.1	7.7	7.3	6.9	6.6	6.3	6.0	5.8
480	12.1	11.3	10.6	10.0	9.5	9.0	8.6	8.2	7.8	7.5	7.2
490	14.6	13.6	12.8	12.1	11.5	11.0	10.5	10.0	9.6	9.2	8.9
500	17.3	16.3	15.4	14.6	13.8	13.2	12.6	12.1	11.6	11.2	10.8
510	20.3	19.2	18.1	17.2	16.4	15.7	15.0	14.4	13.9	13.4	12.9
520	23.6	22.3	21.2	20.2	19.3	18.4	17.7	17.0	16.4	15.8	15.3
530	27.1	25.7	24.5	23.4	22.4	21.5	20.6	19.9	19.2	18.5	17.9
540	30.9	29.4	28.0	26.8	25.7	24.7	23.8	22.9	22.2	21.5	20.8
550	34.8	33.2	31.7	30.4	29.2	28.1	27.2	26.2	25.4	24.6	23.9
560	38.9	37.2	35.6	34.2	32.9	31.8	30.7	29.7	28.8	28.0	27.2
570	43.1	41.3	39.6	38.2	36.8	35.6	34.5	33.4	32.5	31.5	30.7
580	47.3	45.5	43.8	42.2	40.8	39.5	38.3	37.2	36.2	35.3	34.4
590	51.6	49.6	47.9	46.3	44.9	43.5	42.3	41.2	40.1	39.1	38.1
600	55.7	53.8	52.1	50.5	49.0	47.6	46.3	45.1	44.0	43.0	42.0
610	59.8	57.9	56.1	54.5	53.0	51.7	50.4	49.1	48.0	46.9	45.9
620	63.7	61.9	60.1	58.5	57.0	55.7	54.4	53.1	52.0	50.9	49.9
630	67.4	65.6	64.0	62.4	60.9	59.6	58.3	57.0	55.9	54.8	53.8
640	70.9	69.2	67.6	66.1	64.7	63.3	62.0	60.9	59.7	58.6	57.6
650	74.2	72.6	71.0	69.6	68.2	66.9	65.7	64.5	63.4	62.3	61.3
660	77.2	75.6	74.2	72.8	71.5	70.3	69.1	68.0	66.9	65.9	64.9
670	79.9	78.5	77.1	75.8	74.6	73.4	72.3	71.2	70.2	69.2	68.3
680	82.3	81.0	79.8	78.6	77.4	76.3	75.3	74.3	73.3	72.4	71.5
690	84.5	83.3	82.2	81.1	80.0	79.0	78.0	77.1	76.2	75.3	74.4
700	86.4	85.4	84.3	83.3	82.4	81.4	80.5	79.7	78.8	78.0	77.2

# J. Risk Assessment

side 1 av 1 05.06.2013

NTNU	Hazardous activity identification process			Relatordatering	Nummer	Date
				HMS-ved.	HMSRV2601	
HMS				Gjølger av	Side	Erstatler

Unit: Department of Chemical Engineering Date: 10. jan 2013

Line manager: Supervisor: Edd A. Blekkan, Co-supervisor: Andrey S. Volynkin  
 Participants in the identification process (including their function): Operator: Eirik Østbye Pedersen

ID no.	Activity/process	Responsible person	Laws, regulations etc.	Existing documentation	Existing safety measures	Comment
Short description of the main activity/main process: Catalytic dehydrogenation of propane						
1	Bråk av brannfarlig gass	Edd A. Blekkan/ Eirik Østbye Pedersen	bruk i eksplosjonsfarlig område, NEK 420, Forskrift om anlegg og elektrisk utstyr (1929)	HMS datablader	Ekperimentelle prosedyrer er utarbeidet med hensyn på sikkerhet.	
2	Bråk av elektrisk oven	Edd A. Blekkan/ Eirik Østbye Pedersen	Forskrift om sikkerhet ved arbeid		Jording av oven	
3	Håndtering av korrosive kjemikalier	Edd A. Blekkan/ Eirik Østbye Pedersen		HMS datablader	Hansker, varmebriller og labfrakk tilgjengelig	
4	Håndtering av karbon nanopartikler	Edd A. Blekkan/ Eirik Østbye Pedersen			Hansker, varmebriller, støvmaske og labfrakk tilgjengelig	
5	Oppvarming av brennbare væsker	Edd A. Blekkan/ Eirik Østbye Pedersen		HMS datablader	Hansker, varmebriller, avtrekk og labfrakk tilgjengelig	
6	BET analyse	Karin Dragsten/ Eirik Østbye Pedersen	Arbeidsmiljøloven	Apparaturkort, HMS Datablader, Driftsinstruksjoner	Spesialhansker, varmebriller og labfrakk tilgjengelig	
7	TGA analyse	Karin Dragsten/ Eirik Østbye Pedersen	Arbeidsmiljøloven	Driftsinstruksjoner	Gassdetektor, advarselsskilt	
8	Hydrogenkjemioppsjon	Karin Dragsten/ Eirik Østbye Pedersen	Arbeidsmiljøloven	Driftsinstruksjoner	Gassdetektor, advarselsskilt	
9	CO Stripping Voltammetri	A. Volynkin/ Eirik Østbye Pedersen	Arbeidsmiljøloven	Driftsinstruksjoner	Gassdetektor, advarselsskilt	

NTNU	Risk assessment				Umbodet av	Nummer	Dato
					HMS-vedt	4459/2013	04.02.2013
HMS-ACS					Skapem.no	Side	Emne

Unit: Propane dehydrogenation project  
 Department of Chemical Engineering Date: 10 Jan 2013  
 Line manager: Supervisor: Eld A. Brakham, Co-supervisor: Anders S. Volden  
 Participants in the identification process (including their function): Operative: Erik Espire Pedersen

Signatures:

ID no.	Activity from the identification process form	Potential undesirable incident/event	Likelihood (1-5)	Human (A-E)	Consequence:			Risk value	Comments/status Suggested measures
					Environment (A-E)	Economy/ material (A-E)	Reputation (A-E)		
1	Bråk av brannfarlig gass	En liten gasslekkasje	2	A	A	A	2A	Gassdetektor og skum for lekkasjetest bør være lett tilgjengelig.	
1	Bråk av brannfarlig gass	Stor gasslekkasje	1	C	B	B	1C	Alle brukere må ha fått tilstrekkelig trening med bruk av gasser under høy trykk.	
2	Bråk av elektrisk oven	Elektrisk støt	1	C	A	B	1C	Overvåking av kvalitet til elektrisk isolasjon. Uungå kontakt med feteletere deler.	
2	Bråk av elektrisk oven	Ukontrollert oppvarming	1	C	B	C	1C	Alle brukere må ha fått tilstrekkelig trening med bruk av termoelement og kontrollboks.	
2	Bråk av elektrisk oven	Forpennning	1	C	A	A	1C	Omtenksomt arbeid vil minimalisere faren for forpenningskade.	
2	Bråk av elektrisk oven	Brann	1	C	C	D	1C	Omtenksomt arbeid vil minimalisere faren for brann.	
3	Håndtering av korrosive kjemikalier	Flutkontakt	2	A	A	A	2A	Bråk av hanske ved håndtering av korrosive kjemikalier.	
3	Håndtering av korrosive kjemikalier	Øyeblikkontakt	1	C	A	A	2C	Bråk av vernehjeller ved håndtering av korrosive kjemikalier.	
4	Håndtering av karbonanopartikler	Innhaling	2	B	A	A	2B	Bråk av spesialpasset støvmaske ved håndtering av karbonanopartikler	
5	Oppvarming av brennbare væsker	Brennrisikosplosjonsfarlig gassdannelse	1	B	A	B	1B	Bråk av avtrekk og kjølevann.	
6	Håndtering av flyende nitrogen	Flutkontakt	1	D			1D	Bråk av hjerter, spesialhansker og frakk. Ikke ha metall på utsatte steder	
6	Håndtering av flyende nitrogen	Øyeblikkontakt	2	D			2D	Bråk hjeller	
6	Håndtering av prøver	Prøve kommer i kontakt med vakuumpumpe	2			B		Riktig trening. Lapparbeid	
7	Varmebehandling av prøver	Flutkontakt	2	B			2B	Riktig trening. Lapparbeid	
8	Bråk av brannfarlig gass	Brann	2	B			2B	Gassdetektor tilgjengelig	
8	Bråk av oven	Flutkontakt	2	B			2B	Advarselbelysning	
9	Bråk av CO	Innhaling	1	C			2C	Obligatorisk bruk av gassdetektor og avtrekkskap	
9	Bråk av svovelsyre	Flutkontakt	2	A			2A	Bråk av hjerter og frakk	